Design of Broad-band Dual-polarized Microstrip Patch Antennas with High Port Isolation for Millimeter-Wave 5G Applications

by

Mohamed Kamal Nasser

A thesis submitted to the
School of Graduate and Postdoctoral Studies in partial
fulfillment of the requirements for the degree of

Master of Applied Science

Electrical and Computer Engineering

Faculty of Engineering and Applied Science

University of Ontario Institute of Technology (Ontario Tech University)

Oshawa, Ontario, Canada

January 2021

THESIS EXAMINATION INFORMATION

Submitted by: **Mohamed Nasser**

Master of Applied Science in **Electrical Engineering**

Thesis title: **Design of Broad-band Dual linearly polarized Microstrip Patch Antennas with High Port Isolation for Millimeter-Wave 5G Applications**

An oral defense of this thesis took place on January 14th, 2021 in front of the following examining committee:

Examining Committee:

Chair of Examining Committee	Dr. Jing Ren
Research Supervisor	Dr. Langis Roy
Research Co-supervisor	Dr. Ying Wang
Examining Committee Member	Dr. Farhan Abdul Ghaffar
Thesis Examiner	Dr. Ali Grami

The above committee determined that the thesis is acceptable in form and content and that a satisfactory knowledge of the field covered by the thesis was demonstrated by the candidate during an oral examination. A signed copy of the Certificate of Approval is available from the School of Graduate and Postdoctoral Studies.

ABSTRACT

Design of Broad-band Dual linearly polarized Microstrip Patch Antennas with High Port Isolation for Millimeter-Wave 5G Applications

Mohamed Kamal Nasser

Master of Applied Science

Department of Electrical and Computer Engineering University of Ontario

Institute of Technology

Ontario Tech University

2021

In this thesis, multiple broadband dual linearly polarized antennas are designed covering the frequency band for the next generation of 5G communications around 28 GHz. Dual polarization antennas are employed to increase the capacity of the allocated spectrum through frequency reuse. Techniques for improving the impedance bandwidth is one of the most researched areas of microstrip antenna technology. New multi-layer dual linearly polarized design topologies are proposed in this thesis, based on substrate integrated waveguide (SIW) cavity-backed microstrip antennas. Different structures and materials, and antenna types are explored. Wide impedance bandwidths of around 34% to 47% are achieved. In addition to very wide impedance bandwidth, the designs have a profile that is nearly half that of similar antennas reported in the literature without degradation to the antenna front to back ratio or radiation performance. In addition, a technique to improve the port to port isolation of the antenna by more than 10 dB is proposed. All designs proposed here achieve isolation levels above 30 dB across the band of interest. Two antenna arrays, a four - and a sixteen-element are also designed based on the single element

patch and fractal antennas. Their operational bandwidth is around 21% from 24 to 30 GHz, and sidelobe levels are better than 9 dB.

Simulation and optimization are carried out using full wave electromagnetic solver. A prototype of the final design was manufactured and tested. Results of all designs are compared and discussed for their bandwidth and the level of the port isolation in comparison to other millimeter wave dual linearly polarized antennas reported in the literature.

Keywords: Antenna Arrays; dual linearly polarized antennas; Microstrip Antennas; millimeter wave (mm-Wave); Substrate Integrated Waveguide (SIW)

AUTHOR'S DECLARATION

I hereby declare that this thesis consists of original work of which I have authored. This is a true copy of the thesis, including any required final revisions, as accepted by my examiners.

I authorize the University of Ontario Institute of Technology (Ontario Tech University) to lend this thesis to other institutions or individuals for the purpose of scholarly research. I further authorize University of Ontario Institute of Technology (Ontario Tech University) to reproduce this thesis by photocopying or by other means, in total or in part, at the request of other institutions or individuals for the purpose of scholarly research. I understand that my thesis will be made electronically available to the public.

Mohamed Kamal Nasser

STATEMENT OF CONTRIBUTIONS

I, Mohamed Nasser hereby certify that I am the sole author of this thesis and that no part of this thesis has been published or submitted for publication. I have used standard referencing practices to acknowledge ideas, research techniques, or other materials that belong to others.

Part of the work described in Chapters 3 and 4 will be submitted for publication.

For my mother and father Kamal and Eatidal

ACKNOWLEDGEMENTS

I would like to begin by thanking my advisors, Dr. Langis Roy, and Dr. Ying Wang, for their valuable support and mentorship over the past three years. From the two of you, I have learned how to become a better researcher and a better-rounded individual in both my academic and professional life and for that, I am forever grateful. Your passion and positive mindset are truly inspiring. I consider myself truly lucky to have been your student. Farhan Abdul Ghaffar, I have learned a tremendous amount from you over the years you were at Ontario Tech University. You are a great role model and an incredible mentor for any graduate student aspiring for academic success to have. I have learned an immense amount from every single one of you. Thank you for being there for me as mentors and supervisors. The success of this work would not be possible if it were not for you.

I wish to extend my thanks to my thesis examiner Dr. Ali Grami, and Farhan Abdul Ghaffar, my thesis committee members. Thank you, Dr. Grami and Dr. Ghaffar, for taking the time out of your busy schedules to be on this committee and to review this thesis. I appreciate all the feedback and suggestions you have provided.

I am also grateful to my friend and colleague Pedram Karimipour Fard for manufacturing the 3D printed parts used in my prototypes and the microscopic measurements conducted over the past few months.

My incredible parents Kamal Nasser and Eatidal Zumrawe, and my amazing brother Osama, I cannot thank you all enough for supporting me and being there for me during this journey. I would not be the person I am today if it were not for all your advice and support. My words cannot express my gratitude. To the rest of you in my life, who have always

inspired and offered me support when I need it the most, many thanks go to you. You know who you are!

My grad school lab mates and friends, thank you all for an incredible three years and for all the fun memories and times we shared. I will always remember and cherish those times. It has been a treat to have worked with such phenomenal peers and to have made such wonderful friends. You have made these three years of research much more enjoyable.

Finally, I would like to thank the team at CMC Microsystems for their support by providing all the necessary tools and software licenses to simulate the designs in this thesis.

Table of Contents

LIST OF TABLES

LIST OF FIGURES

Chapter 1

Chapter 2

Chapter 3

Chapter 4

LIST OF ABBREVIATIONS

ACMPA	Aperture Coupled Microstrip Antenna
DP	Dual Linearly Polarized
EIRP	Effective Isotropically Radiated Power
EM	Electromagnetic
FBR	Front to Back Ratio
GB	Gigabit
GHz	Giga Hertz
HFSS	High Frequency Structural Simulator
IEEE	Institute of Electrical and Electronics Engineers
5G	Fifth Generation
ISM	Industrial Scientific and medical
LTCC	Low Temperature Co-Fired Ceramics
LTE	Long Term Evolution
MIMO	Multiple-input and Multiple-output
mm	millimeter
MMIC	Monolithic Microwave Integrated Circuits
NR	New Radio
PCB	Printed Circuit Board
PGB	Photonic Bandgaps
PIFA	Planar Inverted-F Antenna
PLA	Polylactic Acid
PTFE	Polytetrafluoroethylene
RFID	Radio Frequency Identified
SAR	Synthetic Aperture Radar
SIW	Substrate Integrated Waveguide
SLL	Sidelobe Levels
VSWR	Voltage Standing Wave Ratio

Chapter 1

Introduction

1.1 Background and Motivation

Since the early 1980s there has been a significant growth in mobile communication technologies. Figure 1.1 shows the evolution of these generations from the first generation of wireless communications (1G) to 5G and what they provided to consumers. 1G brought us voice communications, using mostly analog signals and frequency division multiple access scheme. 2G enabled us to text for the first time, and it provided better quality and user capacity. The 3G launched in 2000 was designed to offer web-based applications, and video file transfer, bringing users online for the first time. 4G provided services like multimedia sharing and higher data rate with 4G LTE (long term evolution) [1].

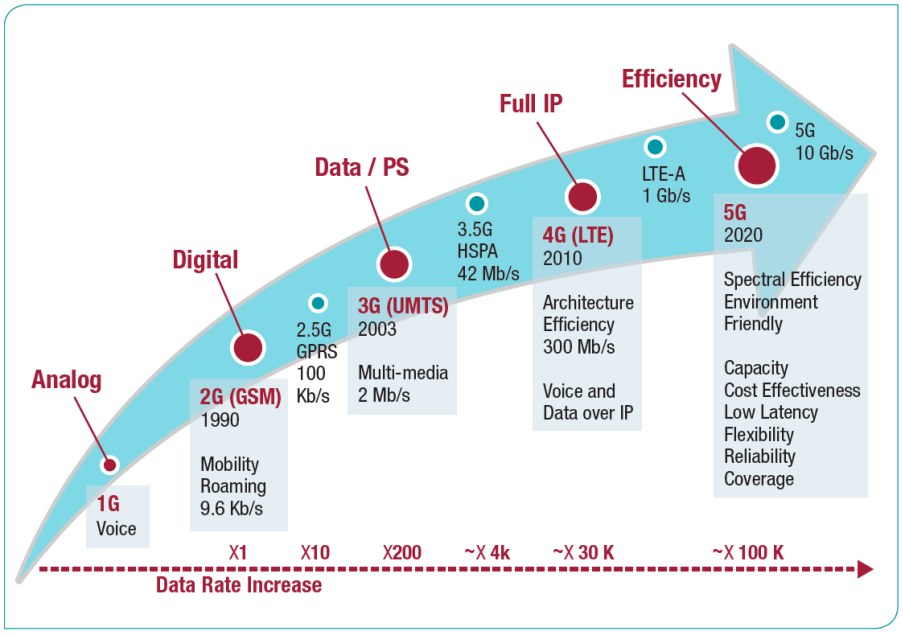

Figure 1.1: Wireless generations and data rates **[2]**

5G is an extension of today's fourth generation communication network. MM-Wave technology is a key enabler for 5G communications, offering end users a new experience in terms of higher data rates, and lower latency [2]. This comes at a time when there is a continuous demand for receiving over the air media content faster, and the current telecommunication system nearly reaching its user capacity. A latency of less than a millisecond will allow for its use in time sensitive applications such as autonomous vehicles [2]. In its latest mobility report (June 2020) Ericsson predicts 2.8 billion 5G mobile subscriptions by 2025 [3].

Larger spectrum availability above 24 GHz in comparison to sub 6 GHz worldwide will help in enabling 5G services. Moving to higher frequencies, however, comes with its own challenges, due to the higher path loss conditions in comparison to lower end of spectrum. Advanced antenna systems are needed to deal with such radio propagation challenges. Base stations need to be equipped with larger antenna arrays as the antenna sizes are significantly reduced at these frequencies. This opens the door for beam forming, where multiple transmit/receive signals can be sent in different directions in comparison to a single omnidirectional transmission. At mm-Waves fully integrated transceivers and antennas (with more than a 100 antennas) will be deployed, enabling beamforming to enhance coverage in more challenging propagation environments [4]. During the past few years the number of base station antenna arrays have considerably grown to meet today's higher capacity requirements[4]. By taking advantage of multiple-input and multiple-output (MIMO), carrier aggregation throughput can be increased.

Microstrip patch antennas have matured into one of the most popular and adaptable PCB (Printed Circuit Board) printed antennas. This is the result of their many desirable features:

such as their light weight, ease of fabrication, conformability, and low production cost. Patch antennas are typically resonant structures, meaning they have excellent efficiencies over a narrow impedance bandwidth. Over the years researchers have developed techniques to improve the impedance bandwidth of these antennas. This however comes at the expense of complexity. The past half a century has seen a great deal of microstrip antenna development[5]. Despite all these developments patch antennas typically suffer from a narrow impedance bandwidth ranging from 1 – 2%, making them not suitable for many applications. Radiation bandwidth, contrary to the impedance bandwidth of a patch antenna, is broadband, with a fractional bandwidth larger than 30%. Two of the most common patch antenna techniques being used to this day are aperture (slot) and proximity coupled excitation techniques [6], [7]. Microstrip antennas were deployed in commercial systems, such as mobile base stations in the 1990s. In addition to the further enhancement of impedance bandwidth, antennas with impedance bandwidth of around 67% were designed[8]. Applications with Photonic Bandgaps (PGB) structure to enhance the efficiency and radiation performance were also investigated [9]. Microstrip patch antennas have also been employed for various applications such as synthetic aperture radar (SAR), millimeter wave (mm-Wave) collision avoidance systems, missiles, aircrafts, satellite systems [10], and mobile communication base stations and handsets[11].

1.2 Thesis Objectives

The 5^{th} generation wireless communication will be a major advancement to today's wireless communication systems by providing higher data rates (many Gigabit (GB)/s) and a massive reduction in response time, while providing better services for densely populated areas. This is possible because of the smaller wavelengths (about 5 mm at 60 GHz) and the

attenuation of about 15 dB/Km, which allows the base stations to be placed closer together in comparison to current wireless communication systems. Quality of service improvements and better energy efficiency are expected to allow users to stream high quality videos and games instantly [2]. Multiple frequency bands are being considered by different countries for the next generation 5G wireless communications. Figure 1.2 shows some of the upper spectrum bands currently proposed in the US, Europe, South Korea, Japan, and China [12]. The 26 and 28 GHz bands, extending from 24.25 to 29.5 GHz, are currently being considered for 5G. The overall objective of this thesis is to design a 5G broadband and dual linearly polarized antenna with high port isolation. Here, multiple dual linearly polarized antennas, and antenna arrays operating from 24.25 to 29.5 GHz will be designed. The required antenna specifications in this thesis are being driven by a leading 5G hardware manufacturer.

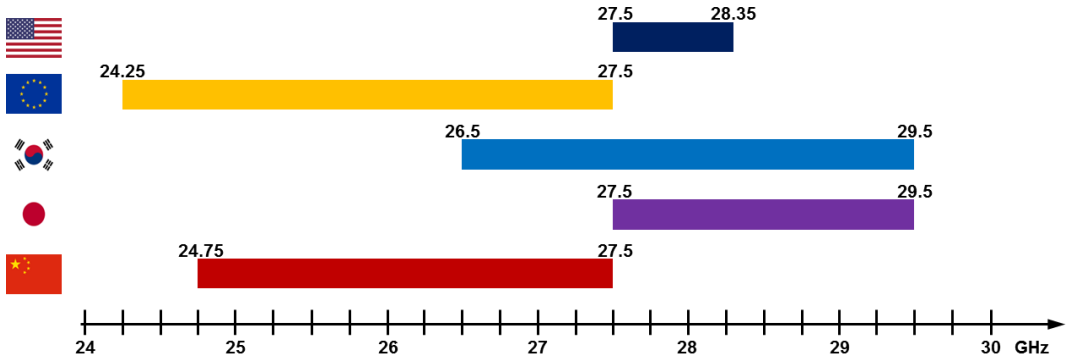

Figure 1.2; Some proposed bands for mm-Wave 5G "© 2018. 3GPP™ deliverables and material are the property of ARIB, ATIS, CCSA, ETSI, TSDSI, TTA and TTC who jointly own the copyright in them. They are subject to further modifications and are therefore provided to you "as is" for information purposes only. Further use is strictly prohibited."

The aim of this thesis is to design a broadband dual linearly polarized microstrip antenna around 28 GHz. Even though there are many publications on the topic of patch antenna bandwidth enhancement, most of them are typically at lower frequencies below 6 GHz and

those that are available have a larger antenna profile. The design goals can be summarized as follows:

- Investigate techniques for patch antenna bandwidth enhancement such as antenna stacking and slot coupling.
- Improve antenna port isolation (magnitude of S_{21}) to be better than 30 dB across the band without degrading other antenna characteristics.
- Design an antenna array with an integrated corporate feed network to make sure the design makes a good candidate for a 5G antenna array.

1.3 Thesis Contributions

The antennas realized in this thesis have a wider bandwidth and a lower profile in comparison to other antennas reported in the literature. Additionally, superior isolation performance is also attained with a newly proposed technique. This method provides an isolation enhancement of more than 10 dB in comparison to conventional microstrip antennas, without degrading other antenna characteristics.

The first design is a microstrip line fed multilayer antenna with two slot coupled radiators and H-shaped slots. Fractal antennas can offer a better impedance bandwidth, therefore a Sierpinski fractal was designed, to investigate their bandwidth and isolation capabilities. The patch antenna has an impedance bandwidth of around 34% and the fractal has a bandwidth of around 28%. Port isolation levels are better than 34 dB and 28 dB for the patch and fractal antenna, respectively. These antennas have the lowest profiles and port isolation levels in comparison to most mm-Wave dual linearly polarized antennas reported in the literature. A four and 16 element antenna array were also simulated using a microstrip line feed network.

Two similar designs using a foam and a 3D printed spacer between the antenna elements are also proposed. The former has a profile of 0.15 λ_0 and an impedance bandwidth of around 47%. To the best of our knowledge this is the largest impedance bandwidth reported in the literature for an antenna of its profile. Port isolation levels are also better than 40 dB in most of the band. The latter has a profile of 0.177 $\lambda_{0,}$ an impedance bandwidth of 34.7%, and better than 37 dB port isolation. As a result of this work some of the best performing dual linearly polarized antennas in terms of bandwidth, isolation levels, and profile are reported.

1.4 Thesis Organization

Chapter 2 provides an overview of the current state of the art of patch antennas, with focus on broadband dual linearly polarized antennas with high levels of isolation. Different patch antenna excitation techniques are reviewed, along with methods for antenna bandwidth enhancement. Broadband mm-Wave antennas from the literature are discussed as well.

In the 3rd chapter three mm-Wave broadband dual linearly polarized antennas are developed, operating around 28 GHz, one of the band candidates for 5G millimeter wave communications. Each of the three designs could achieve an impedance bandwidth of 28% or more with port isolations higher than 30 dB. All designs in this chapter use a second patch antenna for bandwidth enhancement, as this was deemed the best method. A technique for port isolation enhancement is proposed, leading to an isolation enhancement of at least 10 dB, by connecting a shorting post between the slots in the ground plane and the patch antenna. A parametric study on the effect of various parameters on the antenna matching is also carried out using the full wave solver ANSYS HFSS.

The 4th chapter starts with a brief overview of the requirements on antenna arrays for 5G applications. A microstrip feed network, and two antennas arrays, namely a four-element and a sixteen-element arrays, are designed. Array radiation patterns, cross-polarization levels, and simulated array efficiencies are then presented. Concluding remarks and future research developments are covered in chapter 5.

Chapter 2

Broadband Microstrip Antennas: State of the Art

2.1 Introduction

This chapter covers the current state of dual linearly polarized microstrip antennas, focusing on designs for 5G applications. The most common design technique for dual polarization is through the excitation of two orthogonal modes, one for each polarization. Additionally, orthogonal elements such as crossed dipoles or slot antennas can also be employed, although not very common. The use of the term "dual polarization" in this thesis refers to dual linear polarization and not circular polarization. Therefore, the focus of this chapter is on dual linearly polarized designs that are excited using two orthogonal modes. A comparison of the antennas discussed here is carried out in terms of their percent bandwidth and port isolation improvements. Different methods proposed in the literature for port isolation enhancement are also discussed.

Two critical parameters that always pose a challenge when designing dual linearly polarized microstrip antennas are the level of cross-polarization and input port isolation, especially in demanding applications such as mobile and satellite communications. Due to the proximity of the input ports, high levels of isolation are typically difficult to achieve. Over the years, a tremendous amount of research has gone into the investigation of different techniques to reduce this effect.

2.2 Radiation Interaction Between Two Dual linearly polarized Elements

Port isolation and cross-polarization levels are the two performance measures of a dual linearly polarized (DP) antenna. This concept can be simplified using the illustration in figure 2.1, which uses two orthogonal radiating elements, one representing each polarization.

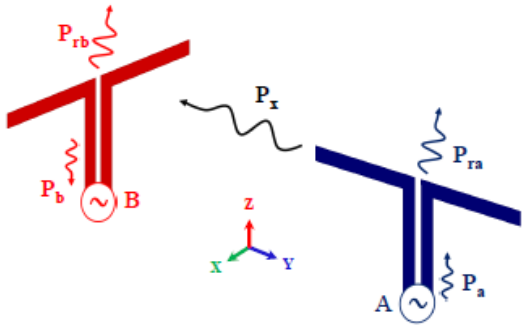

Figure 2.1: Coupling between two radiation elements in a dual linearly polarized antenna © 2019 IEEE

Assume these two elements are lossless and ignore the cross-polarization radiation from both antennas as illustrated in the above figure. When element A is excited, a portion of the power is radiated (P_{ra}), and the rest couples to element B (P_x). P_x then divides into P_b and $P_{rb,}$ where P_b is representative of the port isolation level and P_{rb} the cross-polarization. From figure 2.1, we can observe that the antenna cross-coupling P_x affects both the level of port isolation and cross-polarization. Therefore, if the level of antenna cross-coupling is reduced, both the port isolation and the element's cross-polarization would be minimized [13].

2.3 Achieving Dual Polarization by Exciting Two Orthogonal Modes

Dual linearly polarized (DP) antennas can be realized by exciting two orthogonal modes that generate two polarizations, a vertical and a horizontal. These antennas can be advantageous in wireless communication systems because of their ability to increase channel capacity and reduce multipath fading. It is therefore an ideal choice for multiple-input and multiple-output (MIMO) communication systems currently used for 4G and future 5G applications. Only square patches operating in the dominant mode are considered in this work because of their superior properties in terms of symmetry and compactness [14]. Higher-order modes are also excited beneath the patch antenna, contributing to the port isolation and cross-polarization degradation. Next, we discuss various DP microstrip antenna designs with different feeding configurations, such as slot (aperture) coupled, microstrip-line, and probe feeding, while evaluating antenna characteristics of each system in terms of bandwidth and isolation enhancement. Throughout this work antenna bandwidth refers to the band over which the antenna return loss (S_{11} and S_{22}) is better than 10 dB, and port isolation refers to the magnitude of S_{21}.

2.3.1 Microstrip Line fed DP Antennas

Microstrip lines are the simplest and most compact way of exciting a patch antenna, where the antenna and the feed network are printed on a single layer board. Broadband antennas fed in this manner, however, typically suffer from increased levels of spurious feed radiation and degradation in the antenna polarization purity as a result of increased substrate thicknesses [15]. Dual linearly polarized microstrip antennas with direct feeding through a microstrip line are fed either at the edges [16] or corners of the antenna, as shown in figures 2.2 (a) and figure 2.2 (b), respectively. These types of antennas, however, are

narrowband, offering impedance bandwidths of only a few percent. Corner-fed antennas typically have an isolation margin of 10 dB compared to edge fed ones [17]. Cross-coupling and cross-polarization levels in the techniques mentioned above can be reduced by using balanced differential excitation. Figure 2.2 (c) is an example of a differentially fed microstrip antenna from [18], with an enhanced polarization purity.

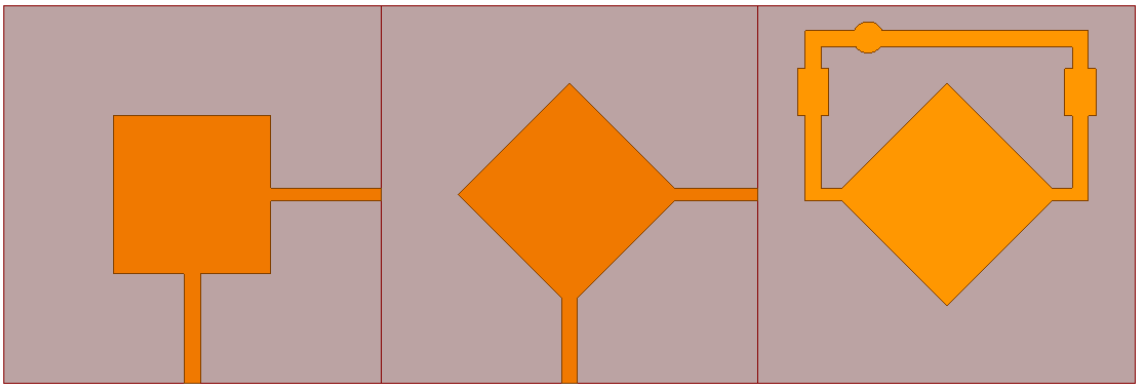

(a) (b) (c)

Figure 2.2: Microstrip line fed dual linearly polarized patch antennas, (a) edge fed (b) corner-fed (c) differentially-fed (*Concept from* **[16]–[18]**)

2.3.2 Coaxial Probe fed DP Microstrip Antennas

Coaxial probe feeding is another common technique for microstrip patch antenna excitation. In this method, a probe is added beneath the patch antenna, allowing for easier matching and lower cross-polarization levels (for relatively thin substrates $\leq 0.05\ \lambda_0$) in comparison to direct feeding. The coaxially fed dual linearly polarized patch antenna shown in figure 2.3 from [14] achieved an impedance bandwidth of 2.2% and a port isolation level better than 30 dB. Increasing the laminate thickness can widen the impedance bandwidth at the expense of higher cross-polarization levels and difficulty in matching due to the inductive nature of the probe as its length increases [19]. Further

discussion on the issues associated with the distance between two probes in a DP antenna configuration in terms of port isolation, cross-polarization levels, and co-polarization distortion due to the probe's leakage radiation can be found in [20] and [21].

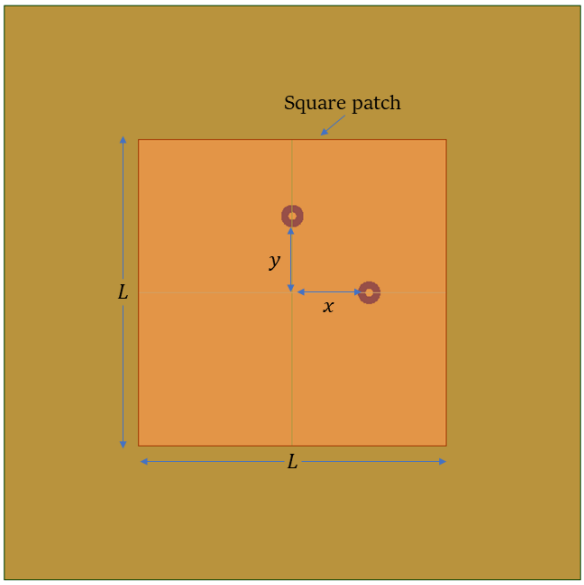

Figure 2.3: Dual linearly polarized coax fed antenna (concept from [14])

2.3.3 Slot (aperture) Coupled Dual linearly polarized Microstrip Antennas

In 1985 D. M. Pozar introduced a new microstrip line fed patch antenna that does not require a direct connection between the antenna element and the feed network [6]. The feed line and the radiating elements are placed on two different substrate layers separated by a ground plane with an etched slot that helps in blocking radiation pattern distortions from the feed network. This excitation method also introduces a new degree of antenna optimization, where the slot dimensions and stub length can be varied to achieve the desired antenna performance. Additionally, this also aids in integrating monolithic phased arrays typically printed on a higher dielectric constant layer (gallium arsenide (ε_r = 12.9), for example) below the radiating element. In this scenario, any active elements would be directly integrated with the feed network. The antenna element is printed on a lower

dielectric constant material for better impedance bandwidth, scan angle performance, and radiation efficiency [6].

A slot coupled dual linearly polarized antenna with 3.5% bandwidth and port isolation of 18 dB was proposed in [22]. Two rectangular slots in the ground plane were coupled to two microstrip lines exciting two dominant modes. The designed antenna is shown in figure 2.4 (a). Replacing the patch with a circular one and modifying the slot placement, the port isolation can be enhanced, as shown in figure 2.5 (b). In [23], a dual linearly polarized patch antenna was designed with an impedance bandwidth of 1.6% and port isolation that is better than 35 dB. This improvement results from further slot displacement in the ground plane, which leads to less coupling. Further discussion on the effect of the slot length and their offset from the patch center on the port isolation can be found in [23].

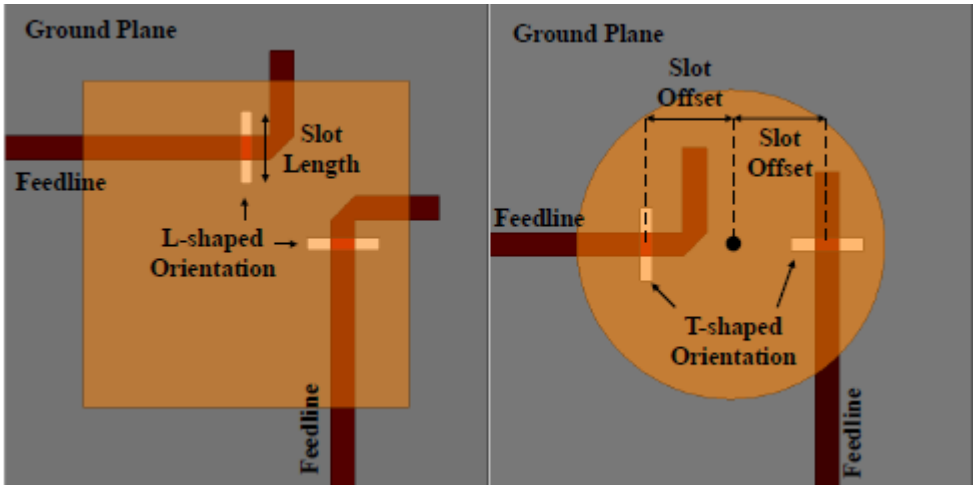

(a) (b)

Figure 2.4: Slot coupled microstrip antennas © 1987, 1993 IEEE [13]

Experimental studies have shown that if the slots are placed further apart, or their length is reduced, better port isolation can be achieved. This is, of course, limited by the antenna dimensions and is not feasible beyond a certain limit. Using slots of different shapes is

another avenue for isolation improvement. In [24] and [25], the effect of various slot shapes on the level of coupling is presented. These experimental studies concluded that a stronger level of coupling to the patch antenna can be achieved by using an H shaped or bow-tie slot in comparison to a rectangular slot. Additionally, the slot length also reduces by approximately 30%. Shorter slot lengths directly translate into better efficiency and lower back lobe radiation levels [24], and for the case of a dual linearly polarized antenna, better port isolation as the offset between the slots increases.

2.3.4 Stripline fed Dual linearly polarized Microstrip Antennas

The authors in [26] proposed the stripline fed dual linearly polarized antenna shown in figure 2.5 to eliminate the parasitic radiation from the feed network while limiting the back radiation from the slot with the lower ground plane. This feeding technique, however, increases the manufacturing complexity and the fabrication cost of the antenna, given the feed lines are sandwiched between two ground plane layers. A few critical parameters must be kept in mind when designing this type of antenna, most notably the return currents via the ground plane and the level of back radiation due to the slots. Different higher-order modes can be excited between the two ground planes depending on the level of back radiation from the slots. For resonant slots, a densely spaced wall of shorting posts can be used to eliminate higher odder modes. However, only light shielding is required for the case of a non-resonant slot, where the vias can be spaced more than $\lambda_g/10$ apart and still suppress parasitic modes. Another technique to reduce the level of back radiation is by using multiple resonators (a parasitic patch), where the resonance frequency of the parasitic patch is close to that of the primary antenna, and the slot size can be reduced below resonance, therefore, decreasing the level of back radiation

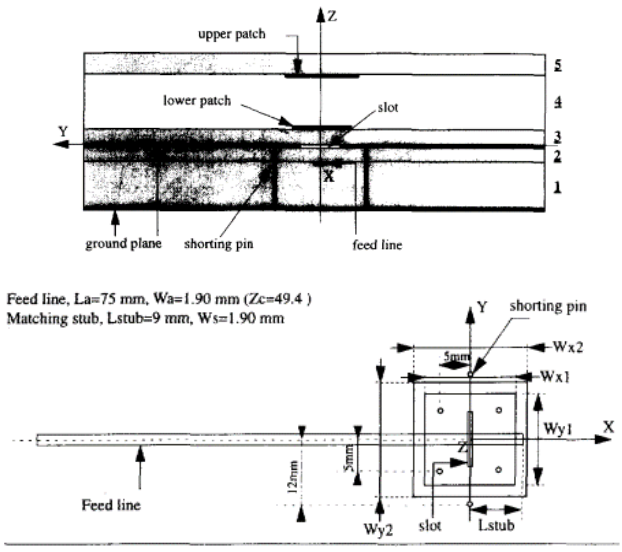

Figure 2.5: Linearly polarized stripline fed antenna © 1995 IEEE

Cross-polarization levels that are better than 37 dB were achieved using this technique. Input port isolation that is better than 35 dB was also attained throughout the bandwidth of interest.

2.3.5 Advantages and Disadvantage of Microstrip Antenna Feeding Techniques

All patch antenna excitation techniques have their own set of advantages and disadvantages. Choosing between them is a matter of tradeoff, depending on the application they are used for. A variety of different patch antenna feeding techniques, along with design procedures, can be found in [5]. Table 2-1 below summarizes some of the advantages/disadvantages of the most common patch antenna feeding techniques discussed in this chapter.

Table 2-1: Advantages and disadvantage of different excitation techniques

	Advantages	Disadvantages
Coaxial Feed	• Easy matching • Low spurious radiation	• Tends to be inductive for thicker substrates • Pin soldering is required

Microstrip Line	• Easy to manufacture • Inset feeding makes it easy to match	• Feedline radiation • Narrow bandwidth • Low efficiency for thicker substrates
Slot (Aperture) Coupled	• Wide bandwidth • Higher dielectric constant substrates can be used, allowing for active element integration • Reduces feed line effect on the radiation pattern	• Increased manufacturing costs because of the use of multiple layers • High levels of back radiation when resonant slots are used

2.4 Techniques for Bandwidth and Isolation Enhancement

Based on the general performance trends of microstrip antennas, two straightforward techniques to increase the operational impedance bandwidth of a microstrip antenna are increasing the substrate thickness and the use of low permittivity laminates. These techniques, however, are limited to maximum impedance bandwidths of around 10%. Additionally, a series of issues could arise, such as low radiation efficiency due to the excitation of surface waves, and the appearance of grating lobes in array applications. To substantially improve the bandwidth of a microstrip antenna (greater than 15% or 20%), the addition of an air gap between the feed network and the radiator, as for the case of L-probe fed patch antennas, or more resonant radiators are typically needed. Here, L-probe based designs are discussed first, and the rest of the section is dedicated to bandwidth enhancement techniques using additional resonators.

As a result of the limitations of conventional probe fed patch antennas mentioned earlier, L-shaped probes, as shown in figure 2.6, have been introduced [27]. These antennas

achieve a broader bandwidth and reduce the cross-polarization levels typically seen in traditional probe fed patch antennas. The horizontal section of the probe is designed to be close to a quarter wavelength, forming an open-circuited stub and compensating for the inductive nature of the vertical probe. This type of feeding can lead to impedance bandwidths of up to 40%. Single-sided antennas like the one in figure 2.6 are known to disrupt the normal distribution of the dominant mode and cause higher levels of cross-coupling between polarizations. An L-shaped probe fed dual linearly polarized antenna was proposed in [28], achieving an impedance bandwidth above 37% and around 40 dB port isolation. The design presented in [29] achieves an impedance bandwidth of 24% and a port isolation level that is better than 30 dB across the band. Both of those designs were differentially fed, with each branch having the same amplitude and a 180° phase difference between them, leading to coupling cancelations between the two feeds. The leakage radiation also cancels out in the far-field since they have the same amplitude but opposite directions, resulting in lower cross-polarization [20]. An example illustrating differential feeding of a DP patch antenna proposed by the authors in [29] is shown in figure 2.7. Antennas fed in this manner do not suffer from the same problems that single-sided antennas do. Complications can arise when designing differentially fed antennas like those shown in figure 2.7, especially on the array level, but that is a small price to pay in comparison to the performance enhancement they can provide. Further port isolation improvement may be achievable by reducing the length of the feedline before the split point, leaving the door open for further optimization. This can be beneficial on the array level, where the overall array performance is tied to how well the feed network performs.

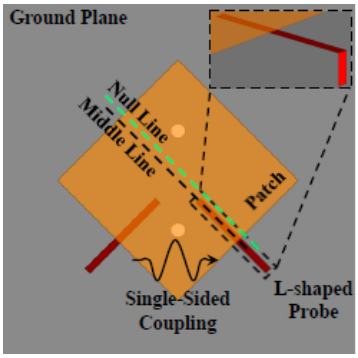

Figure 2.6: L-probe fed dual linearly polarized patch antenna © 1998 IEEE **[13]**

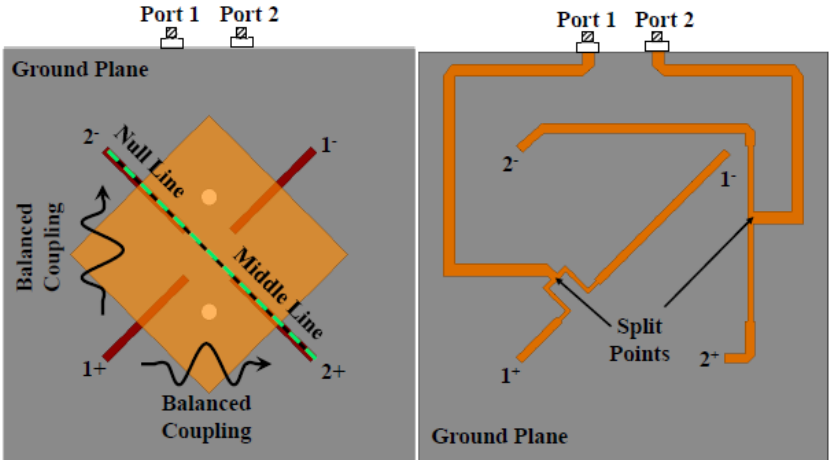

Figure 2.7: Differentially fed dual linearly polarized antennas, (a) L-shaped probe, (b) differential feed © 2004 IEEE **[13]**

Next, we move on to discuss the achievable bandwidth using additional resonators by showing different patch antenna examples with parasitic patches and comparing their performance. This technique can lead to impedance bandwidths of more than 50% through the addition of multiple resonators, typically supported by foam substrates. Most of these designs are fed using different configurations of slots from H or dog-bone shaped to crossed slots [30]. These coupling slots can also be used as resonators to achieve a broader bandwidth. To the best of our knowledge, antenna stacking has not been attempted using L-shaped probes, and those with traditional probe feeding typically offer a lower impedance bandwidth.

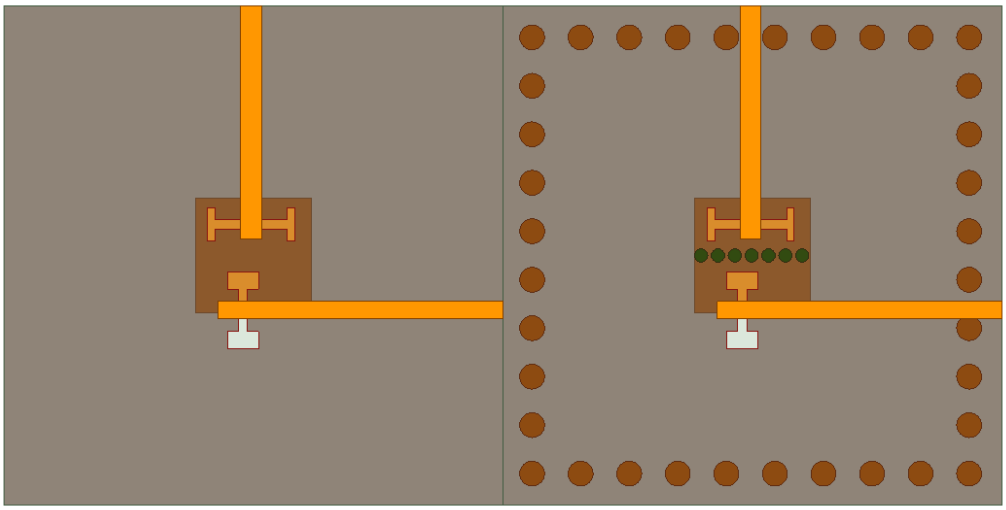

(a) ***(b)***

Figure 2.8: Dual linearly polarized microstrip antennas with H-shaped coupling slots (*Concept from* [31], [32])

Two broadband dual linearly polarized designs fed using H shaped slots from [31] and [32] are shown in figure 2.8 (a) and (b), respectively. The antenna in figure 2.8 (a) achieved an impedance bandwidth of 25% and isolation (≥ 40 dB). In comparison, the design in figure 2.8 (b) achieved a 10 dB bandwidth of 28% and port isolation (≥ 40 dB). A better level of coupling and a wider impedance can be achieved by placing the coupling slot closer to the center of the patch [6]. However, this is not feasible for the case of a dual linearly polarized patch antenna because it reduces the offset between the slots and worsens port isolation, unless a via wall is added between the slots as done in [32]. An isolation improvement of around 10 dB was achieved using this technique at the expense of increased design complexity and longer simulation times. Plots of the ground plane electric were provided to show the improvement in coupling with the vias.

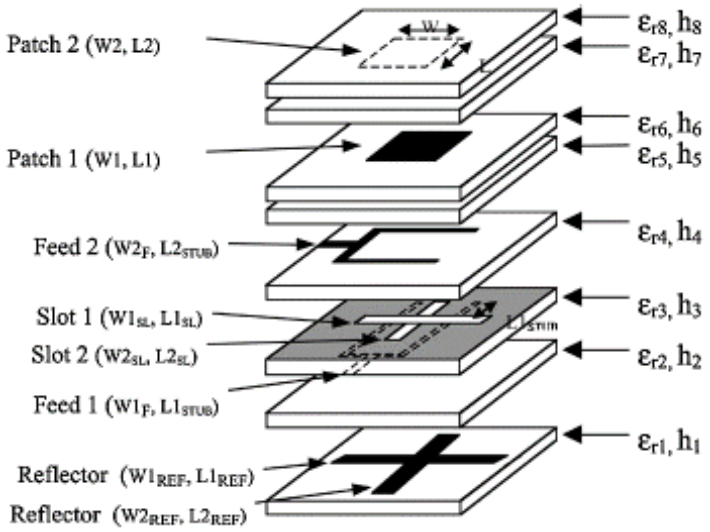

Figure 2.9: Broadband dual linearly polarized aperture stacked patch antenna © 2004 IEEE

The antenna shown in figure 2.9 is a crossed slot coupled patch antenna operating around 2 GHz for cellular base station applications. This antenna can achieve an impedance bandwidth above 50% with port isolation (≥ 35 dB) across the band [33]. Two balanced feeds that are symmetric with the patch center and the slots are used here, one for the excitation of each polarization. This design also has other advantages, such as higher-order mode suppression and better port isolation [34]. One disadvantage, however, is the low front to back ratio (typically between 6 to 12 dB) when resonant slots are used. A reflector can be used to improve the antenna front to back ratio to acceptable levels.

2.5 Broadband Millimeter-Wave Dual linearly polarized Antennas

Most of the designs discussed in the previous sections operated at lower frequencies near L and S bands. In some cases, such as the L-probe fed antenna, duplicating those designs at higher frequencies would pose significant challenges because of the antenna size. L-probe fed patch antennas are typically supported by a little plastic post with a diameter of around 1 mm. Manufacturing this at higher frequencies without causing alignment issues

would be a difficult task. In this section, a few mm-wave dual linearly polarized antennas from the literature are discussed and compared in terms of their impedance bandwidth, profile, and input port isolation. Other examples of mm-Wave designs not discussed here are [35]–[37].

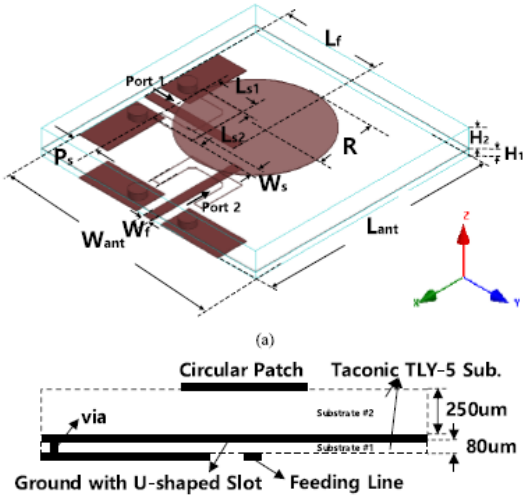

Figure 2.10: U-slot coupled patch antenna © 2019 IEEE

A low profile dual linearly polarized circular patch antenna coupled through U-shaped slots was proposed in [38], as shown in figure 2.10. The antenna has a low profile of 0.066 λ_0 while offering an impedance bandwidth of 15%, which covers the entire 60 GHz industrial, scientific, and medical (ISM) band from 57 to 64 GHz. A significant improvement in port isolation (from 23 dB to better than 37 dB over the frequency band) was achieved by using a circular patch antenna. The currents from each of the feeds circulate near the edge of the circular patch antenna. Given that the feeds are orthogonally oriented, the currents cancel each other out because they flow in opposite directions. The current in port 1, for example, flows in the clockwise direction, while the currents due to port two flows in the counterclockwise direction, therefore canceling each other out and increasing the port isolation. There was a good agreement between the measured and simulated results of the

manufactured prototype, except for a small difference in the S_{11} and S_{22} return loss bandwidth because of layer miss-alignment.

This design, however, is likely going to suffer from larger levels of back radiation because of the resonant slots. As mentioned earlier, it is always desirable to keep the operating frequency of the slots well below the operating frequency of the patch antenna to avoid high back radiation levels.

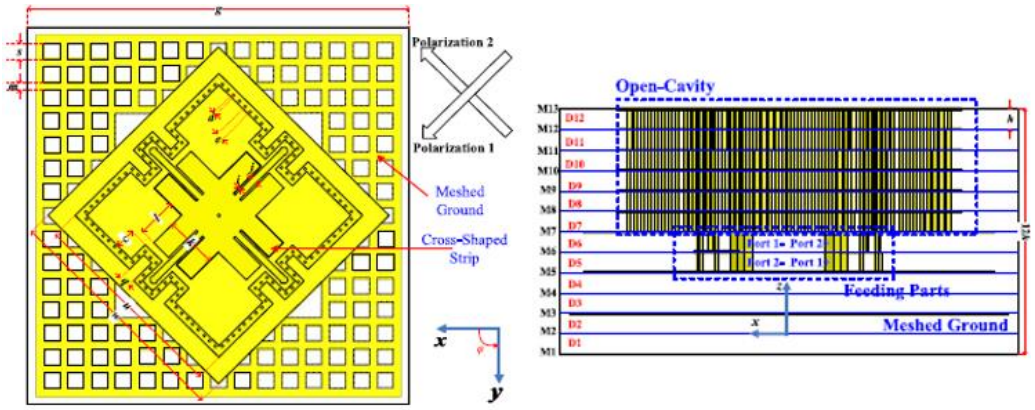

Figure 2.11: LTCC based dual linearly polarized antenna © 2017 IEEE

In [39], a dual linearly polarized low temperature cofired ceramics (LTCC) based planar aperture antenna for a 60 GHz CMOS differential transceiver chip is proposed. The impedance bandwidth of the antenna covers the entire 60 GHz ISM band, and the port isolation level is better than 26 dB across the band. Antenna-in-Package solutions such as the one proposed in this article started gaining research attention in the early 2000s because they can easily be integrated with other mm-Wave wireless systems. The antenna is made up of multiple thin layer stack-up of LTCC substrates with a cross-shaped strip, a meshed ground plane, and a metallic cavity extending through various layers in the stack-up as shown in figure 2.11.

A 4x4 slot coupled dual linearly polarized microstrip antenna array for mm-Wave RFID tag readers operating in the frequency range from 22 to 26.5 GHz is proposed in [40]. The antenna offers an impedance bandwidth of 18% with port isolation that is better than 35 dB across the band. The antenna structure and stack up are like that proposed by [41], where a balanced feed is used for each polarization on different substrate layers and a crossed slot in the ground plane for coupling.

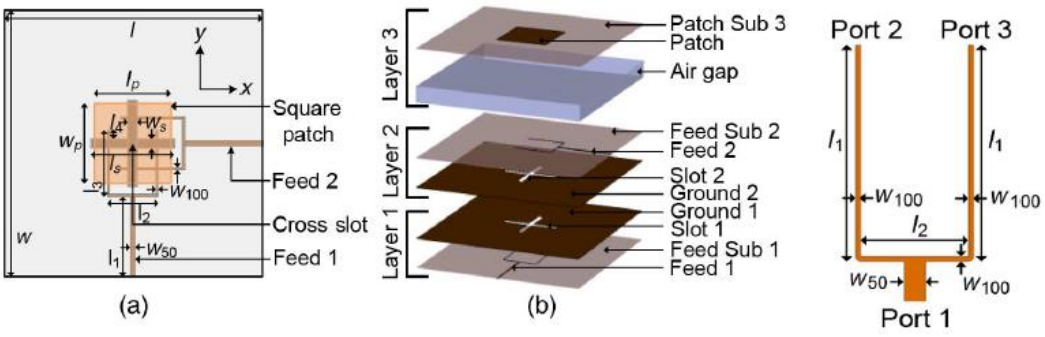

Figure 2.12: mm-Wave crossed slot patch antenna © 2015 IEEE

The use of the crossed slots does improve the port isolation at the expense of an additional substrate layer and the possibility of increased back radiation [42]. Even though the exact level of back radiation is not reported in the article, it is most likely close to 15 dB. This conclusion was reached because the design does not use a resonant slot, which further reduces the front to back ratio. If resonant slots were employed here, the impedance bandwidth would be close to 50%, with the back-radiation levels around 10 to 15 dB. A reflector patch can be added below the ground plane to increase the front to back ratio to acceptable levels. The proposed antenna structure is shown in figure 2.12. A foam airgap is used between substrate feed two and the patch antenna. A thick laminate layer is typically needed here to avoid direct coupling between the feed and the patch antenna since one of the feeds is above, and the other is below the ground plane. Another issue that could arise

is the compression of the foam layer if bond ply layers are used since heat and pressure are typically applied to glue the layers together. Applying pressure reduces air bubbles within the foam and increases its permittivity.

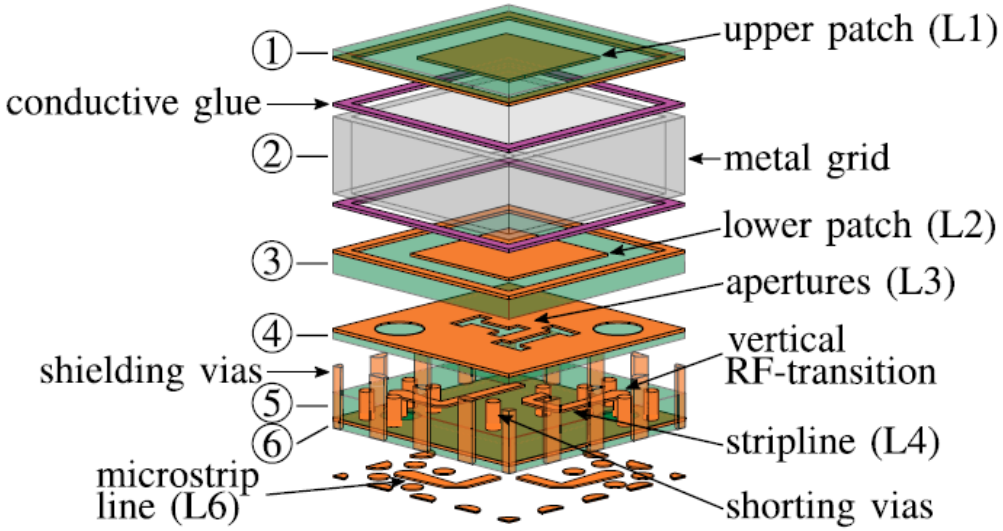

Figure 2.13: Cavity-backed mm-Wave dual linearly polarized patch antenna © 2016 IEEE

In [43], another dual linearly polarized microstrip antenna operating at Ka-band is presented. The antenna structure is similar to that proposed by Adrian and Schaubert in [22] and discussed earlier in this chapter. The antenna is designed for wide-angle scanning Satcom on the move applications (airplanes, trains, and ships) from 27.8 to 30.8 GHz, offering a scan performance up to ±60°. The antenna unit cell is made up of a multilayer design where two patch antennas, a metallic airgap and stripline and microstrip feed networks are used. The second resonator and the airgap below the radiating patch increase the operating bandwidth of the antenna, and the stripline and microstrip line feed network reduces the level of back radiation. The reason is that another metallic layer is added below the slots and only a small portion of the feed network is exposed at the back therefore reducing feedline spurious radiation. A wall of vias forming a cavity are also employed

around the antenna element to supress surface waves and reduce the levels of interelement coupling. An exploded view of the antenna element is shown in figure 2.13.

2.6 Cavity-backed Antennas

Cavity-backed antennas are known to offer excellent performance characteristics in comparison to traditional microstrip antennas [44] such as reducing back-lobe radiation and increasing the antenna radiation efficiency by suppressing surface and leaky-wave excitation [3]. Better scan performance and inter-element coupling in antenna arrays with thicker substrates are also achieved due to the suppression of leaky waves. Metallic walls were employed in [45] between elements of a slot array antenna to reduce inter-element coupling due to parallel plate waveguide modes. Microstrip antennas built on a thicker substrate typically suffer from low radiation efficiency and the appearance of grating lobes even at scan angles close to broadside, because of surface and leaky waves. Guided waves in a microstrip antenna substrate can be minimized similarly, by using a metallic cavity that surrounds antenna elements. This leads to larger scan angles in microstrip antennas with thick substrates due to the suppression of leaky-wave resonances [46]. In [47], the probe-fed microstrip antenna with a metallic cavity backing shown in figure 2.14 was proposed to achieve broadband antenna performance. Techniques to compensate for the reactive nature of the feeding probe were also investigated and analyzed. The proposed antenna layout was made of two layers, a thick foam layer with a dielectric constant close to that of air to prevent the excitation of surface wave while increasing the antenna bandwidth, and a thin PTFE layer for the realization of the parasitic patch. Antenna bandwidth of around 35% for VSWR $\leq$ 2 and good scan performance because of the metallic cavity were achieved. A microstrip antenna using SIW technology with similar

scan performance was proposed in [48] as an alternative low-cost solution to the machining of metallic cavities. Another is the design proposed in [49] for x-pol suppression.

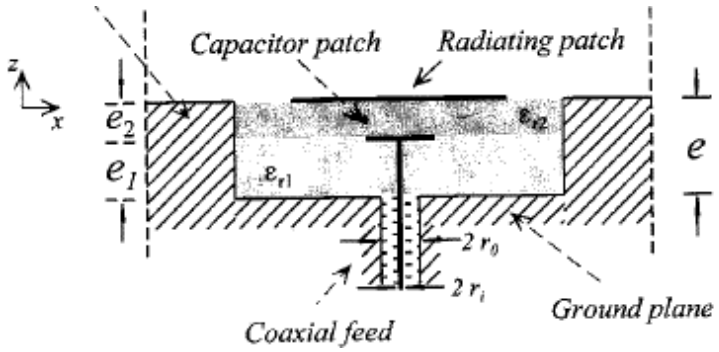

Figure 2.14: Probe-fed cavity-backed antenna © 2000 IEEE

Chapter 3

Antenna Design

In the previous chapter, various techniques for bandwidth and isolation enhancement of dual linearly polarized microstrip antennas were discussed. Multi resonator antennas were deemed to be the most promising in terms of bandwidth enhancement. Other feeding techniques such as L-probe feeds were able to produce a broad bandwidth with high levels of port isolation. However, their application was limited to lower frequencies because of their manufacturing complexity.

In this chapter, three planar antenna designs are proposed, which operate in the sub-millimeter wave frequency range around 28 GHz for the next generation of mobile communications, 5G. Each of the antenna type uses a different substrate for layer 2. The first uses an RT/Duroid 5880 laminate, which is used for all antenna layers. The second uses a low permittivity foam (Rohacell 31 IG/A ε_r = 1.05), and the third is a 3D printed airgap made from polylactic acid (PLA). In each design, a substrate integrated waveguide (SIW) cavity-backing was simulated, except for the case of the PLA. A stacked patch antenna without a cavity or a shorting post was also simulated as a baseline for isolation and radiation pattern comparison. Each of the three proposed dual linearly polarized antennas can achieve an impedance bandwidth above 30% and port isolation better than 30 dB.

3.1 Antenna Design I

The design proposed here is a SIW cavity-backed patch antenna operating in the submillimeter-wave range around 28 GHz. Metallic posts connecting the ground plane to the top surface of the antenna are used to form a cavity. SIW cavity-backed antennas have similar characteristics and are easier to manufacture in comparison to conventional cavity-backed antennas since they can be realized using traditional PCB manufacturing techniques [48], [50], [51]. Other SIW design equations such as post diameter and spacing can be found in [52], [53].

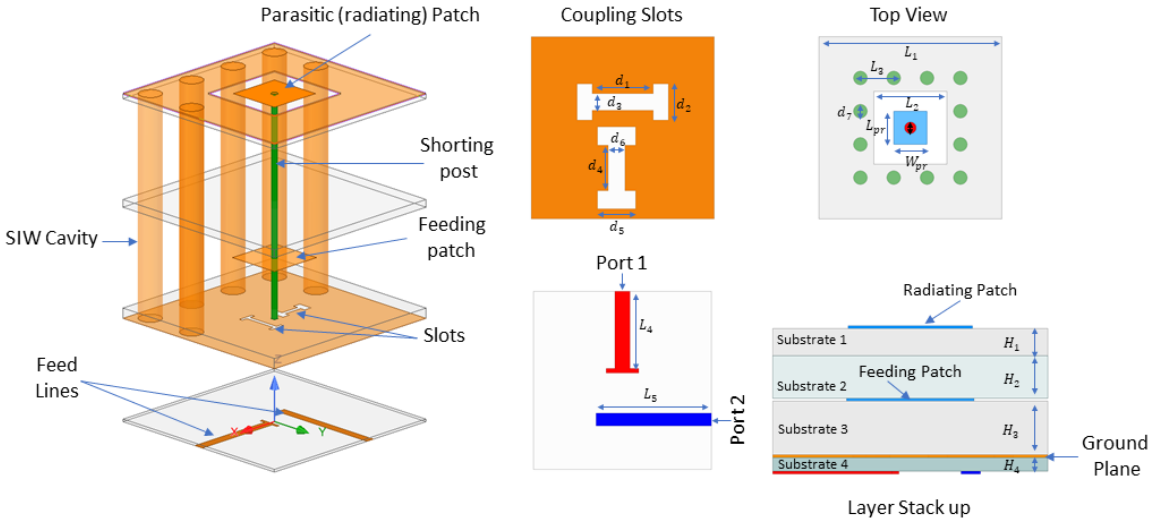

Figure 3.1: Proposed antenna stack up

Figure 3.1 shows the geometry of the proposed slot coupled microstrip patch antenna, and table 3-1 shows the antenna dimensions. Lpar, Wpar, Lp, Wp, T1, and T2, are the length and width of the parasitic patch (radiating patch), the length and width of the main (feeding) patch, and the feedline widths for port one and port two, respectively. The proposed design is to be manufactured on a four-layer Rogers RT/Duroid 5880 substrate with a relative permittivity of 2.2. Microstrip line feeds for both the vertical and horizontal polarizations are etched on the bottom of substrate 4. The ground plane with two coupling slots and the

feeding patch is etched on the bottom and top of substrate 3, respectively. The radiating patch (parasitic patch) can be etched on the top or bottom (this is referred to as the inverted configuration) of substrate 1, and it is separated from the feeding patch by a gap. This gap can be realized using an air gap if 3D printed spacers, posts, or a foam substrate is used. Each patch antenna introduces a resonance, as shown in figure 3.2, by the peaks in the real part of the input impedance.

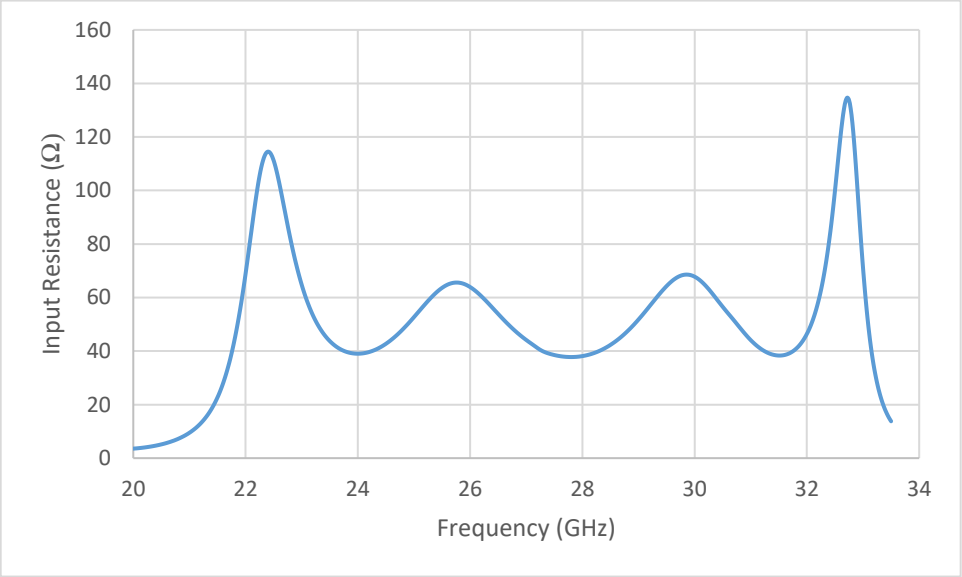

Figure 3.2: Real part of the input impedance

The structure can then be optimized for the slot to antenna coupling and good matching in the desired frequency range. Designs with spacers or foam tend to yield a higher impedance bandwidth. However, they have a slightly larger thickness, and they are more challenging to manufacture, not because of the difficulty in 3D printing spacers but because of alignment issues that can deteriorate the antenna performance. Using foam raises another problem since the bonding process used to glue multi-layer PCB structures together can compress the foam and push out air bubbles in it increasing its permittivity and reducing thickness. The only way to remedy this might be to use aircraft-grade rigid foam that can

handle the heat and pressure applied during the bonding process (LAST-A-FOAM RF-2200 made by General Plastics Manufacturing Company) [54]. Many S and C band antennas have been reported employing foam airgaps because the antenna sizes are relatively large (30 mm or more in comparison to 3 to 5 mm at 28 GHz). At these frequencies, antennas are less sensitive to small misalignments, making it easier to glue the layers together or, in some cases, even apply a thin double-sided tape to hold them together. As a result of these issues, a Duroid 5880 substrate is used here instead of an air gap, allowing for easy manufacturing of metallic posts, and ensuring that most PCB manufacturers can prototype them. The tradeoff associated with this is typically a reduction in the bandwidth of the antenna. Simulations show that, with proper optimization of the design, the reduction in bandwidth is less than 5%.

Table 3-1: Antenna parameters

Parameter	***Dimension (mm)***	***Parameter***	***Dimension (mm)***
L_1	25	H_1	0.254
L_2	7	H_2	0.381
L_3	2.73	H_3	0.508
L_4	12.1	H_4	0.127
L_5	13.4	D_1	1.73
L_{par}	2.71	D_2	0.81
W_{par}	2.71	D_3	0.22
L_p	2.78	D_4	1.02
W_p	2.78	D_5	0.75
T_1	0.42	D_6	0.22
T_2	0.51	D_7	1.1

3.1.1 Design Features

The simulation results of the optimized ANSYS HFSS antenna are shown in figure 3.3. The antenna has an impedance bandwidth of 34.2% and an isolation better than 34 dB over the band, where the port isolation is better than 40 dB over most of the band.

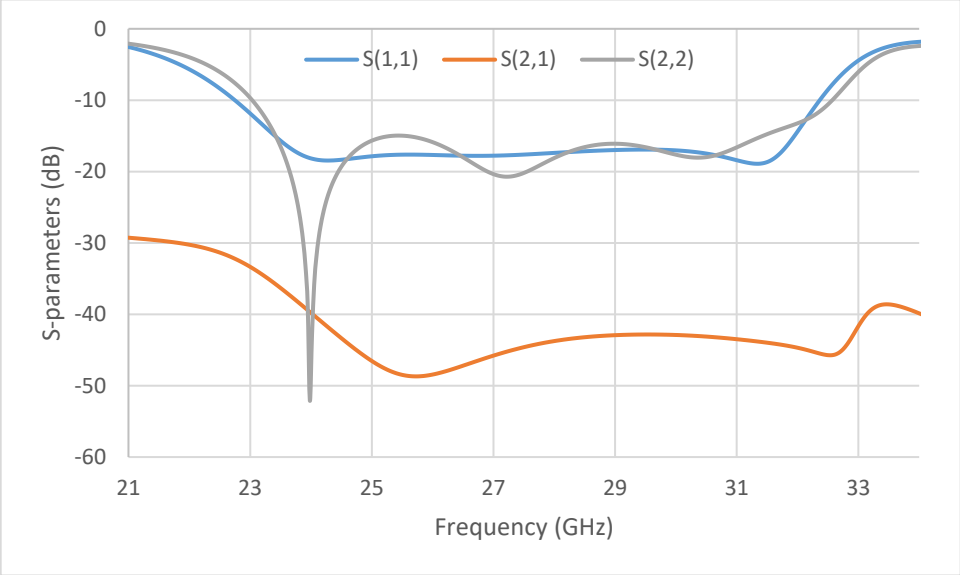

Figure 3.3: Optimized antenna S-parameters

It is important to understand that achieving a good level of port isolation over such a large bandwidth is a cumbersome task. Here, a shorting post is added at the center between the ground plane and the radiating patch, as shown in figure 3.1. This shorting post improves the port isolation of the antenna (|S21|) by 5 to 10 dB's across the entire band. Since this is the zero-voltage point of the patch antenna, other antenna parameters, such as efficiency and bandwidth, were not affected. Only a small drop in the antenna gain of 0.2 dB was noticed in the simulated results. This shorting post excites a current in the non-radiating slots of the patch antenna, therefore reducing the level of coupling between port 1 and port 2. The via diameter is varied to achieve the optimal values of S_{21}, as shown in the parametric study section. The magnitude of the electric field on the ground plane before

and after adding the shorting post when port one is excited is shown in figure 3.4 (a) and (b), respectively. This figure illustrates the reduction in the coupling between the two ports. The field reduction is evident, especially near the port excitations. Both simulations were generated using Ansys HFSS at the center frequency of the design (around 28 GHz).

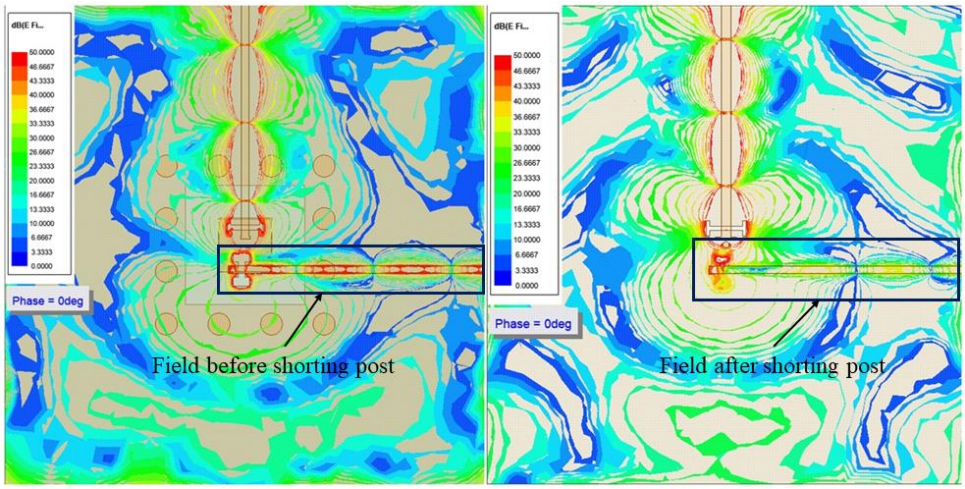

(a) (b)

Figure 3.4: Magnitude of the electric field on the feed substrate

As can be seen from the simulation results in figure 3.5, this technique yields better than 10 dB isolation improvement across the entire frequency band. Shorting posts have been utilized to improve other characteristics of microstrip antennas such as frequency agility and polarization diversity since the late 1980s [55], and this is another application of how they can be used to improve other antenna characteristics.

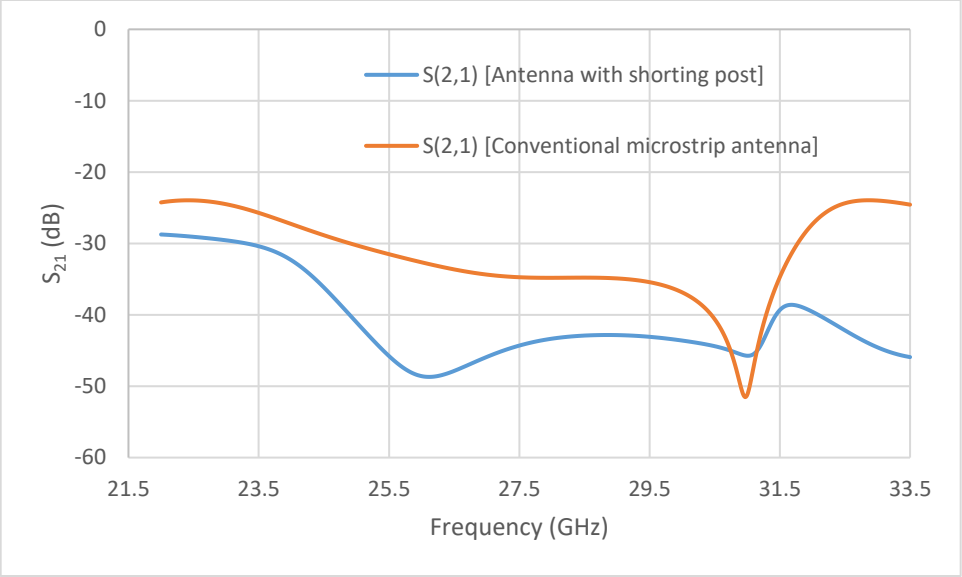

Figure 3.5: Improvements in the antenna port isolation by using a shorting post

3.1.2 Design Parameters

This section outlines important design considerations based on the design guidelines proposed for slot-coupled patch antennas [5], [56], [57]. The effect of the essential parameters on the antenna performance is studied. These are the antenna airgap, the patch dimensions, the antenna laminate thicknesses, and the slot lengths. Besides, the SIW cavity dimensions and its relation to the antenna gain and S-parameters are also studied. The reader can refer to appendix A for a detailed description of the substrate selection methodology along with other crucial antenna parameters such as antenna and slot dimensions. These are of course not exact equations but rather a good starting point for the simulations. Once the initial design is simulated the designer can then change the antenna parameters (these are the antenna substrate heights and slot and patch antenna dimensions) to achieve the desired results (bandwidth, isolation, gain, and front to back ratio) for that specific application.

Slot coupled patch antennas have many degrees of freedom in comparison to antennas fed using other excitation techniques. Giving the designer the freedom to control which parameter they vary. For example, if a high front to back ratio is desired for an antenna built on a thick substrate, the width of the patch can be decreased instead of increasing the slot length to achieve a good match, at the expense of a slight reduction in the impedance bandwidth.

The appropriate substrate thickness depends on the application and the desired percent bandwidth along with radiation efficiency, gain, and back radiation levels. Using thicker antenna substrates and modifying other antenna parameters, a larger impedance bandwidth can be achieved. Low dielectric constant laminates are usually employed for the antenna substrate since they offer the best achievable impedance bandwidth, radiation efficiency, and scan angle performance in phased array applications. Assuming that the feed substrate is kept constant, four parameters are used to obtain optimal matching, namely patch width and length, the antenna substrates, open-circuited stub, and the slot length.

Like antennas excited using other techniques, the patch length controls the resonant frequency of the antenna. The width of the patch also affects the percent achievable bandwidth, as seen in other types of patch antennas. Any portion of the feedline extending beyond the slots is considered a stub that can be used to tune the imaginary part of the input impedance leading to better matching.

H or dog-bone shaped slots have proven to offer better coupling between the slot and the antenna and lower back lobe radiation in comparison to their counterpart, the rectangular slot, as mentioned in the previous chapter. For these reasons, they are employed in all designs throughout this chapter. The level of coupling between the antenna and the slot

resonance can be controlled using the slot length. Increasing the slot length increases the level of coupling and vice versa, where longer slots are typically needed for antennas mounted on thicker substrates. Here the level of back radiation must be monitored when varying the slot length as there is a tradeoff between the two parameters. A slot length equal to roughly half that of the patch is a good starting point while monitoring the coupling loop on the smith chart and the level of back radiation when increasing this parameter. If the impedance response is confined to the edge of the smith chart, it would be difficult to obtain a good match because of the high input impedance of the antenna. The best level of impedance matching can be achieved by varying the slot length to get the closest match to the desired input resistance value.

3.1.3 Parametric Study

The data presented in this section is shown in the form of S-parameters plots, input resistance plots, and input impedance smith chart plots. Input resistance plots show the antenna impedance matching, while the smith chart plots are used to show the level of coupling between the slots and the antennas. Figure 3.6 shows a loop near the center of the smith chart, which implies that the antenna is coupling to the slot resonance. When the patch ratio increases in comparison to slot size, the circle deviates from the chart center, indicating a reduction in the coupling. Similarly, the coupling decreases if the slot length is reduced. The level of antenna coupling can be described as critically coupled when the input impedance is well matched to 50 **Ω**, under coupled when less than 50 **Ω**, and over coupled when the input impedance is larger than 50 **Ω**.

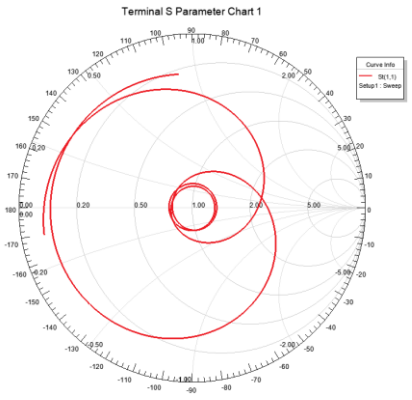

Figure 3.6: Impedance loop of a coupled antenna and slot

Whenever the loop disappears, or deviates off the center the smith chart, this is considered a decrease in the slot to patch coupling. Varying the slot length and observing the changes in the antenna input impedance and coupling level, the optimum slot length can be determined. Similarly, other critical antenna parameters, such as substrate thickness and patch dimensions, can be determined.

The effect of varying the dimensions of the feeding and radiating patch antennas are studied next. The S-parameter results in figure 3.7 show the impact of the patch size on the matching, where the yellow curve is for the nominal value of 2.71 mm. As the length of the patch increases, the matching starts to deteriorate, and we only see the effect of the lower resonance (2.9mm). A change of 5% or less tends to produce acceptable results (S_{11} $\geq$ 10 dB), keeping in mind, of course, that this is still a minimal change between 1 to 4 mils.

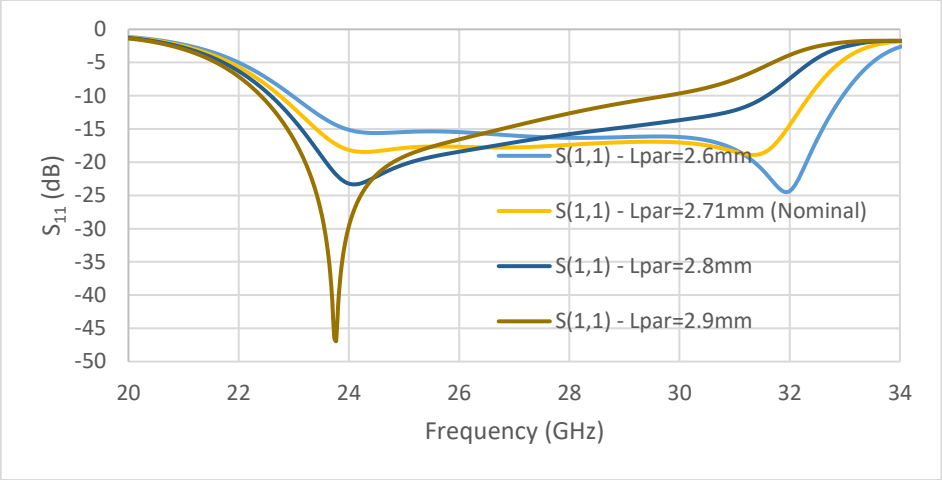

Figure 3.7: Antenna return loss for different radiating patch lengths

When the length of the feeding patch is varied, somewhat similar results to those seen for the case of the radiating patch are observed. Figure 3.8 shows the effect of these changes for a nominal patch length of 2.78 mm. As the length of the primary patch decreases, only the resonance of the radiating patch appears. This scenario can be seen for the case of L_p=2.65mm, for example, from the single dip in S_{11} around 26 GHz. Like the radiating patch, this antenna is also somewhat tolerant of small dimensions variations due to the fabrication process.

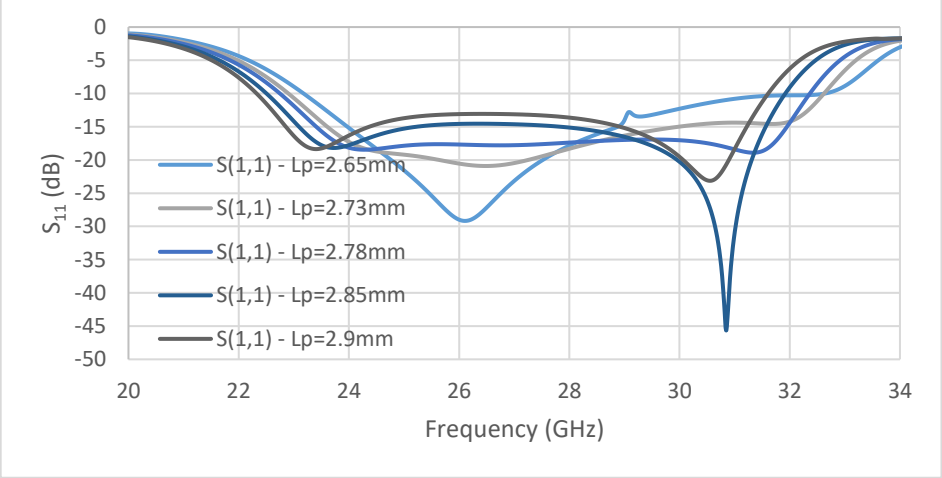

Figure 3.8: Antenna return loss for different feeding patch lengths

Figure 3.9 presents the real part of the input impedance for port 1 for various patch lengths. The resistance starts increasing around 30 GHz, explaining the mismatch that occurred in the S-parameter plot. An increase in the lower resonance input resistance is seen for shorter patch lengths while at longer patch lengths for the upper resonance. If the size of the feeding patch were further reduced, only the response from the upper patch would be seen. This single peak tells that the dimension of these antennas affects both the upper and lower resonance behaviors.

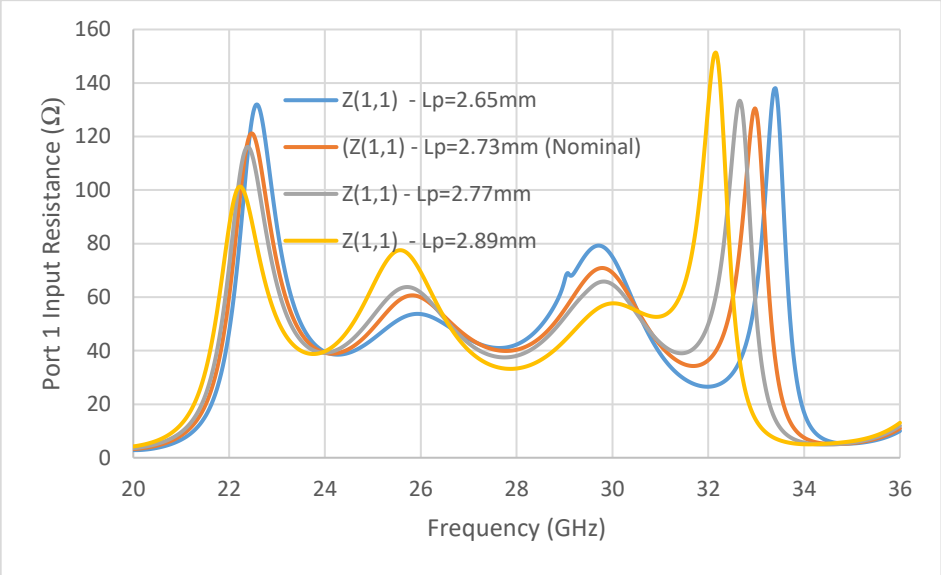

Figure 3.9: Port 1 input resistance for different feeding patch lengths

The real part of the input impedance for port one is shown here again in figure 3.10, where the length of the radiating patch is varied, and for a nominal patch length of 2.71 mm. As Lpar is decreased, the upper resonance around 32 GHz starts to disappear to the extent where the effect of the lower patch dominates. On the other hand, increasing the radiating patch dimension, the upper resonance resistance becomes very high, and another smaller resonance around 29 GHz starts to appear.

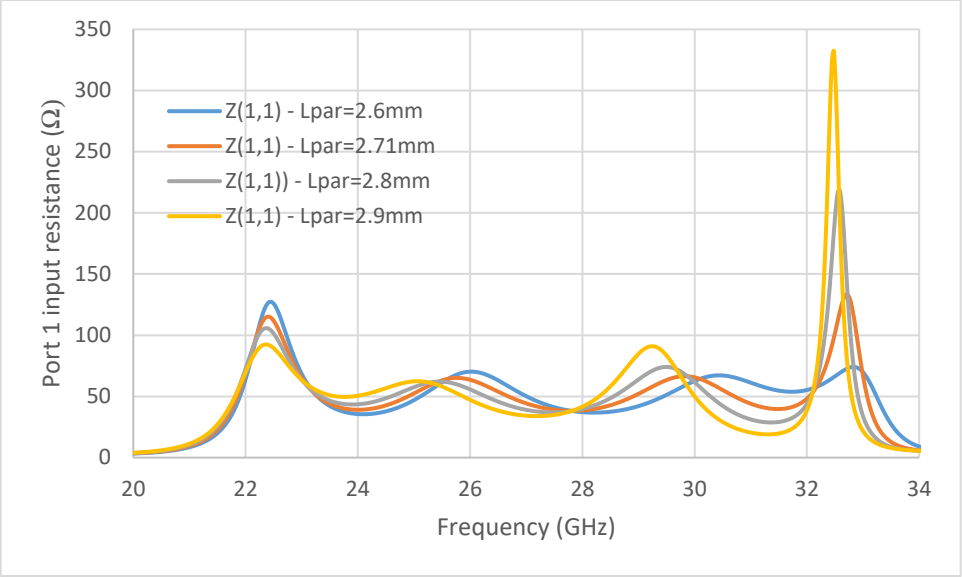

Figure 3.10: Port 1 input resistance for different radiating patch lengths

The coupling can explain this behavior seen when the patch dimensions decrease beyond a certain point to the fringing fields of each of the patches. For example, when the size of the radiating patch becomes very small in comparison to the feeding patch, it no longer couples to its fringing fields and vice versa [57].

Next, the substrate thickness of both patch laminates is varied for several commercially available RT/Duroid 5880 substrate thicknesses. Figure 3.11 shows the results of this parametric for the primary antenna substrate. The matching becomes gradually worse as the substrate thickness deviates from the nominal value of 0.508 mm. It can also be seen that the bandwidth is getting narrower for antennas on thinner substrates as expected. Looking at both the smith chart and input resistance plots gives us more insight into the coupling behavior, where we can see a degraded level of coupling as h_2 is increased.

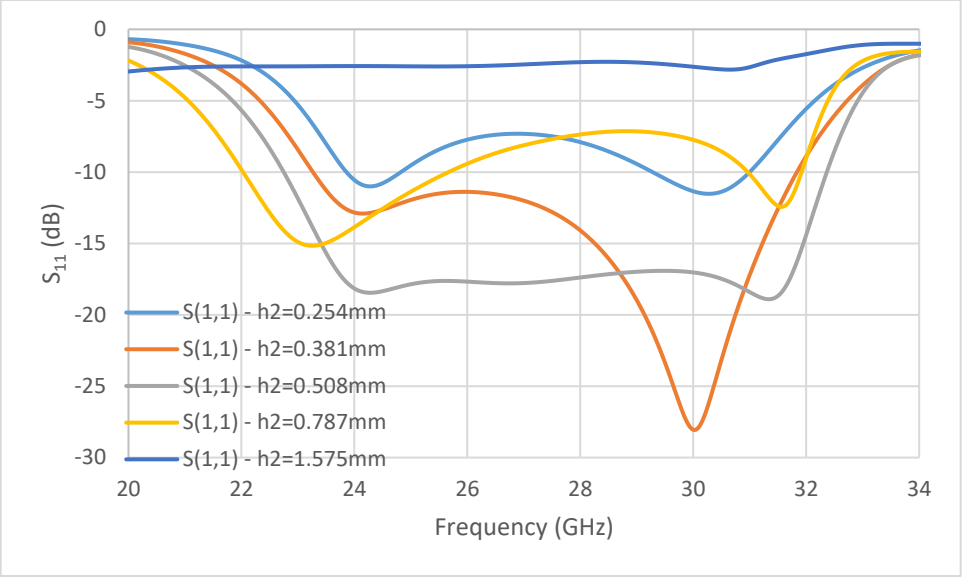

Figure 3.11: Antenna return loss for different feed antenna substrate thickness

The effect of the radiating patch substrate on the antenna matching is shown in figure 3.12, for a nominal thickness of 0.381 mm. Observing the changes in the S-parameter plot, it is apparent that for lower values of h_3, only one resonance dominates. This single resonance is seen from the S_{11} result for a thickness of 0.127 mm. From the slot point of view, only one patch antenna is seen, the top patch in this case. Similar behavior can be seen for thicker substrates. For example, when the substrate thickness is set to 0.508 mm, only the lower patch is seen, and the impedance matching gets worse at higher frequencies around 30 GHz. This behavior can be attributed to the weak coupling between the slot and the radiating patch.

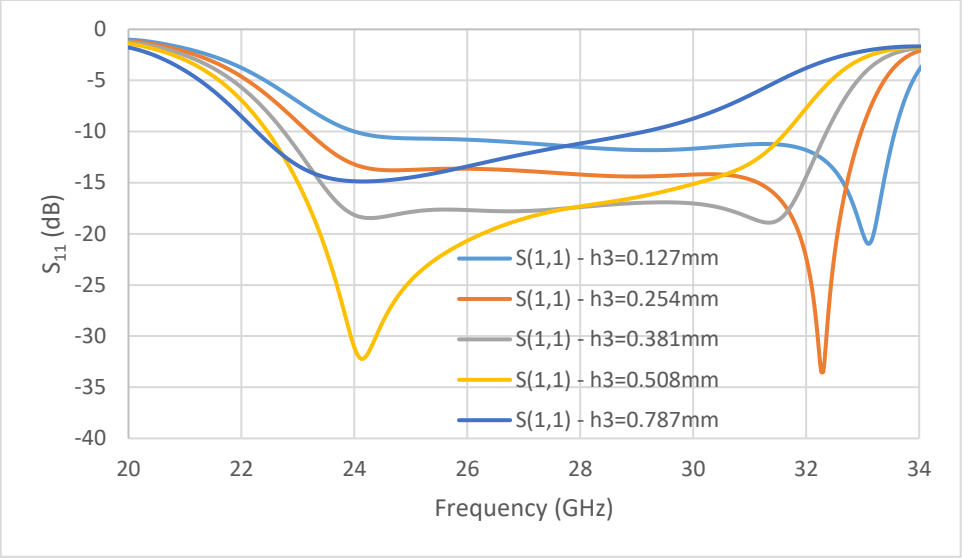

Figure 3.12: Antenna input impedance for different h3 values

The influence of the slot length variation on the impedance matching is plotted in figure 3.13. Here the best match was achieved for a slot length of 1.73 mm. In this design, where two patch antennas are employed, the slot length influences the resonance frequency of the antenna, unlike the single patch antenna configuration, where the dimensions of the patch antenna mainly control the resonance frequency.

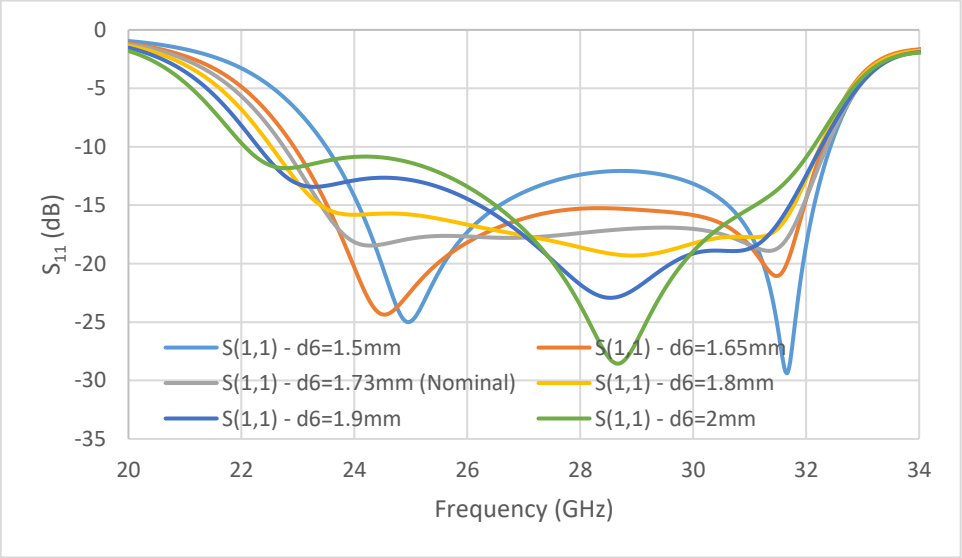

Figure 3.13: Antenna return loss for different slot lengths

From the S-parameter results, it can also be seen that the antenna is matched (≥ 10 dB) for a range of slot length, implying that the antenna performance should not be degraded too much with PCB fabrication tolerances. A slot length of 1.73 mm yields the best results here, and it was the value chosen for the manufactured prototype. The slot effect on the resonance frequency also implies that the three resonators, the slot length, and the two patch antennas interact together and that there is a mutual coupling between them. This coupling allows for acceptable design tradeoffs between them that the antenna designer can use to design the best antenna for a given application. Figure 3.14 shows the changes in the input impedance for port one as a function of the slot length. This parameter, in addition to the width of the microstrip feed line, can be used to achieve the best impedance matching results for the antenna being designed. For example, if low levels of back radiation are required, the designer can reduce the slot length by reducing the thickness of the feeding patch substrate. This reduction in slot length will, however, increase the quality factor of the antenna, and hence reduce the percent impedance bandwidth.

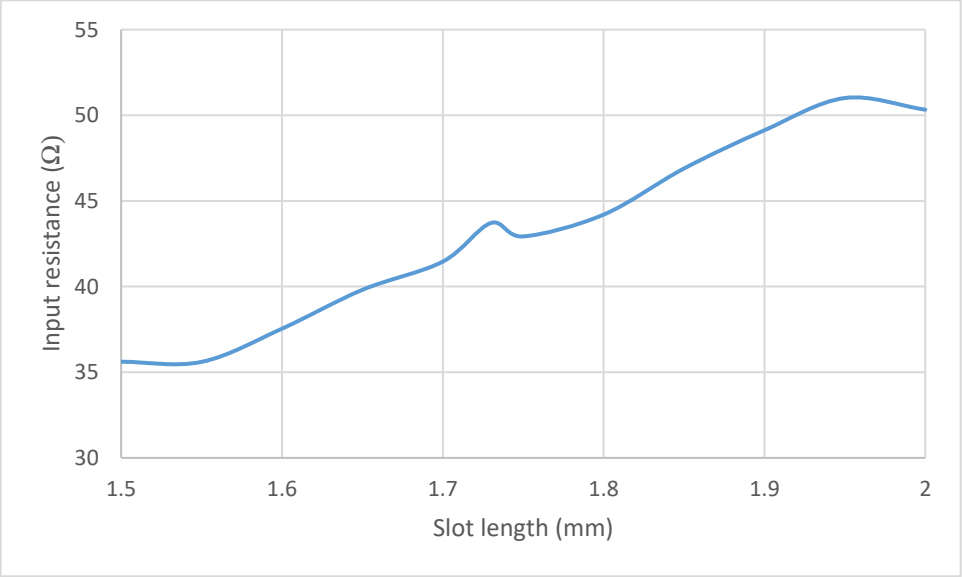

Figure 3.14: Input resistance for different slot lengths

The parametric study outlined in this section can be used as a guideline to design broadband microstrip antennas. Given the fact that the design being proposed here employs a SIW cavity surrounding the antenna for enhanced array performance and a shorting post for isolation enhancement, their influence on the matching and performance of the antenna must be considered. Figure 3.15 shows S_{11} results for a range of cavity dimensions. As we can see, changes in the cavity dimension barely influence the antenna matching ($S_{11} \geq 10$ dB). The effect of this parameter, as shown in figure 3.16 on the port isolation $S_{21,}$ however, are more pronounced and must be kept in mind when designing the antenna. From the plot, we can see the level of isolation getting worse near the upper edge of the band. Using the dimension of the SIW cavity, this can be pushed further away to a higher frequency outside of the band of interest by increasing the cavity dimension. This increase, however, is limited by the inter-element spacing in array applications, where it is desired to keep the distance around $\lambda_0/2$ to avoid grating lobes.

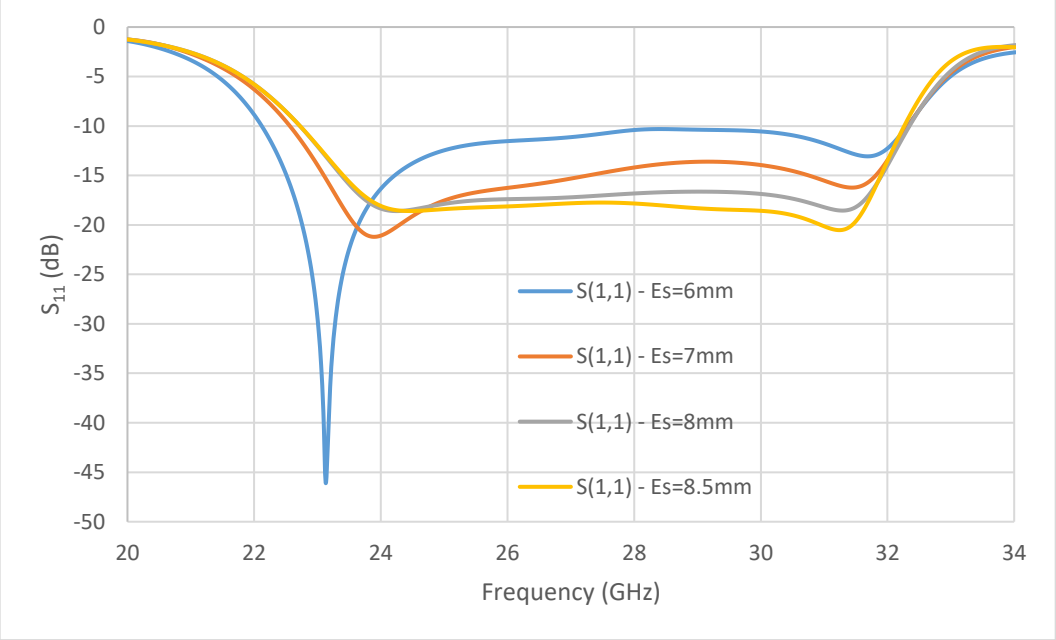

Figure 3.15: SIW cavity dimension effect on antenna return loss

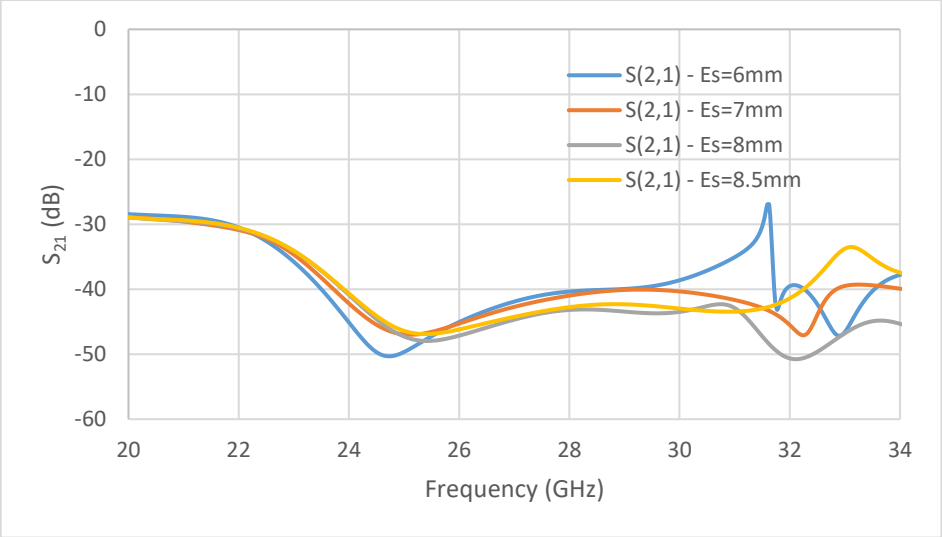

Figure 3.16: Effect of SIW cavity dimensions on input port isolation

A via extending from the ground plane to the radiating patch center is shown to improve the port isolation. Vias with smaller diameters led to a better port isolation level, as shown in figure 3.17. The shorting post diameter, however, is limited by the manufacturing capability. PCB manufacturers have recommendations on the aspect ratio of drills based on the antenna thickness and number of layers.

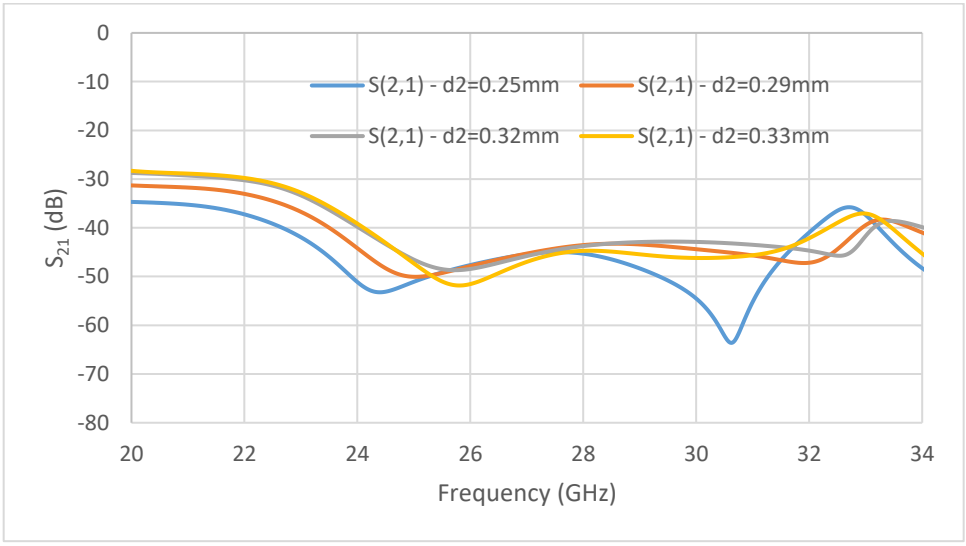

Figure 3.17: Port isolation for different shorting post diameter

3.1.4 Sensitivity Analysis

The effects of small airgaps and dimension changes due to the manufacturing process and laminate properties could be more pronounced at mm-Wave frequencies in comparison to similar antennas designs at lower frequencies. Therefore, they must be considered when designing aperture coupled antennas at these frequencies. Figure 3.18 shows the changes in S_{11} as the feeding patch antenna is offset in the x-direction from – 0.4 mm to + 0.4 mm about the antenna center. A good match ($S_{11} \geq 10$ dB) is achievable for a patch misalignment of less than ± 0.3 mm. Comparison of this result to similar designs at S-band from [56] where misalignments in the range of 0.5 to 1 cm can still yield acceptable results, shows how well the layers must be aligned to produce a successful prototype. S_{22} results are also similar.

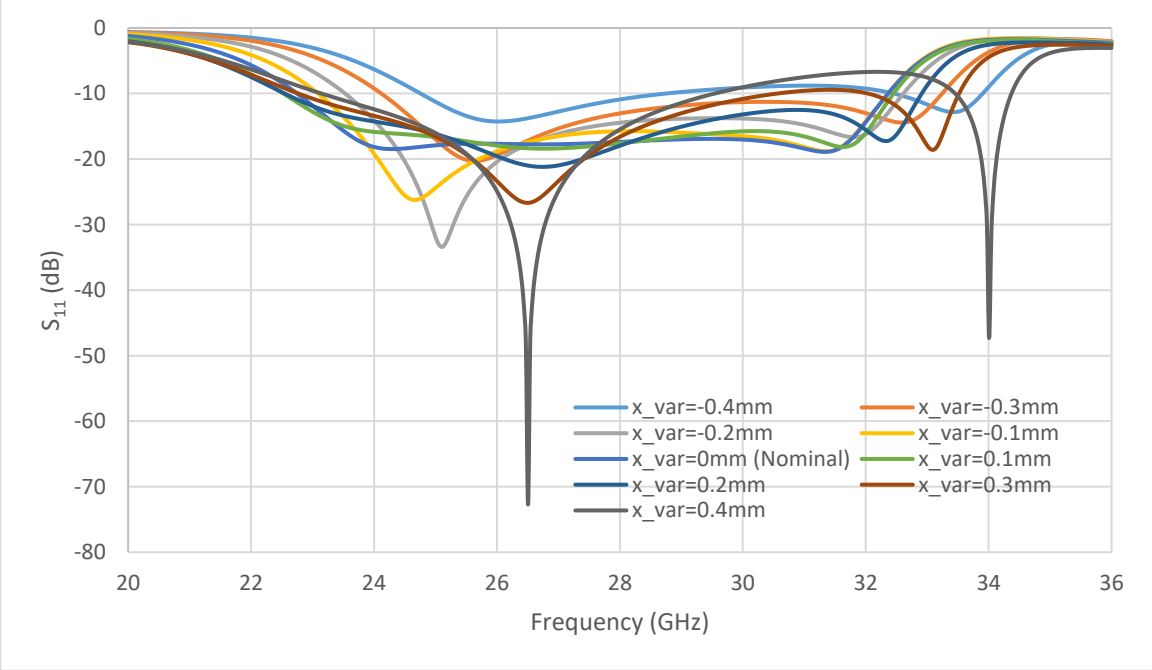

Figure 3.18: Antenna return loss for patch variation in the x-direction

Slot coupled antennas achieve the best level of coupling when the slots are centered about the patch. As the slot moves closer to the edge, resonant loops move from the center

towards the short circuit point of the smith chart on the inductive side, indicating deterioration of the matching [56].

The changes in S_{11} due to the slot movement in the y-direction is almost negligible, as shown in figure 3.19. $S_{22,}$ however, becomes mismatched for offsets larger than ± 0.3 mm. P. L. Sullivan studied the effect of patch misalignment at S-band for a linearly polarized slot coupled microstrip antenna [56]. His studies concluded that movement of the slot in the x-direction caused little change in coupling and impedance matching, given that the entire slot remains underneath the patch.

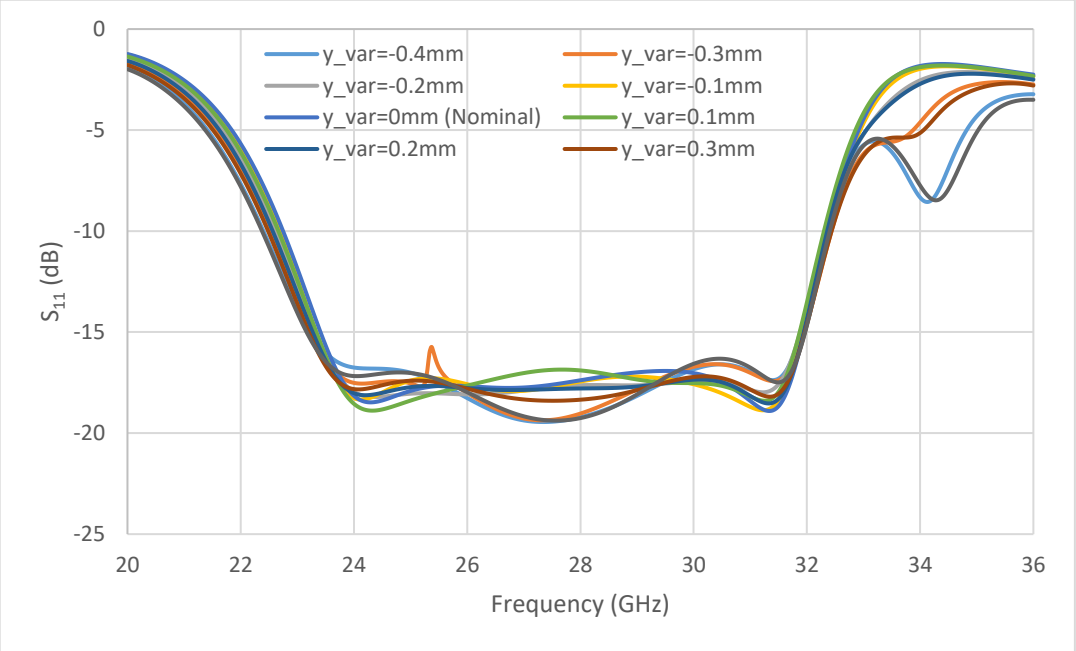

Figure 3.19: Antenna return loss variation for patch variation in the y-direction

In contrast, offset in the radiating patch alignment causes little change in impedance matching, as can be seen from figures 3.20 and 3.21 for S_{11} when the patch is moved in the x and y-direction, respectively.

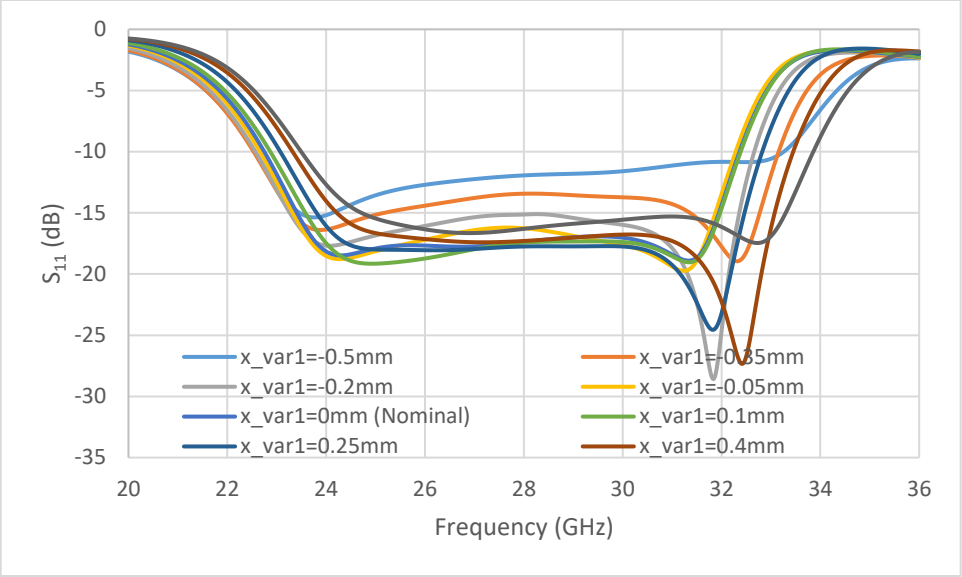

Figure 3.20: Antenna return loss for radiating patch in the x-direction

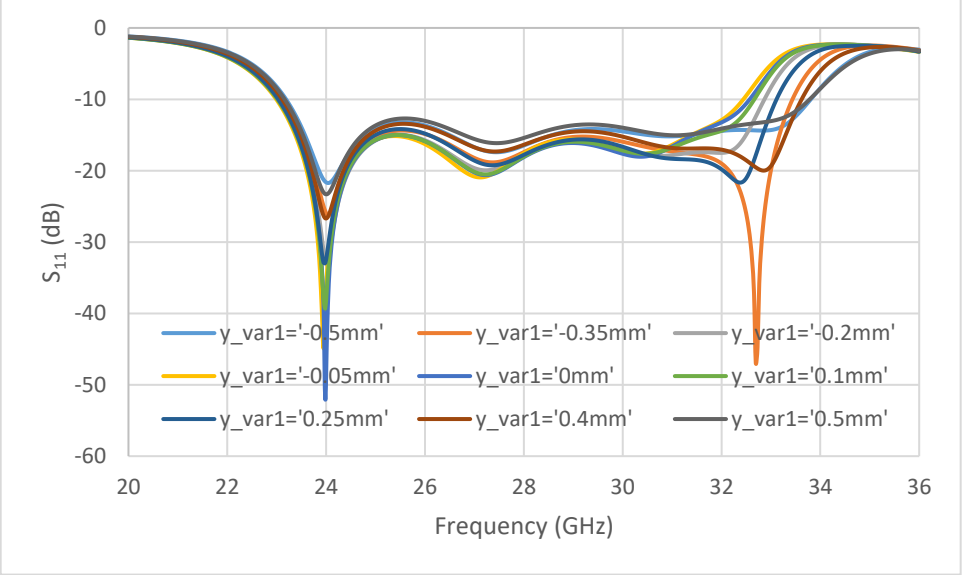

Figure 3.21: Radiating patch offset in the y-direction on return loss

A thin 127 µm Duroid 5880 substrate layer was chosen for the realization of the feed network. If the feed substrate thickness is increased, much beyond 150 µm, it will have detrimental effects on the impedance matching, as shown in figure 3.22. Even though the figure only shows S_{22} plots, the same holds for S_{11}. These results do not account for the changes in the microstrip line width with the variation of the substrate thickness. Once the

microstrip line width has been adjusted, a good match (VSWR ≥ 2) can be achieved for a laminate thickness of 0.254 mm. Going beyond that would require slot length and stub variation to account for the coupling changes.

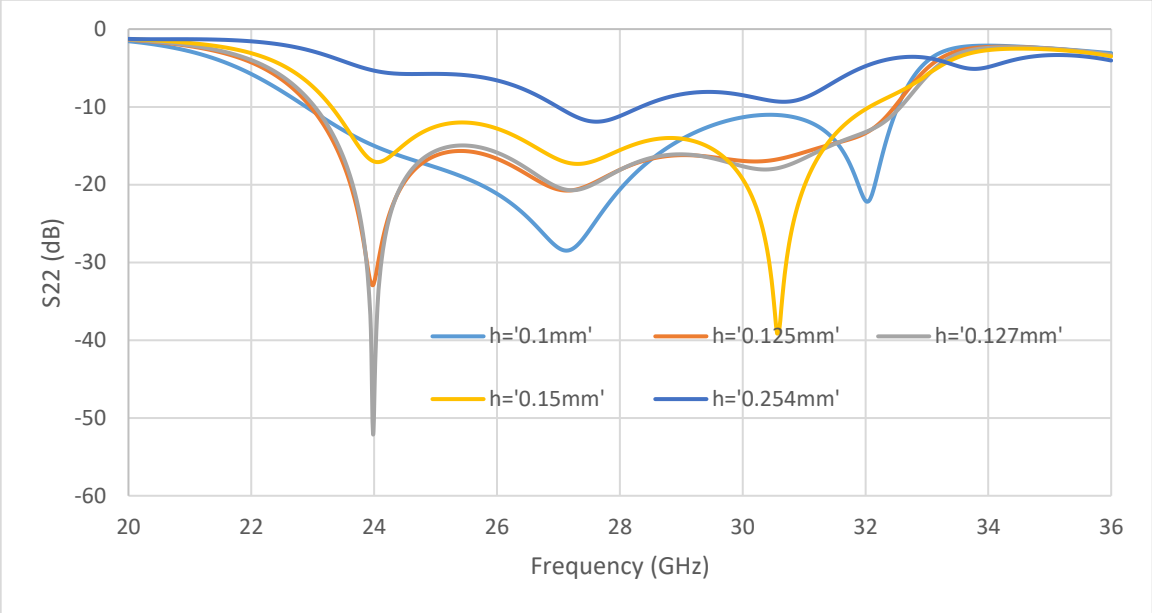

Figure 3.22: Antenna return loss for different feed laminate height

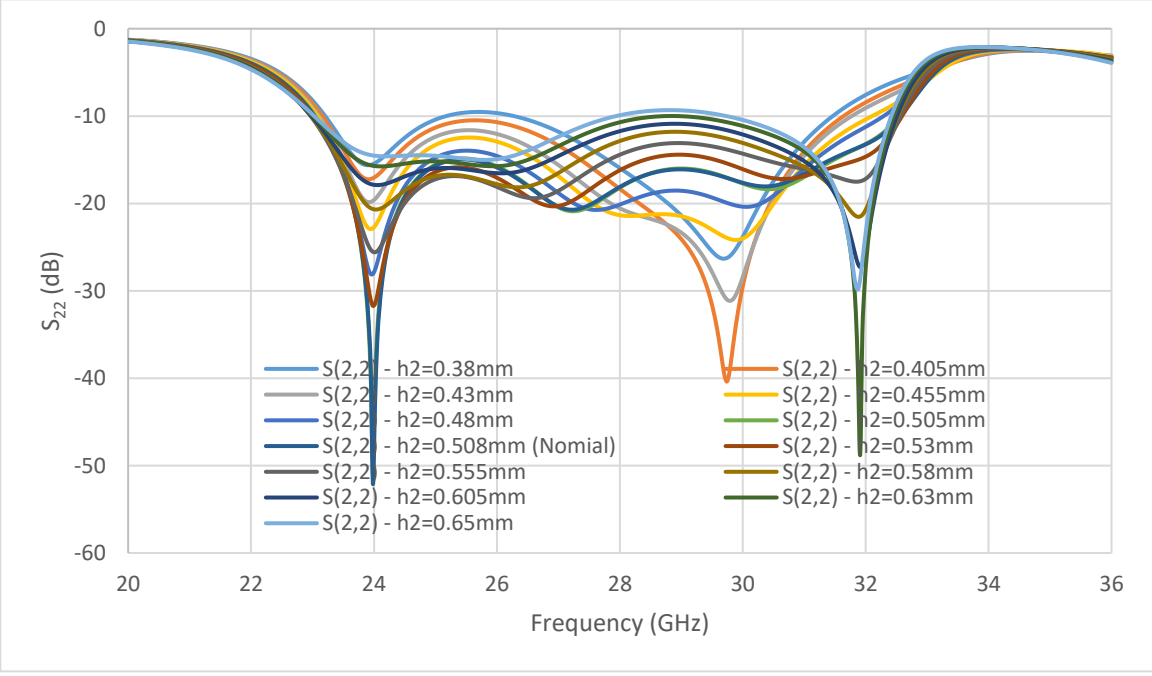

Figure 3.23: Antenna return loss for different feed antenna substrate heights

Small variations in the feeding antenna substrate thickness do not have much of an effect on the impedance matching ($S_{22} \geq 10$ dB is considered acceptable), as shown in figure 3.23 for S_{22}. Changes in the profile of the other substrates also have similar effects, where good matching can still be achieved for small variations in the laminate thickness. The level coupling degrades as the antenna substrate thickness increases and can be compensated for by increasing the slot length, which in turn increases the level of back radiation. This increase explains the scenario of the cross-coupled DP antenna mentioned earlier and why a reflector is needed to attain acceptable levels of back radiation. Levels of back radiation are worsened by increasing the slot dimensions and the use of a thicker substrate, which is employed to increase the antenna bandwidth. Increasing the ground plane thickness also has similar effects on the back radiation, with a severe deterioration in performance when its thickness is increased beyond 0.1 λ_0 [58].

This design is also tolerant of changes in the dielectric constant of the antenna substrates. The antenna results were evaluated for a ± 0.2 difference in the dielectric constant without much degradation in the antenna matching and port isolation. Figure 3.24 and 3.25 show the single element S-parameters for feeding antenna (h_3) and gap (h_2) substrates, respectively. Where dielectric constant of 2, 2.2 (nominal), and 2.4 are evaluated. The S-parameter results tell us that the design can withstand more than 9% change in the substrate dielectric constant without much degradation to the antenna impedance matching and port isolations. Similar results were also seen when the radiating patch dielectric constant was changed. The gain and cross-polarizations levels in both E and H planes were also not affected by these changes in the laminate dielectric constant.

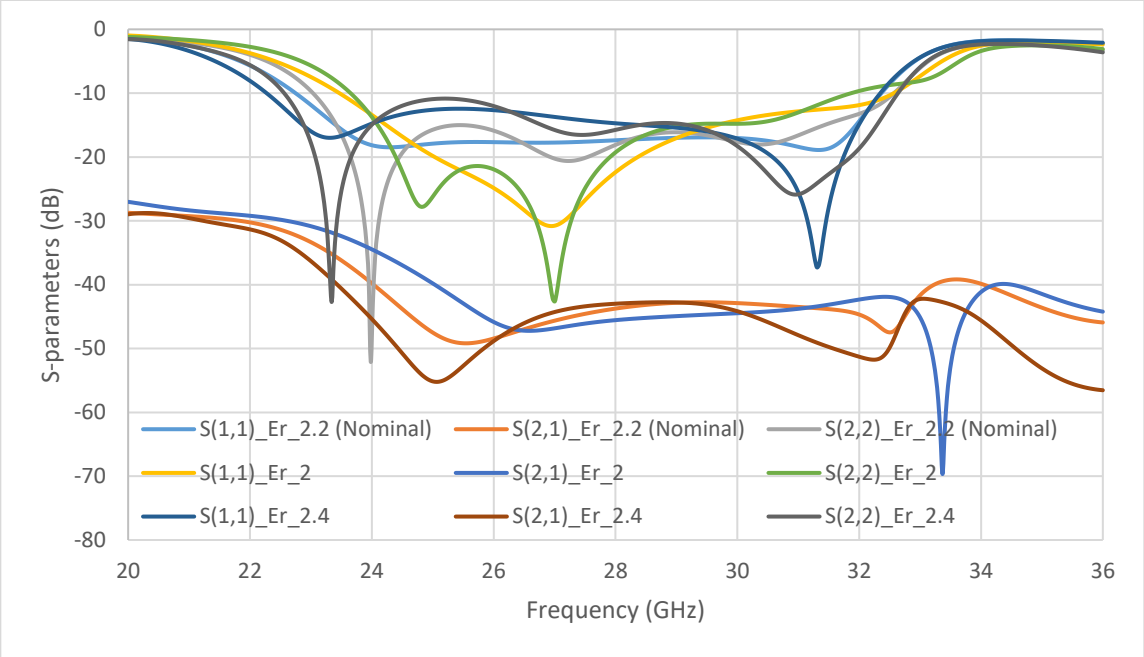

Figure 3.24: Relative permittivity variation effect on S-parameters

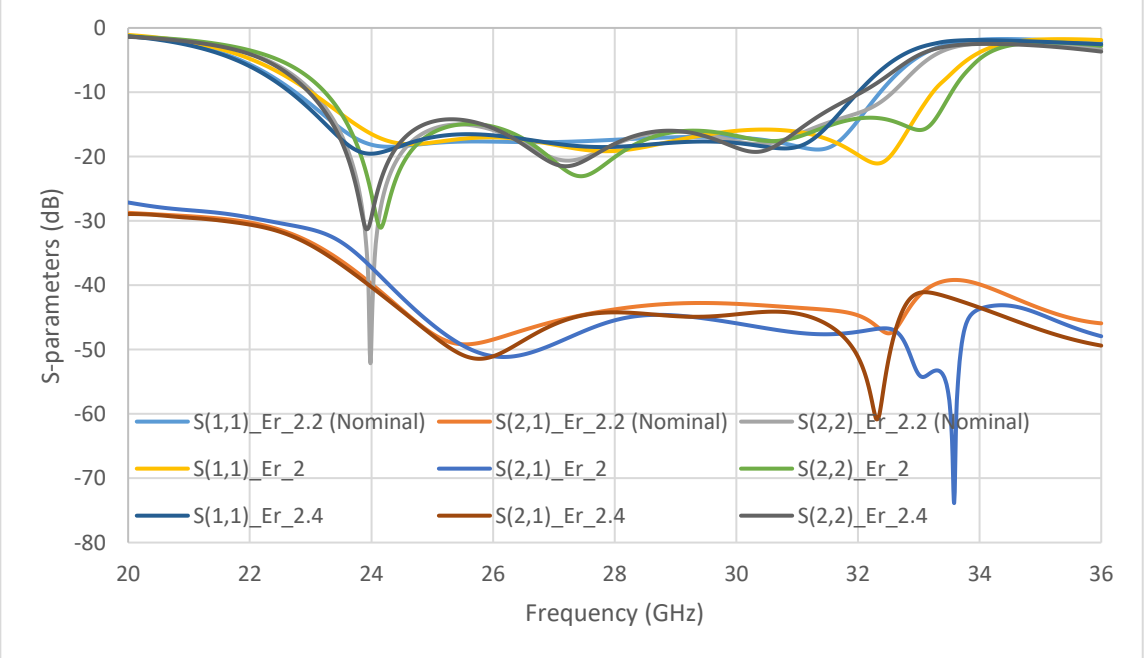

Figure 3.25: Relative permittivity effect on S-parameters

3.1.5 Radiation Patterns

The E_Θ and E_Φ radiation patterns at the center frequency of 28 GHz in the $\Phi = 0$ and $\Phi = 90$ planes are shown in figure 3.26 (a) and (b), respectively. As expected from a patch antenna, this design has broad radiation and a gain of 8.1 dB. The cross-polarization levels for both $\Phi = 0$ and $\Phi = 90$ planes are 30 dB below the main beam at boresight.

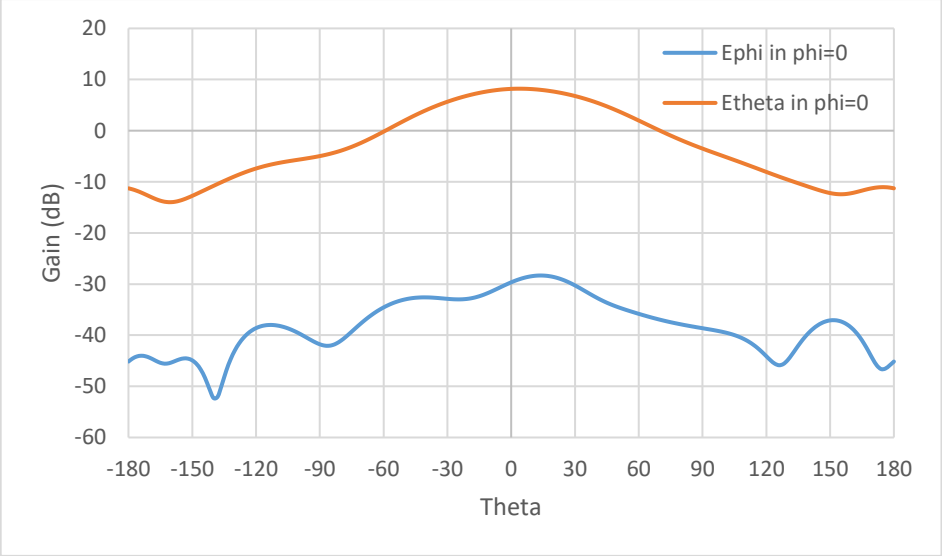

(a)

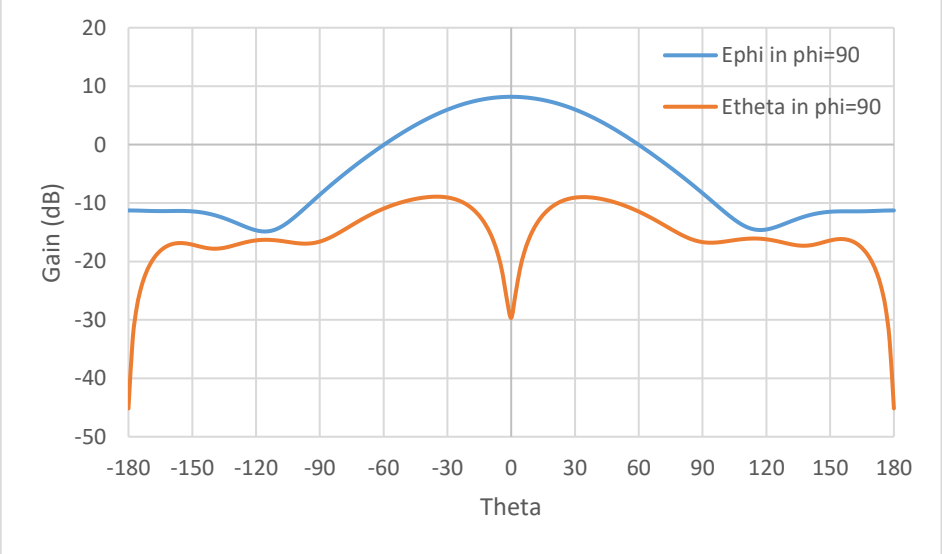

(b)

Figure 3.26: Gain patterns in (a) Φ = 0 and (b) Φ = 90 at 28 GHz

The simulated antenna gain over frequency is shown in figure 3.27. As we can see from the figure, the gain is very stable, with less than one dB variation over the entire bandwidth of interest. One thing to notice here, however, is that the gain decreases rapidly at both edges of the frequency band. The decrease at the lower end can be attributed to the increase in the return loss or worse impedance matching. Where the upper band decrease is likely due to the increase of back radiation as the antenna radiation efficiency reduces.

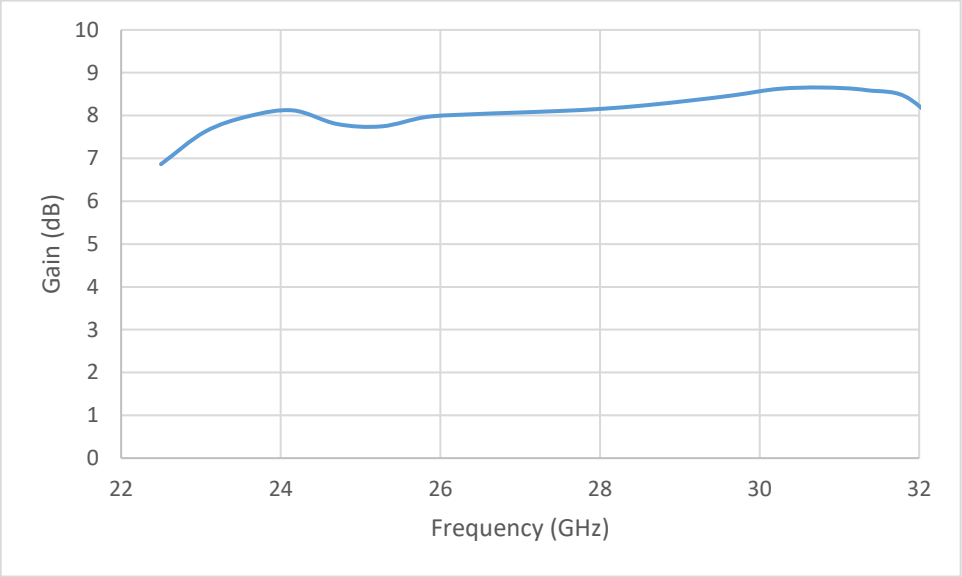

Figure 3.27: Antenna gain vs. frequency

Figure 3.28 shows the antenna front to back ratio (FBR), an important figure of merit for slot coupled patch antennas, given how closely the slot length and the antenna FBR are related. The simulated front to back ratio for this antenna element is better than 17 dB over the entire impedance bandwidth. If a resonant slot were used here to increase the impedance bandwidth, FBRs as low as 6 dB could be seen at the band edges.

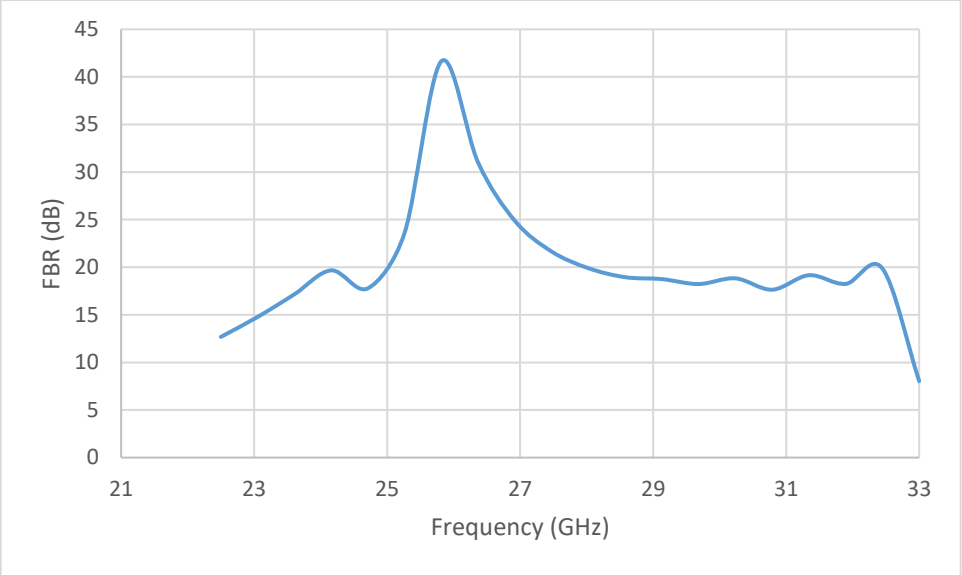

Figure 3.28: Antenna front to back ratio over frequency

3.1.6 Fractal Antenna

Here a broadband fractal antenna is proposed based on the single-layer designs in [59], [60]. Sierpinski carpet fractals replace the patch antennas in the antenna proposed earlier in this section. The slot configuration is shown in figure 3.29 for the first, second, and third iterations. Slot dimensions are as follows; the first, second, and third iterations are one third, one-ninth, and one twenty-seventh the size of the patch [60]. By increasing the order, the bandwidth of the antenna can be improved. However, no noticeable increase can be seen beyond the third iteration. Plus, manufacturing such a design is also challenging and expensive, especially at mm-Wave frequencies because of PCB manufacturing limitations. The advantages of using this design are reduced antenna dimensions and better port isolation when compared to conventional patch design. A silicon-based Sierpinski carpet fractal antenna with 13% impedance bandwidth at 24 GHz was designed in [59], and an LTCC based fractal was proposed in [60].

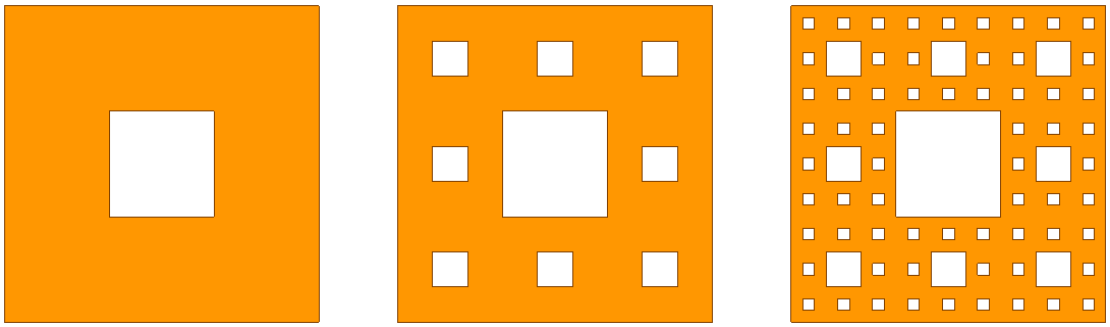

(a) (b) (c)

Figure 3.29: Fractal antenna iterations: (a) 1st iteration (b) 2nd iteration (c) 3rd iteration

The stacked fractal antenna has the same number of layers and stack-up as the microstrip patch antennas proposed earlier. Here a multilayer PCB based fractal design on RT/Duroid 5880 is presented, making use of two fractal antennas on different layers that are capacitively coupled to each other and fed through a slot in the ground plane.

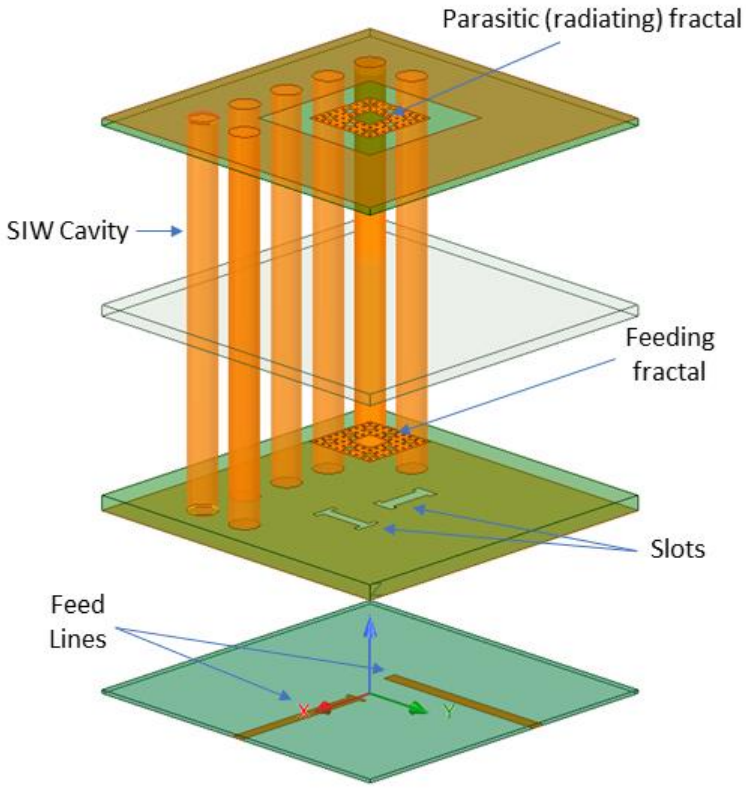

Figure 3.30: Fractal antenna stack-up

Figure 3.30 shows the stack-up of the proposed antenna. An impedance bandwidth of 26.5% for 10 dB impedance bandwidth with a port to port isolation of 30 dB is achieved over the band. Figure 3.31 shows the S-parameter results of the optimized antenna. A parametric study like that in section 3.1.4 was carried out to optimize this design.

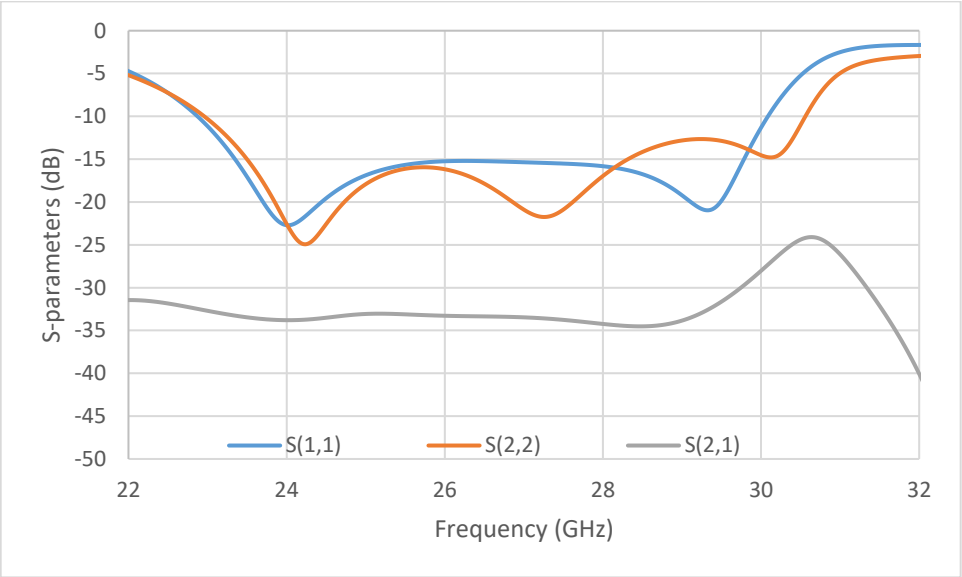

Figure 3.31: Optimized antenna S-parameters

This antenna has a slightly lower gain of 6.8 dB in comparison to a conventional patch antenna, due to the reduced radiator size. Figure 3.32 shows the E_Θ and E_Φ plots in the Φ = 0 and Φ = 90 planes respectively at the center frequency of 26.5 GHz. The cross-polarization levels for both Φ = 0 and Φ = 90 planes are 30 dB below the main beam at boresight.

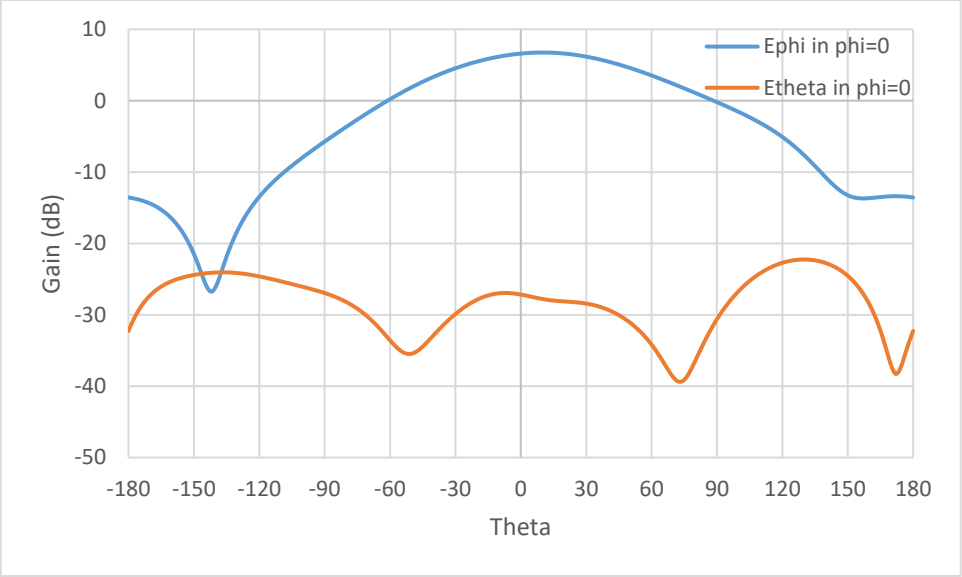

(a)

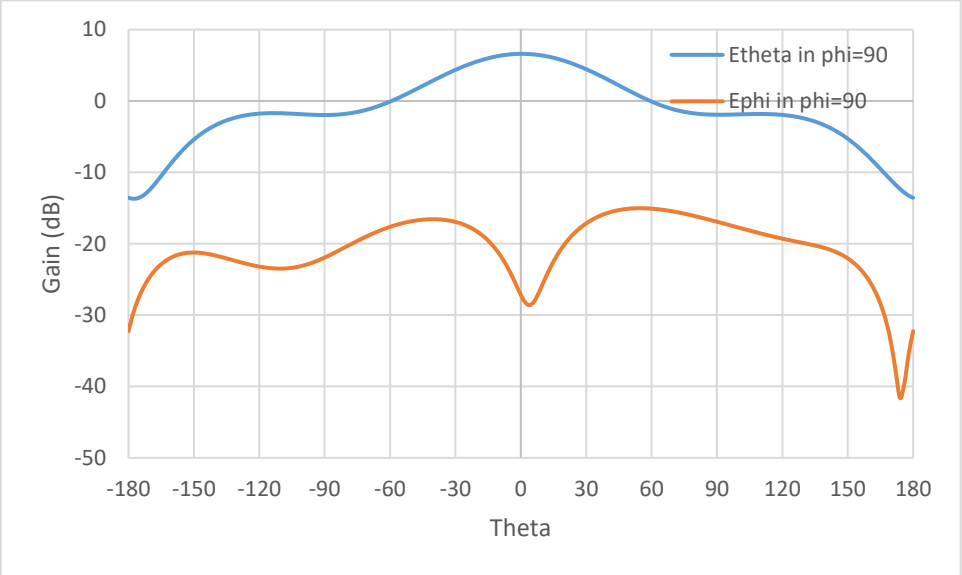

(b)

Figure 3.32: Gain patterns in (a) Φ = 0 and (b) Φ = 90 at 26.5 GHz

Antenna gain over the frequency of interest is also very stable, as shown in figure 3.33, with less than 0.5 dB variation. The simulated efficiency in figure 3.34 also shows that the antenna has a radiation efficiency above 85% from 23 to 30 GHz.

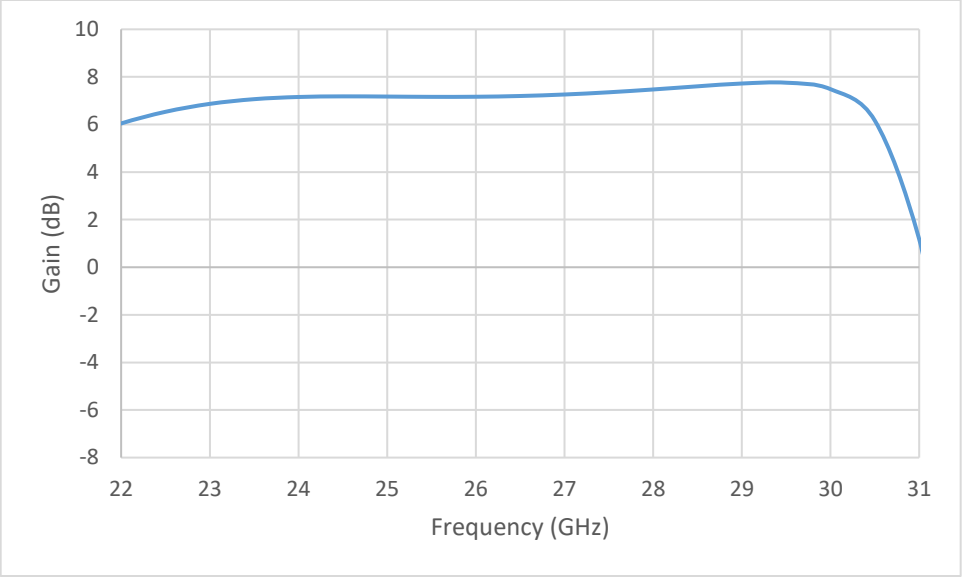

Figure 3.33: Antenna gain vs. frequency

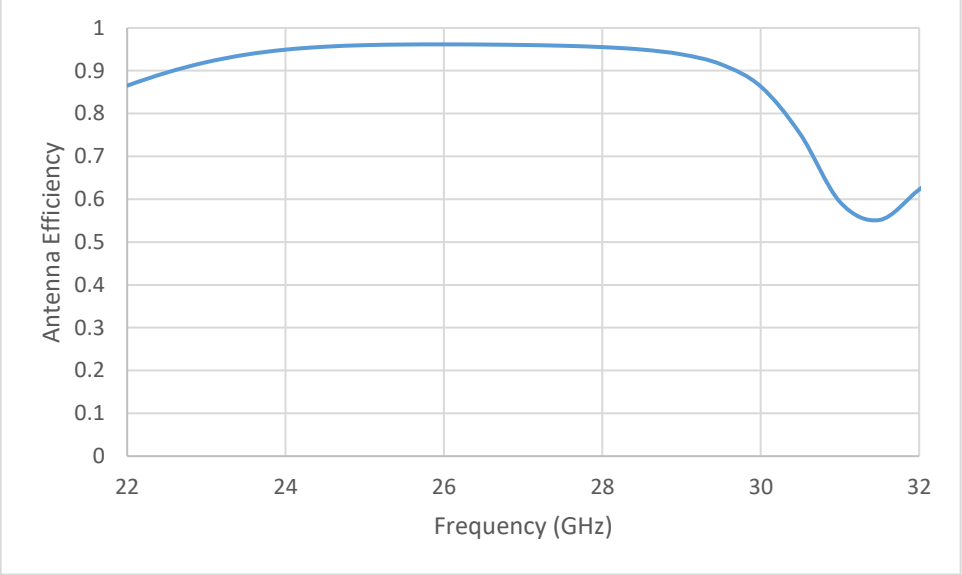

Figure 3.34: Antenna efficiency vs. frequency

The antenna front to back ratio from 24.25 to 29.5 GHz is higher than 15 dB and rapidly becomes worse at both edges of the band, as shown in figure 3.35. This reduction is likely due to the slot dimensions and the gain degradation at the higher frequency end.

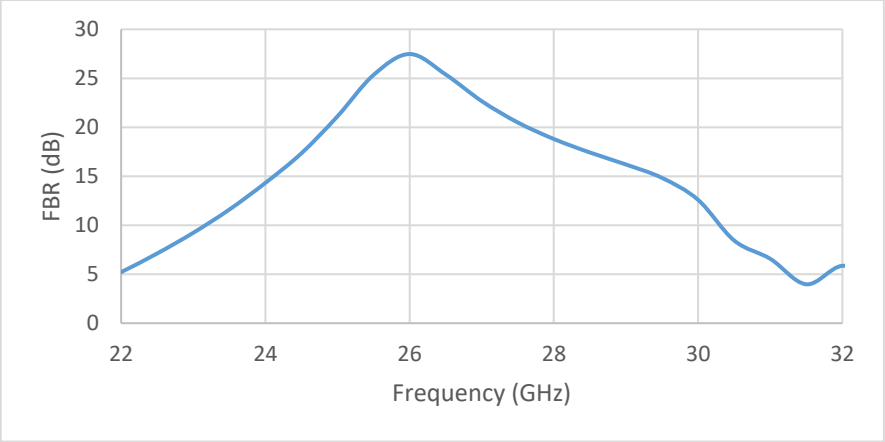

Figure 3.35: Antenna front to back ratio vs. frequency

3.2 Antenna Design II

Figure 3.36 shows the exploded view of the proposed antenna. This antenna is very similar to the one analyzed in the previous section, except that substrate two is replaced with a foam layer (Rohacell 31 IG/A), and a Rogers 4350 laminate was used for the feed network. The total thickness of the antenna prototypes is 1.703 mm (0.15 λ_0). Foam has very desirable characteristics when designing patch antennas primarily due to their relative permittivity, which is close to that of air. Having a low permittivity can be beneficial in eliminating surface waves and improving the antenna radiation efficiency. Surface waves are typically excited at the interface between dielectric and air in a patch antenna, and the higher the dielectric constant, the sooner surface waves are excited as a function of substrate thickness [61]. The authors in [62] proposed a linearly polarized five-layer Ka-band (26-40 GHz) antenna with a broadband impedance bandwidth. The layers were made up of a mixture of foam and RT/Duroid 5880 laminates with a total thickness of 2.495 mm (0.274 λ_0). Using a resonant aperture, an impedance bandwidth of 42.4% was achieved with a gain of 6 dB. Our proposed design outperforms the one in [62] in terms of impedance bandwidth by about 5%. In addition to wider bandwidth, the designs has a profile that is

nearly half that of the antenna in [62], without degrading the antenna front to back ratio or radiation performance.

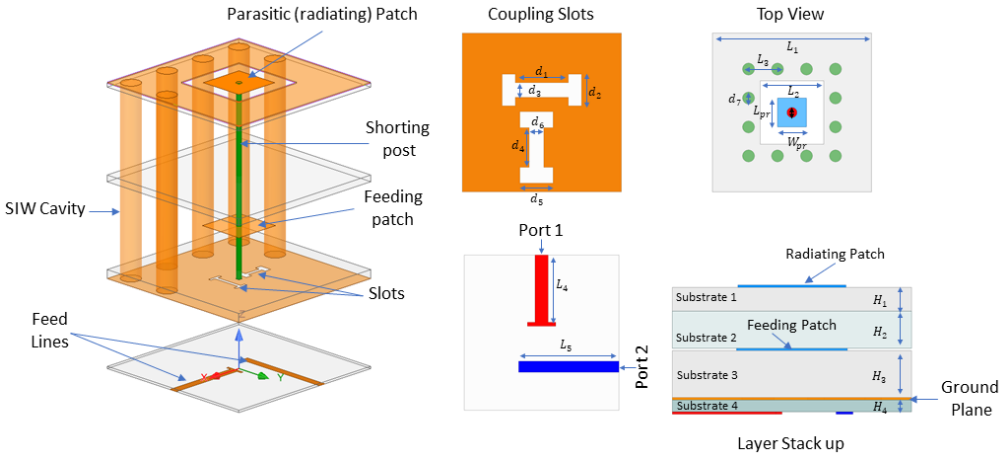

Figure 3.36: Antenna layout

Due to the difficulty in etching or manufacturing antennas on foam, a thin laminate is typically used above it where the antenna can be etched. Another advantage of using foam or spacers is the fact that substrate one can act as a protective layer for the antenna, and a given range of airgap thicknesses provides a lower input resistance for the upper resonance. Lower input resistance translates into easier matching because the antenna can easily be matched to 50 or 75 Ohms, in comparison to an antenna with a higher input impedance [63]. This reduction holds for the inverted antenna configuration, where the radiating antenna is etched on the bottom of substrate 1.

Figure 3.37 shows the simulated return loss for both polarizations and the port isolation between the two. An impedance bandwidth of 46.8% (VSWR $\geq$ 2) is achieved with port isolation levels better than 34 dB across the band. This antenna outperforms the antenna proposed in [62] without increasing the antenna substrate thickness or degrading the level of back radiation by increasing the slot size. The profile of the antenna being proposed here is almost half the size, 0.15 λ_0, in comparison to a profile of 0.274 λ_0.

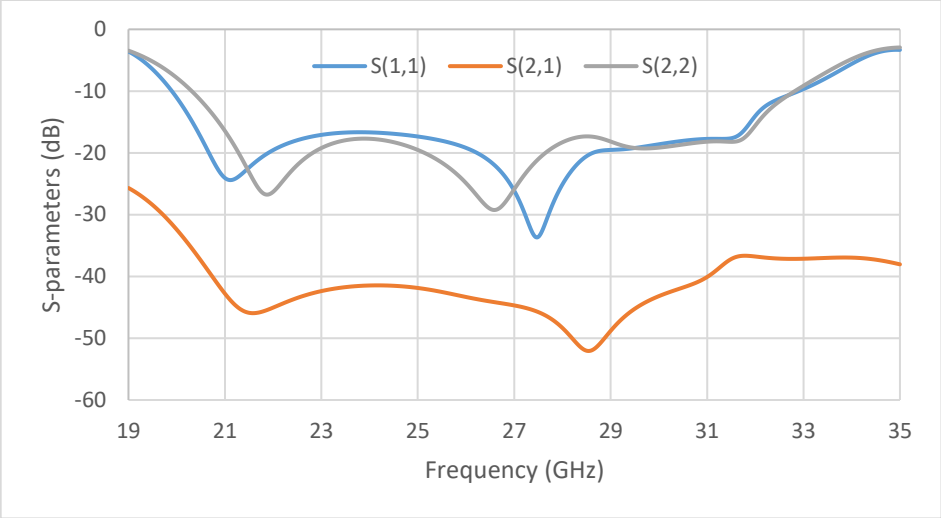

Figure 3.37: Optimized antenna S-parameters

A shorting post is also added here at the center of the antenna between the radiating patch and the ground plane to improve the port isolation. Simulations show that better than 10 dB of isolation improvement is achieved using this technique. Figure 3.38 compares port isolation S_{21} for an antenna with and without a shorting post, and the antenna with the shorting post greatly enhances the isolation.

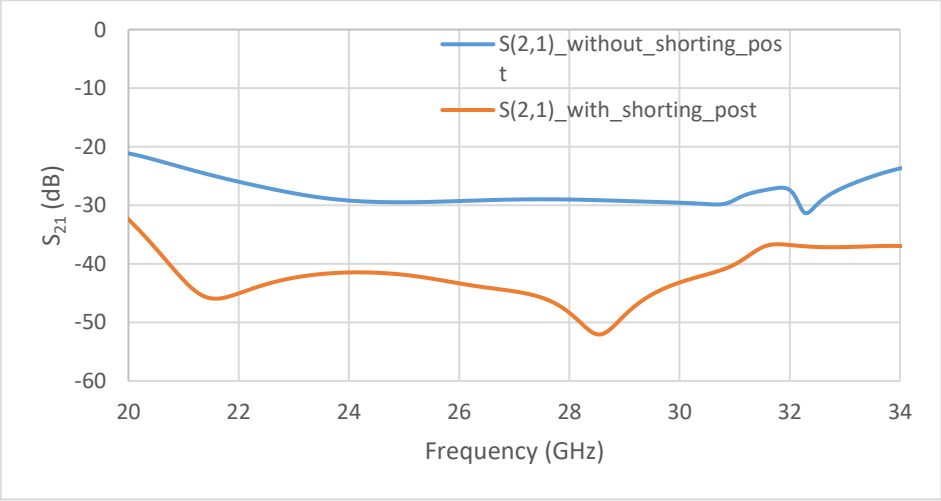

Figure 3.38: Antenna S21 with and without shorting posts

3.2.1 Radiation Patterns

This antenna has a gain of 7.2 dB, which is comparable to other multilayer slot coupled designs. Figure 3.39 shows the E_Θ and E_Φ radiation patterns in the $\Phi = 0$ and $\Phi = 90$ planes, respectively at the center frequency of 26.575 GHz. The cross-polarization levels for both $\Phi = 0$ and $\Phi = 90$ planes are 35 dB below the co-polar patterns at boresight.

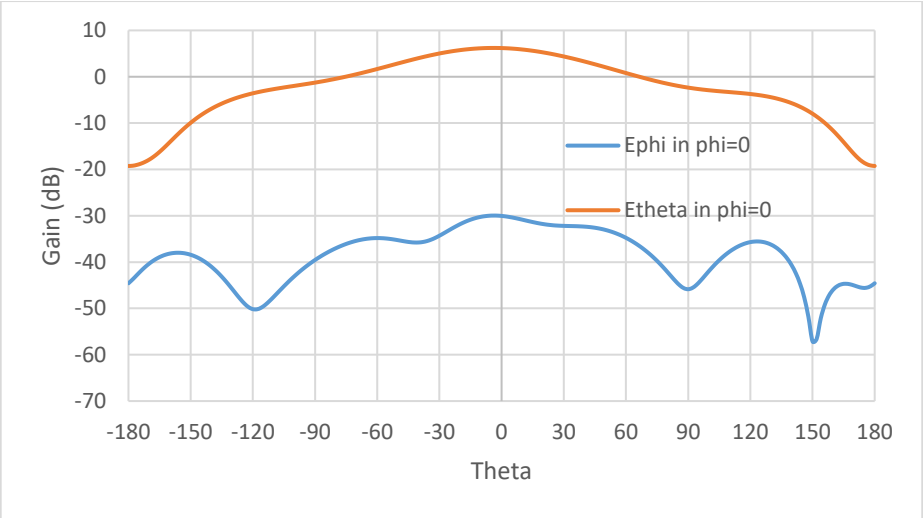

(a)

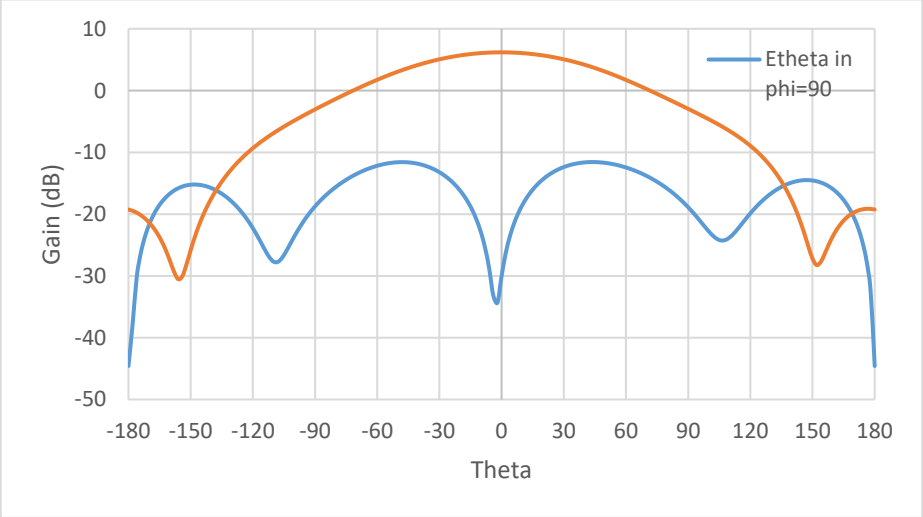

(b)

Figure 3.39: Gain patterns in (a) Φ = 0 and (b) Φ = 90 at 26.575 GHz

Figure 3.40 shows the antenna gain across the matched frequency band. The antenna gain over frequency is better than five dB with a gain variation below 1.6 dB. Which is comparable to other multilayer slot coupled patch antennas proposed in the literature.

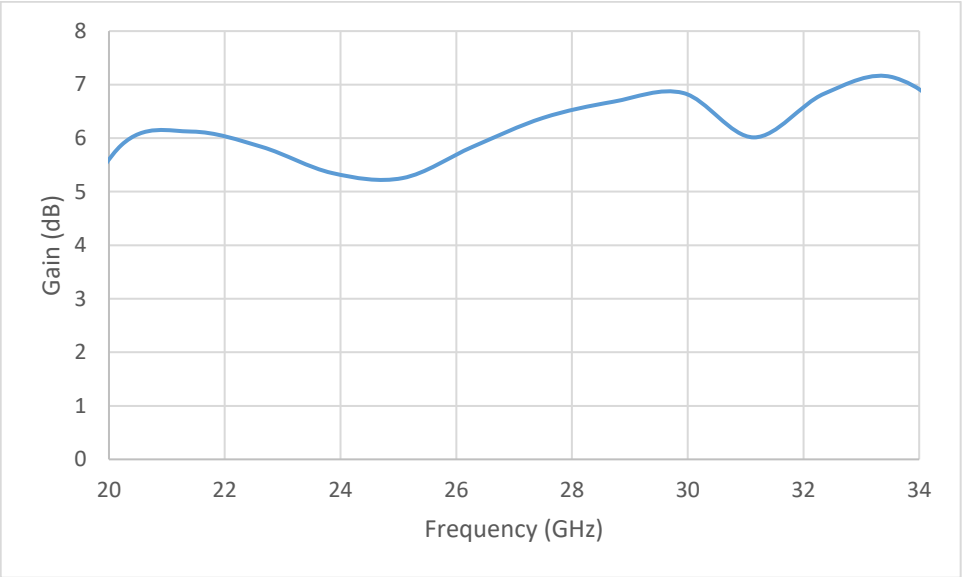

Figure 3.40: Antenna gain vs. frequency

Simulated antenna efficiency is excellent, and the antenna has an efficiency above 85% across the frequency band. Having a high radiation efficiency tells us that surface waves are not deteriorating the antenna efficiency, as can be seen on single-layer patch antennas on thicker substrates. High radiation efficiency is one of the main advantages of using slot coupled patch antennas. Surface wave efficiency can be improved above 95% by using foams and thin laminates for manufacturing the antenna [5]. Figure 3.41 is a plot of the simulated antenna efficiency.

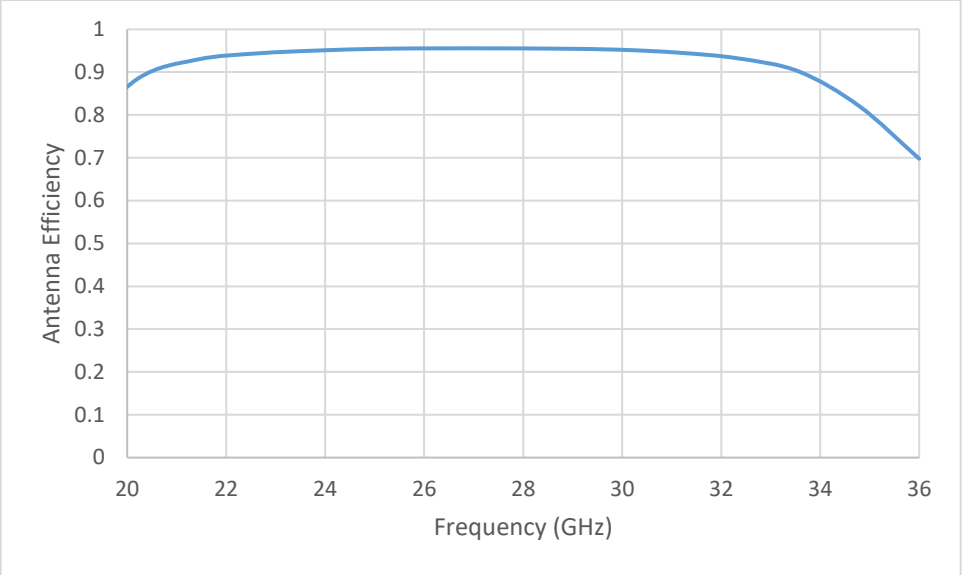

Figure 3.41: Antenna efficiency vs. frequency

Front to back ratio of the antenna is better than 12 dB, as shown in figure 3.42 across the frequency band and better than 15 over most of it. Slot coupled microstrip antennas with resonant slots typically have a worse front to back ratios, especially those with crossed slots. Front to back ratios of patch antennas with crossed slots can go below 7 or 8 dB at the edges of the band.

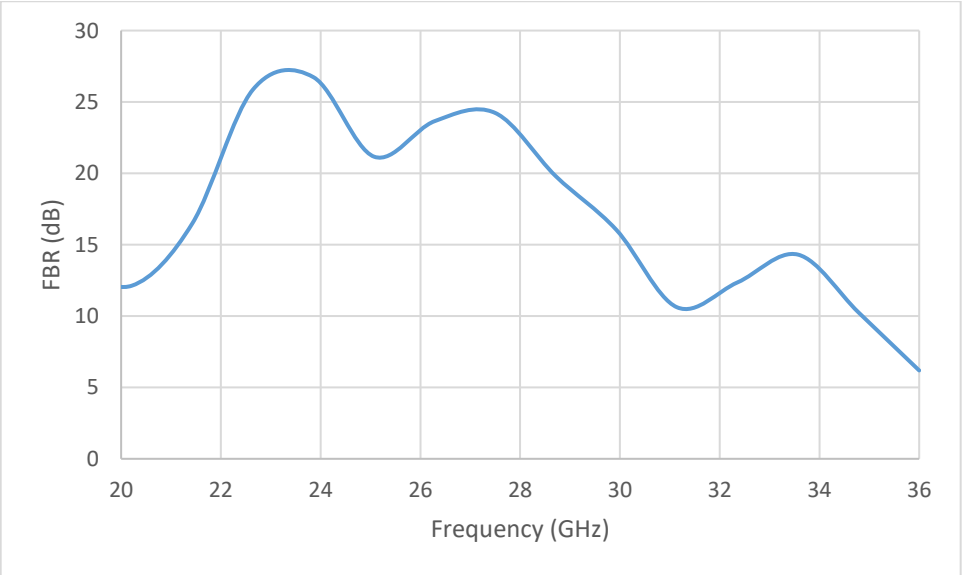

Figure 3.42: Antenna front to back ratio vs. frequency

3.2.2 Fractal Antenna with a Foam Airgap

A dual linearly polarized fractal antenna like the one proposed in section 3.1.6 is designed here, but with a different stack-up. A foam layer again replaces substrate two, and the feed network is manufactured on a Rogers 4350B laminate. Antenna S-parameter results are shown in figure 3.43. These results indicate that a good match is achieved for both ports. S_{11} and S_{22} are better than 14 dB in most of the frequency band. An impedance bandwidth of 39% is achieved here, slightly lower than the antenna proposed in the previous section. Port isolation levels are also comparable. This design has port isolation levels better than 37 dB across the band.

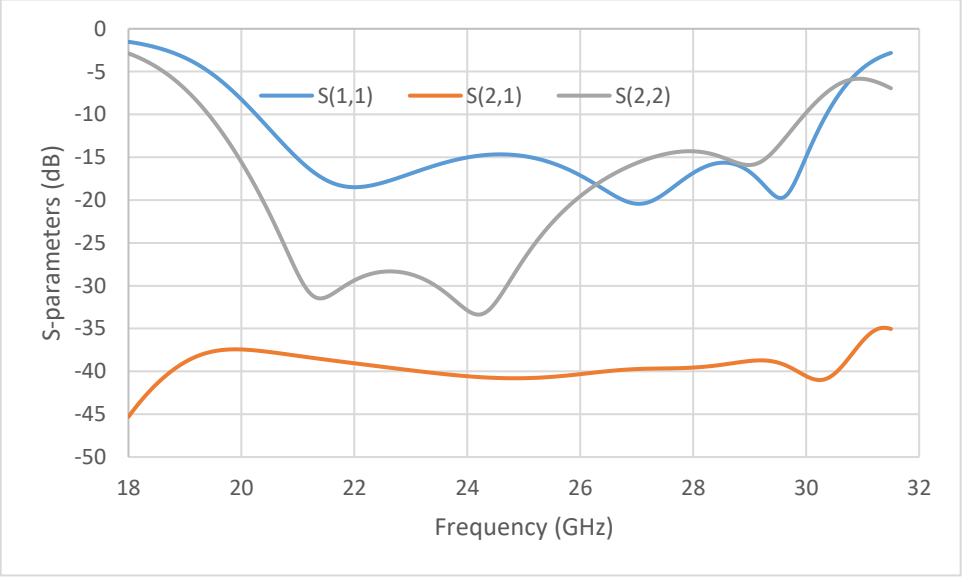

Figure 3.43: Optimized antenna S-parameters

In comparison to all designs proposed so far, this design has the best cross-polarization levels in both the E and H planes. This antenna has a gain of 6.5 dB, which is comparable to the previous fractal antenna design. Figure 3.44 shows the E_Θ and E_Φ plots in the $\Phi = 0$ and $\Phi = 90$ planes respectively at 25 GHz. The cross-polarization levels for both $\Phi = 0$ and $\Phi = 90$ planes are 40 dB below the co-polar patterns at boresight.

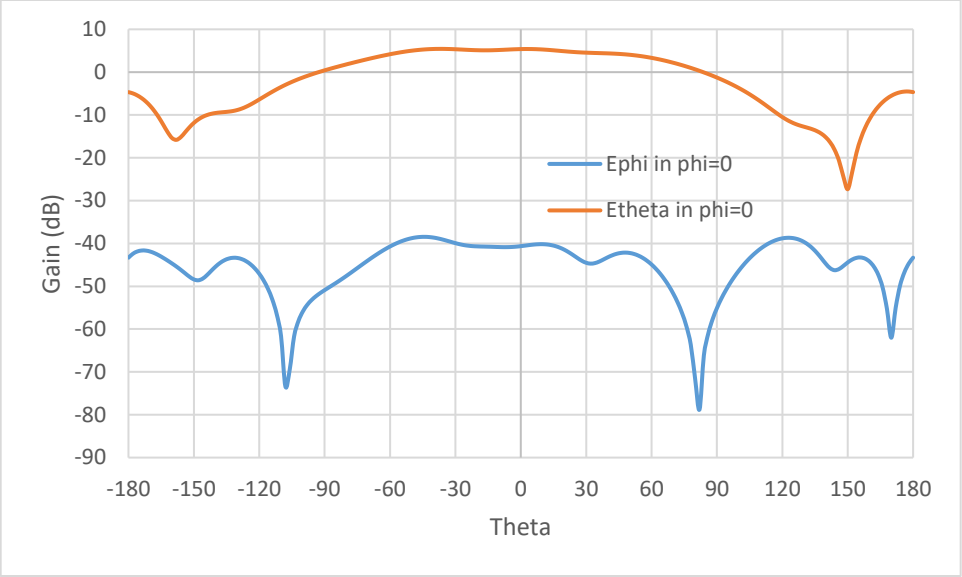

(a)

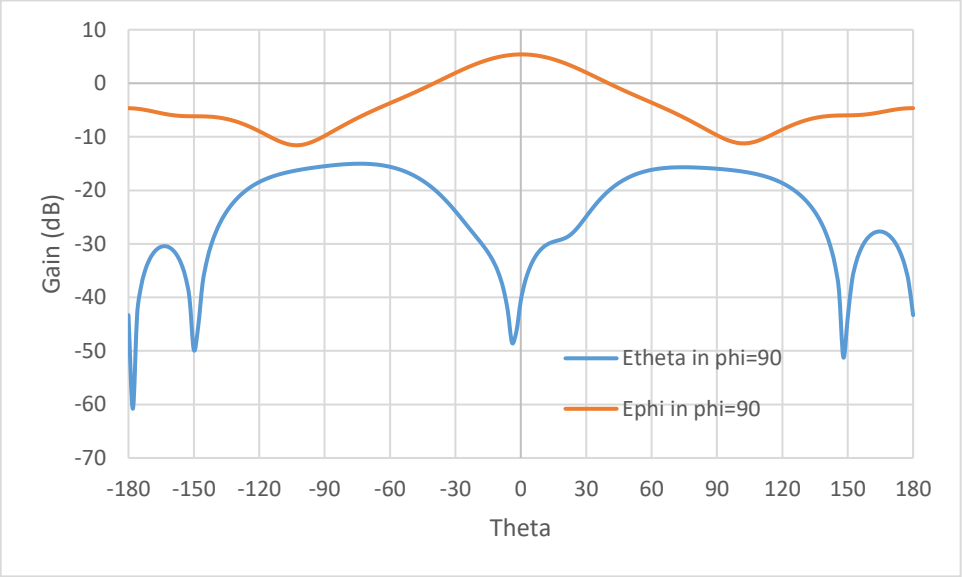

(b)

Figure 3.44: Antenna gain patterns in (a) Φ = 0 and (b) Φ = 90 at 25 GHz

The antenna gain over frequency does fluctuate, varying anywhere from 5.2 to 7 dB, as seen in figure 3.45. These gain values, however, are still in line with the radiation results obtained for the previous fractal antenna proposed in section 3.1.6. Removing the SIW cavity, however, can reduce this effect to some degree.

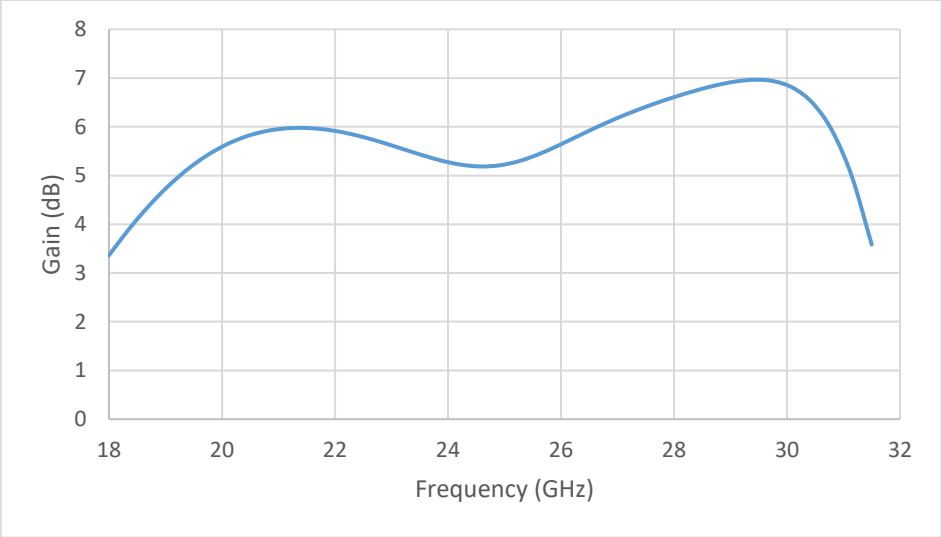

Figure 3.45: Antenna gain vs. frequency

The plot of the simulated radiation efficiency in figure 3.46 is also consistent with other antennas that have been proposed so far. Efficiencies greater than 85% are achieved across the band. Figure 3.47 shows the front to back ratio of the proposed fractal antenna. FBR is better than 15 dB across most of the band, but it gets worse at the band edges with FBR values around 10. This reduction in FBR can be attributed to matching degradation or gain drops as the antenna become a worse radiator.

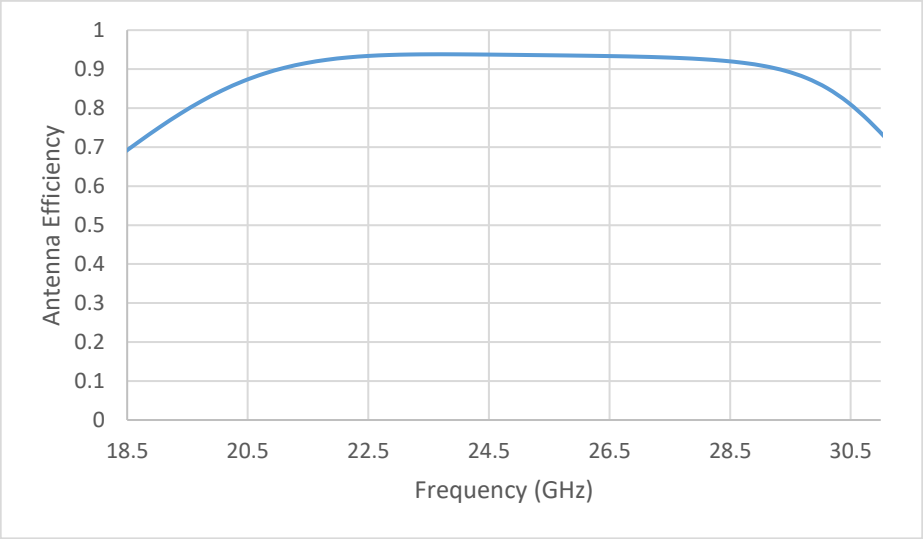

Figure 3.46: Antenna efficiency vs. frequency

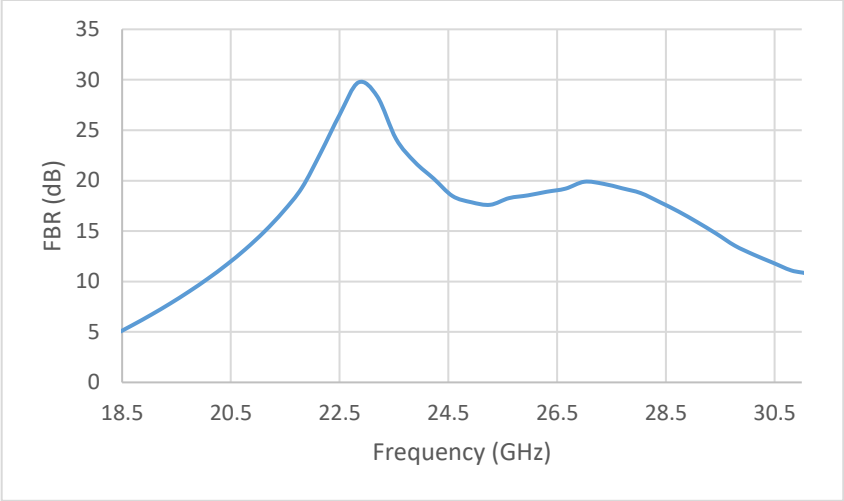

Figure 3.47: Antenna front to back ratio vs. frequency

3.3 Antenna Design III

In this section, a dual linearly polarized microstrip antenna with a polylactic acid (PLA) 3D printed spacer is designed. PLA is one of the most used materials in polymer 3D printing because it is relatively inexpensive in comparison to other polymers. Many publications over the past few years have been dedicated to the study of the electrical characteristics of PLA. In [64], dielectric properties of PLA were characterized from 0.5 to 67 GHz, as shown in figure 3.48.

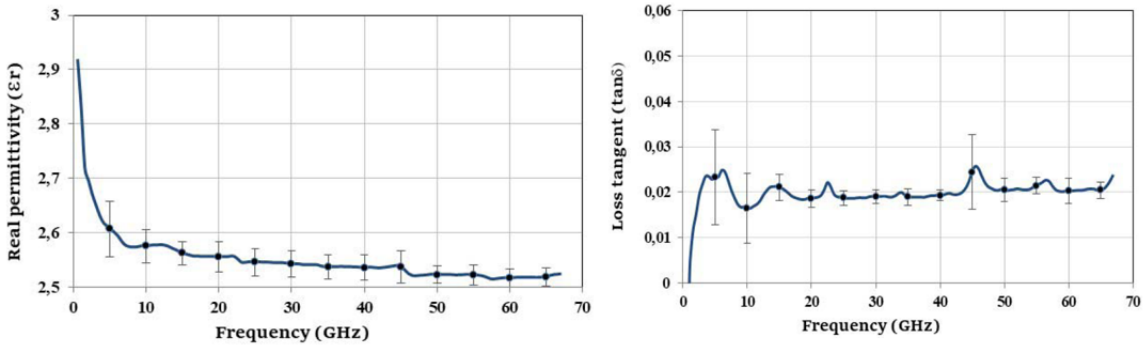

Figure 3.48: Relative permittivity and loss tangent of PLA from 0.5 to 67 GHz © 2018 IEEE

A hollow 3D printed layer replaces substrate 2 in this design, and the feed network is made on a thin layer of Rogers 4350 laminate. Figure 3.49 shows the antenna stack-up, and 3D printed spacer.

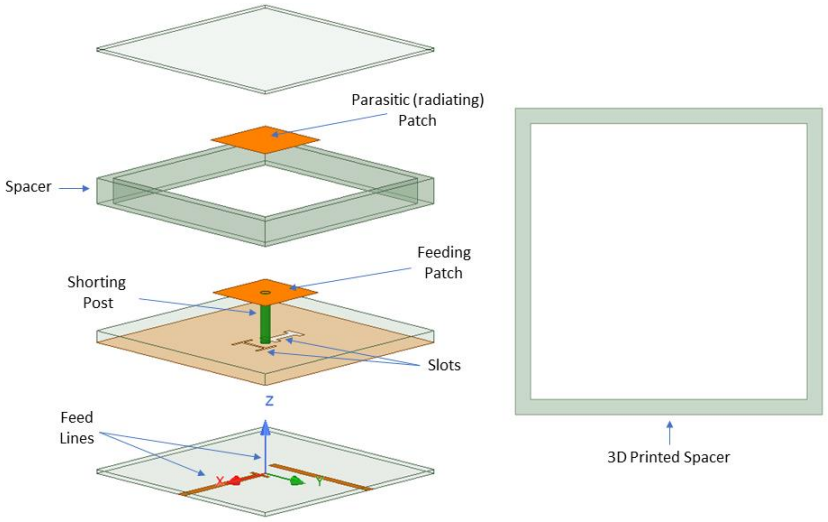

Figure 3.49: Stack up of the microstrip antenna with a 3D printed spacer

Simulated S-parameters of the antenna are shown in figure 3.50. This antenna has an impedance bandwidth of 34.7% (VSWR ≥ 2) and port isolation levels that are better than 37 dB across the band. A shorting post extending from the ground plane to the feeding patch is used here to improve port isolation.

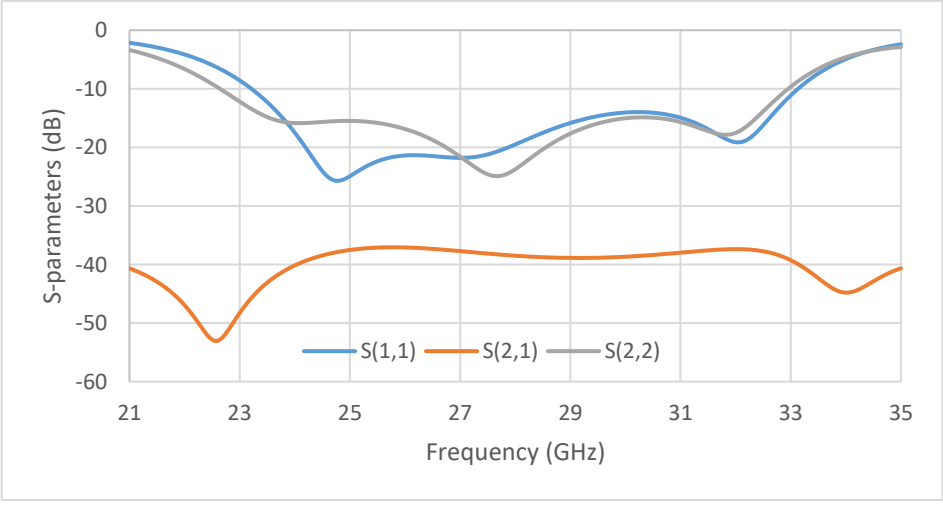

Figure 3.50: Optimized antenna S-parameters

This antenna has a gain of 8.2 dB, which is comparable to other stacked patch antennas. Figure 3.51 shows the E_Θ and E_Φ plots in the $\Phi = 0$ and $\Phi = 90$ planes respectively at 28 GHz. The cross-polarization levels for both $\Phi = 0$ and $\Phi = 90$ planes are 38 dB below the main beam at boresight. Cross-polarization levels in the phi 90 plane degrade off-boresight, which can be attributed to the small size of the ground plane (1 cm).

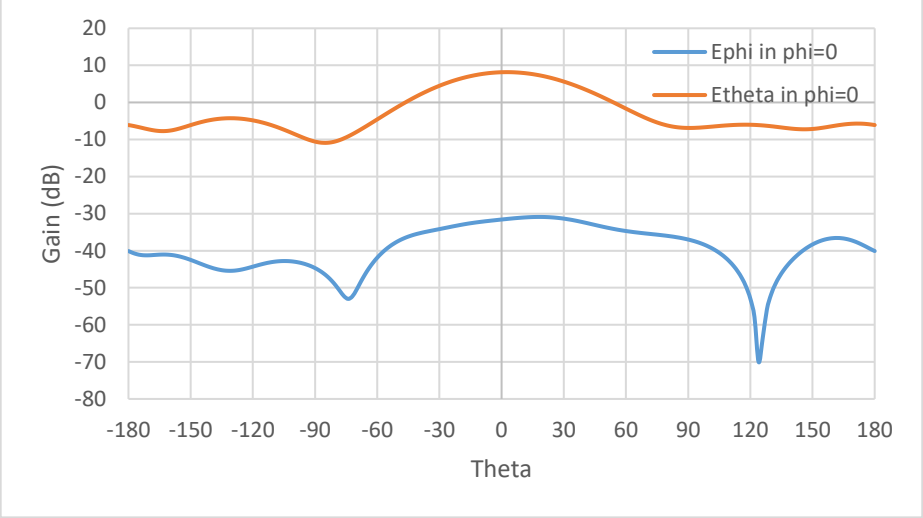

(a)

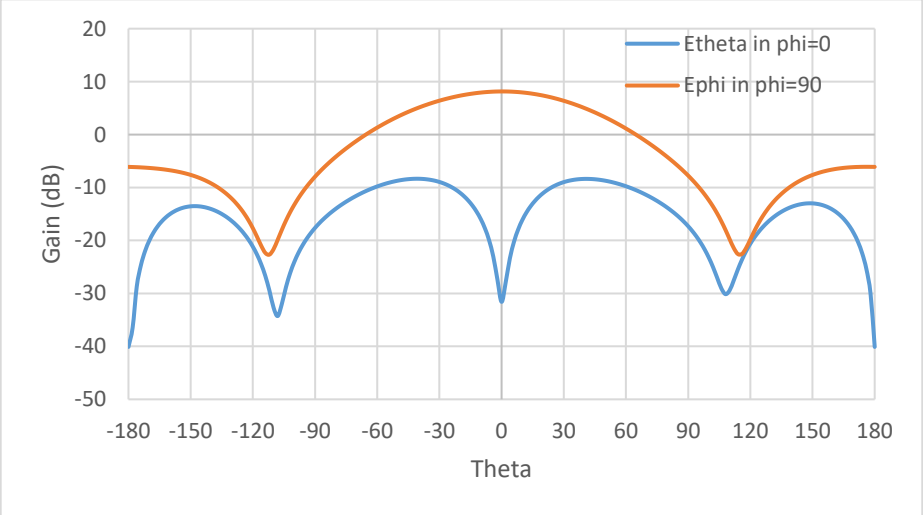

(b)

Figure 3.51: Gain patterns in (a) Φ = 0 and (b) Φ = 90 at 28 GHz

The antenna gain over the frequency band of interest is better than 7 dB, with gain levels as high as 9 dB at the upper-frequency edge. Gain levels of this antenna are comparable to other stacked patch antennas. Figure 3.52 shows the antenna gain in the frequency band of interest.

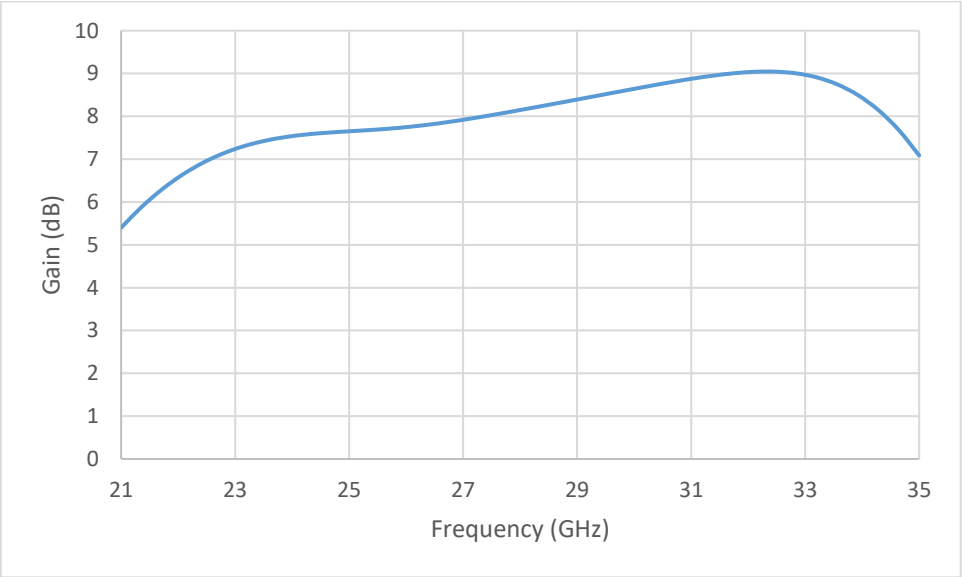

Figure 3.52: Antenna gain vs. frequency

One of the main disadvantages of using slot coupled antennas is their back radiation, especially when designing antennas with broad bandwidth. This design has a front to back ratio that is better than 14 dB across the band, as shown in figure 3.53. Coupling slots are not resonant with the antennas here, which is why an adequate level of back radiation is achieved. Having a high FBR is essential in many applications, mainly when active devices are used below the ground plane. If high FBR is not an issue or the design allows for the addition of a backing cavity, the antenna bandwidth can be increased by using resonant slots.

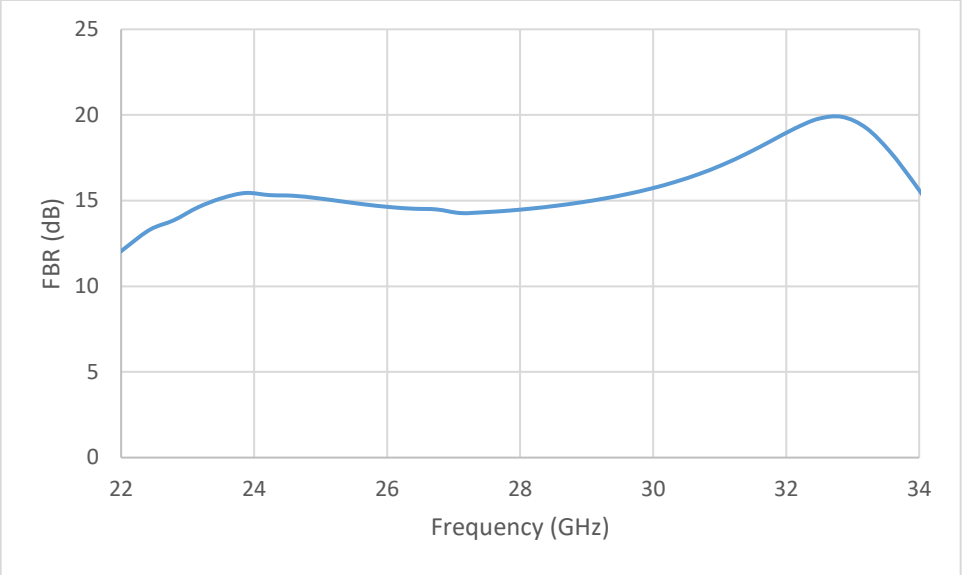

Figure 3.53: Antenna front to back ratio vs. frequency

Figure 3.54 shows the simulated radiation efficiency of the proposed antenna. The efficiency of the antenna is better than 90% from 23 to 33 GHz. High radiation efficiency is one of the main advantages of using stacked patches to increase the antenna bandwidth. Even though thicker substrates are used to improve the operational bandwidth, efficiencies are still higher than 80%.

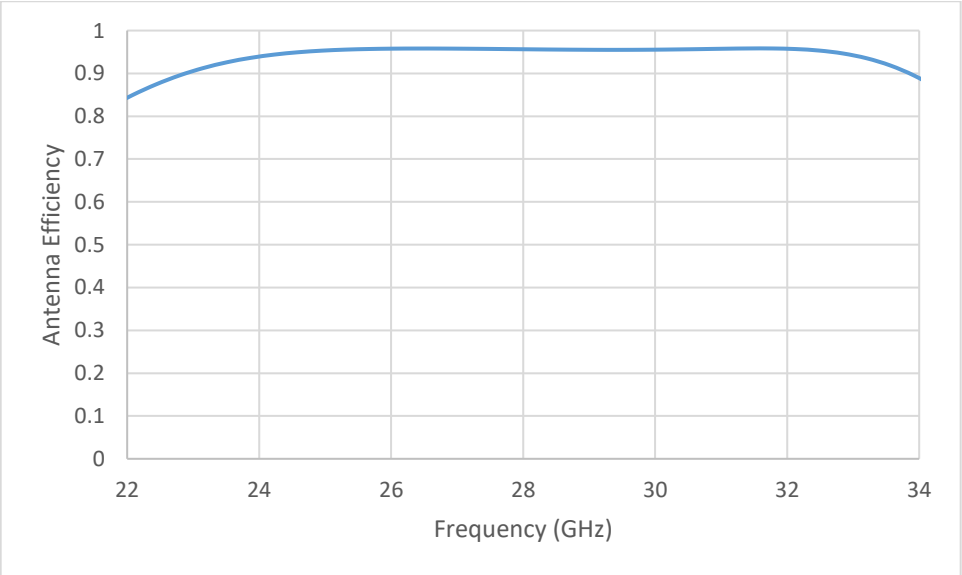

Figure 3.54: Antenna efficiency vs. frequency

3.4 Measurement Results

Measurement results of the manufactured antenna designs from sections 3.1 and 3.3 are presented here. A prototype of the design proposed in section 3.2 was also manufactured. However, satisfactory results could not be obtained as a result of the foam compression which occurred during the bonding process used to glue the layers together. As discussed earlier the use hard foams that can withstand higher heat and pressure, is one way to resolve this. Therefore, only the results of the two antennas made on Rogers RT/Duroid 5880 substrates and designs with a 3D printed spacer are presented.

When designing antennas at mm-Waves there are many things to consider that do not typically pose a great challenge at lower portions of the frequency spectrum. Some of the challenges are the variation in material properties in comparison to substrate datasheets, PCB manufacturing limitations, connector effects, the presence of airgaps between layers, and layer misalignment in multilayer designs. These changes can cause a shift in the center frequency of the design or worse yet a mismatch in the antenna return loss.

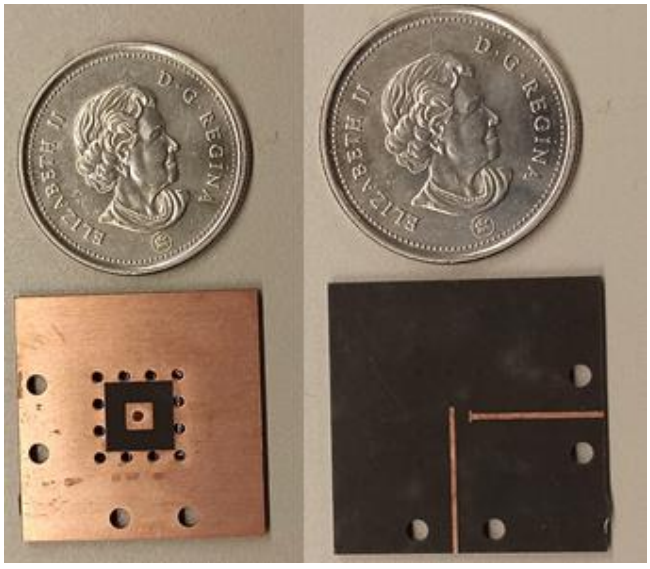

Figure 3.55: Manufactured single element antenna

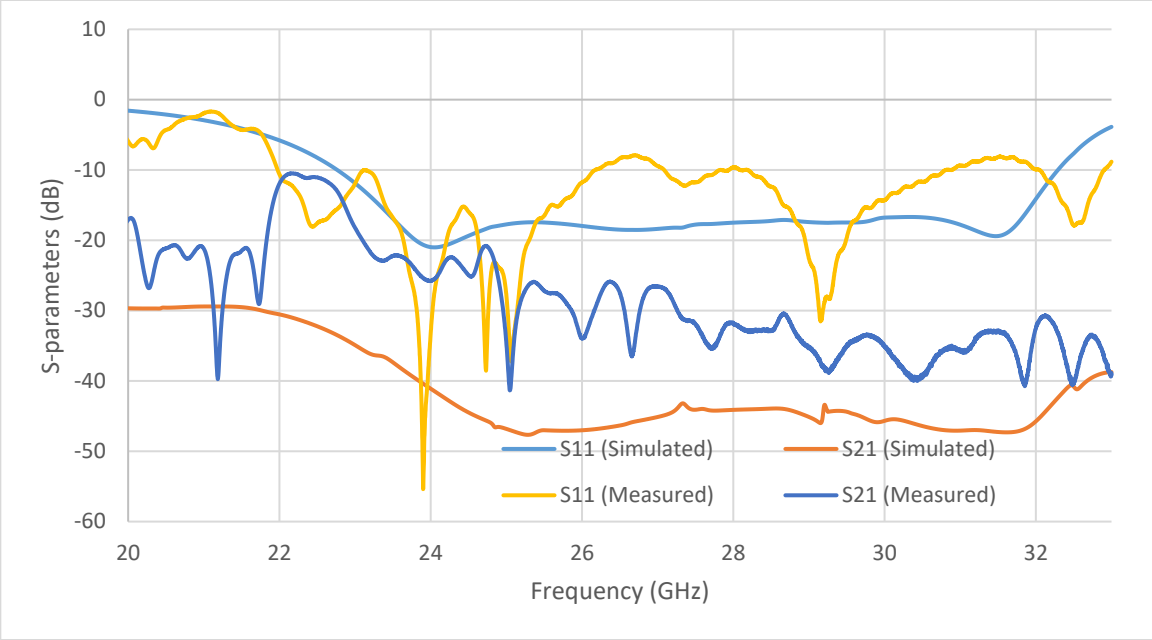

Figure 3.56: Measured and simulated S_{11} and S_{21} of the single element antenna

Figure 3.55 shows the top and bottom layers of the fabricated single element antenna, and figure 3.56 shows the comparison of the measured and simulated S_{11} and S_{22} results. As we can see the measured and simulated results do not perfectly agree. S_{22} return loss is much worse than S_{11}, hence not shown here. Measured S_{11} also shows a similar trend when compared to the simulated values except for the return loss peaks around 27 and 32 GHz. These mismatches can be a result of connector misalignment in relation to the microstrip line, or mismatches do the connector itself. The width of the microstrip line being around 0.4 to 0.5 mm and the connector pin diameter around 0.17 mm, makes it difficult to perfectly align the pin to the center of the line. These issues in addition to manufacturing tolerances can worsen the antenna performance. S_{22} measurement results also suffer similarly from connector effects, but it seems that the manufacturing errors are more detrimental in this case. S_{22} performance is much worse than S_{11} in most of the measurements, which lead us to believe that the issue is most likely due to a fabrication error.

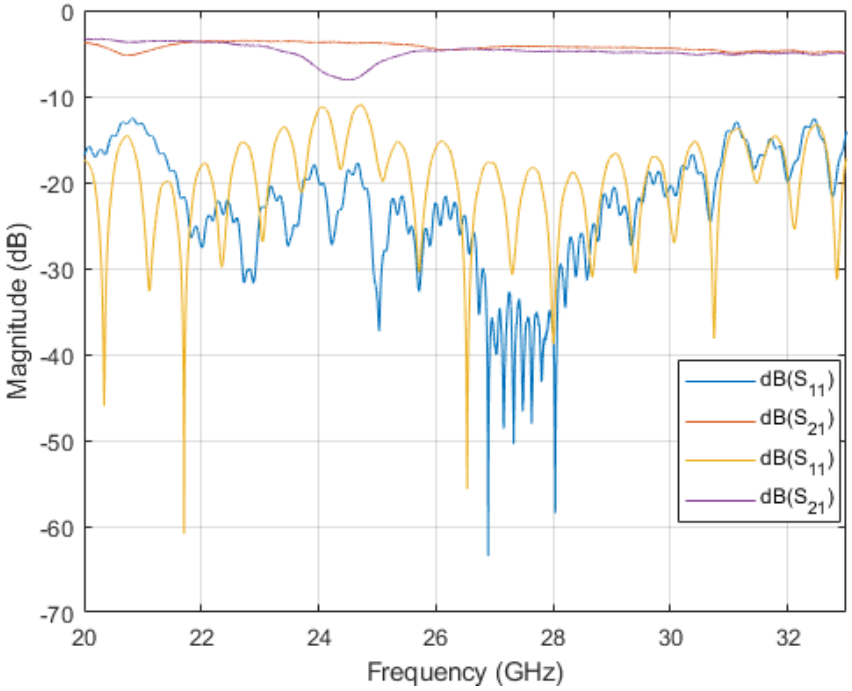

Figure 3.57: Two S-parameter measurements of the same transmission line

Figure 3.57 compares two S-parameter measurements made on the same transmission line using the same connectors. The width of the 50 Ω microstrip line is around 0.3 mm, which proves the earlier point made regarding return loss and insertion loss variation due to connector misalignments. To resolve this issue several measurements will be made on each antenna and their results will be compared to select the best of them.

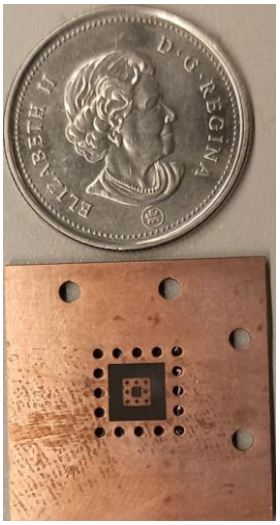

Figure 3.58: Single element fractal antenna

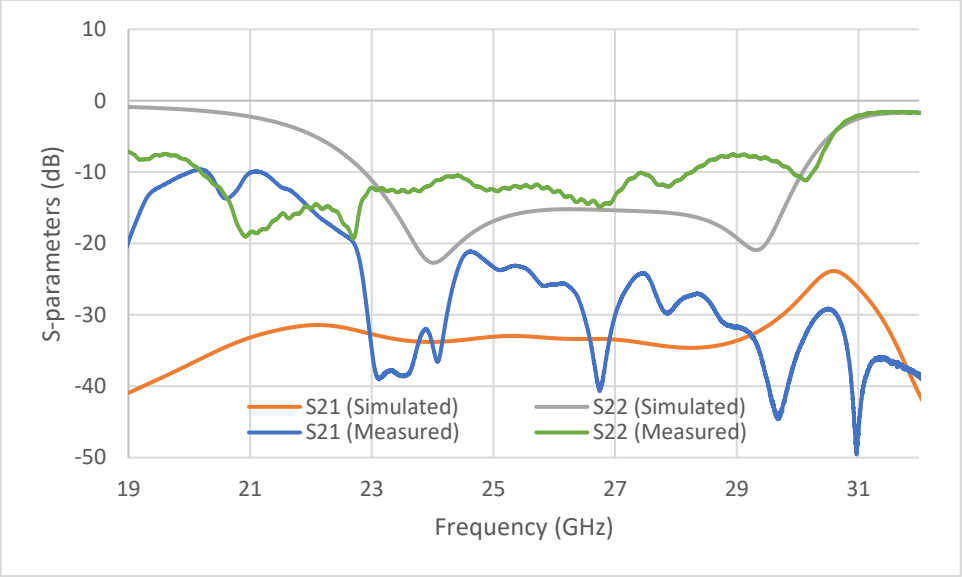

Figure 3.59: Measured and simulated S_{22} and S_{21} results of the single element fractal antenna

Measured and simulated S_{22} and S_{21} of the single element fractal antenna element in figure 3.58 is shown in figure 3.59. S_{22} is matched from around 20.4 GHz to around 28 GHz, indicating a shift in comparison to the simulated results. Shifts in the resonant frequencies can arise because of changes in the material properties. The slot dimension of the 3rd iteration of the fractal antenna (around 0.1 mm) is also very close to the manufacturing limitation of most PCB manufacturers (0.076 mm). These issues along with other manufacturing errors such as slot misalignments and dimensions are the main reason for such mismatches.

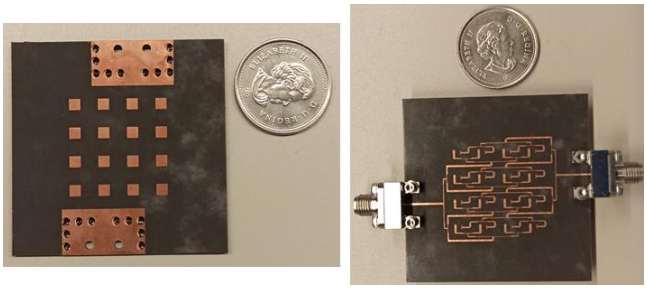

Figure 3.60: 16-element array

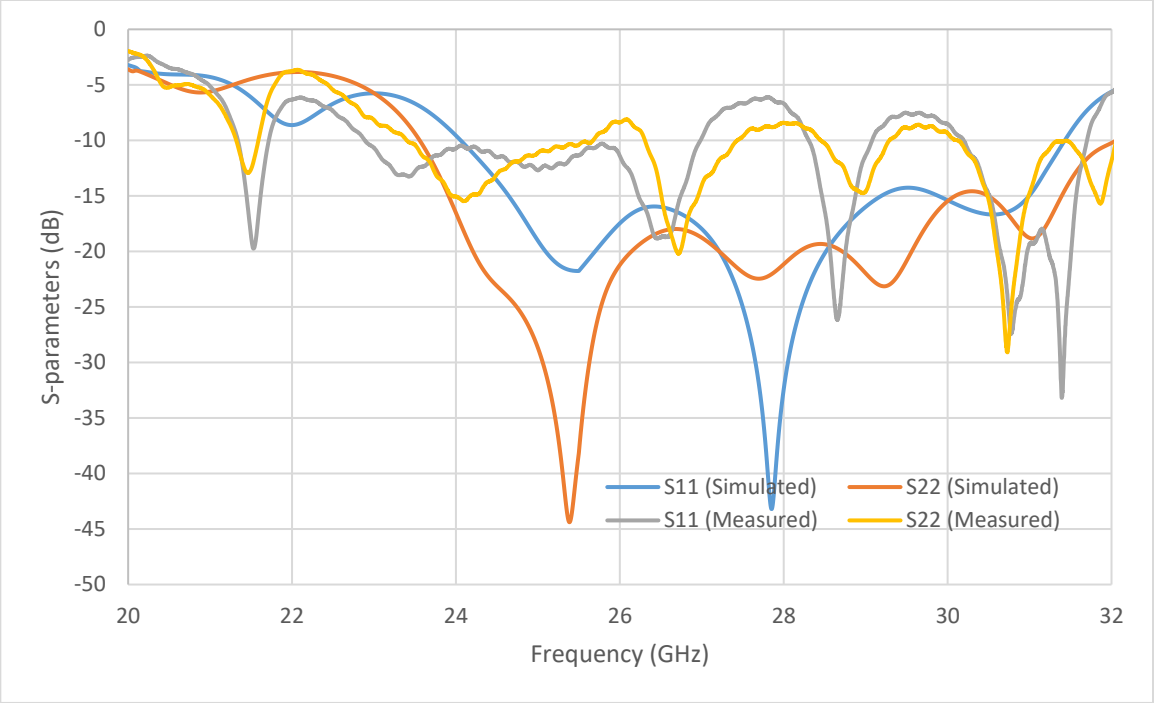

Figure 3.61: Measured and simulated s-parameters of the 16-element array

Figures 3.60 and 3.61 show the manufactured 16- element array and its measured S-parameter results. Here again the antenna is only match over a small portion of the band, which can be a result of similar issues to those encountered on the single element level.

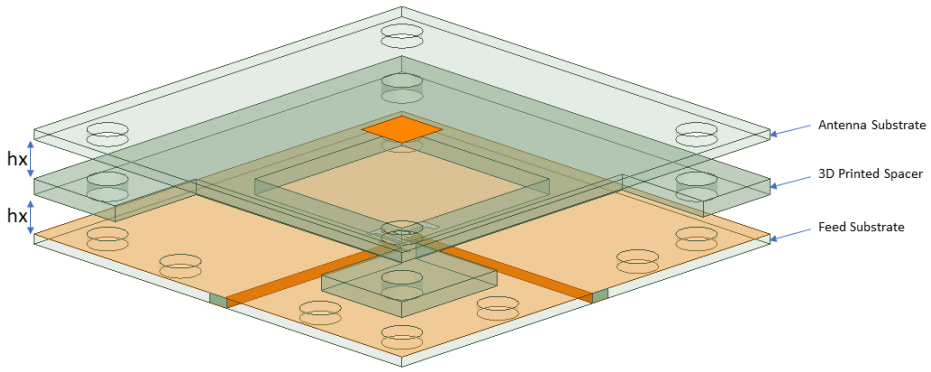

Figure 3.62: Airgaps between the 3D printed spacer and antenna substrates

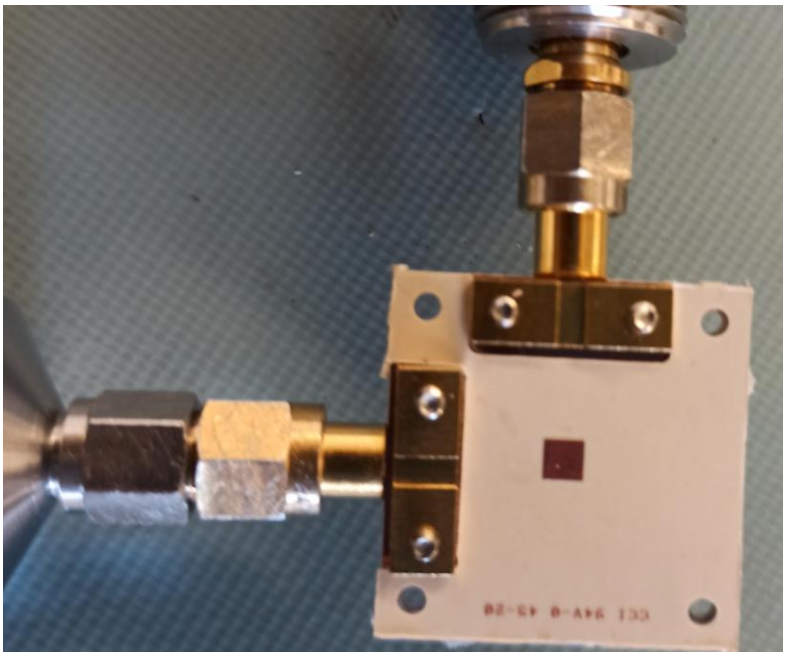

Figure 3.63: 28 GHz antenna with a 3D printed spacer

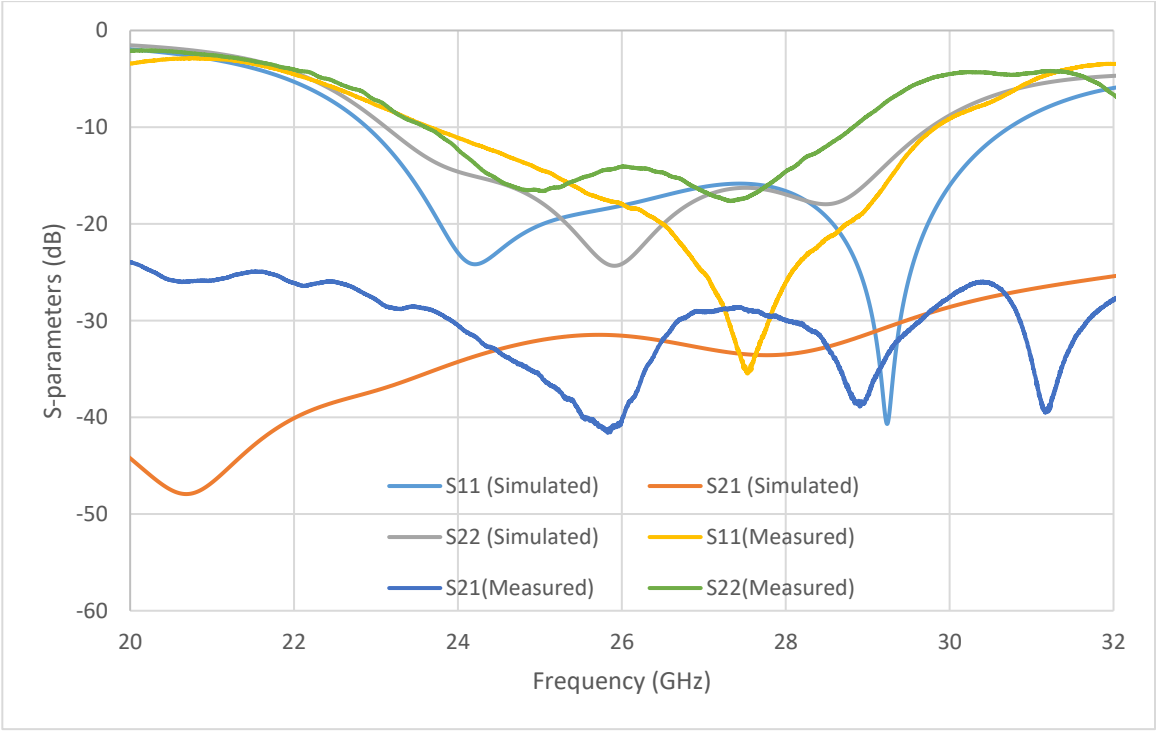

Figure 3.64: Measured and simulated s-parameters of 28 GHz antenna with a 3D printed spacer

To reduce the manufacturing costs a modified version of the design proposed in section 3.3 is manufactured. Instead of using two radiating elements only a single antenna is used as shown in figure 3.62. Both the feed network and the antenna were built on a 0.508 mm thick Rogers RT/Duroid 6002 substrate and are separated by a spacer 3D printed from PLA. This type of stack-up is more sensitive to manufacturing variations and typically has higher levels of back radiation in comparison to a multilayer stack-up. A picture of the manufactured prototype is shown in figure 3.63 and a comparison of the measured and simulated results are shown in figure 3.64. The measured antenna bandwidth is reduced in comparison to simulation results, S_{11} has a bandwidth of 16.5% instead of 28% and S_{22} shows an impedance bandwidth of 21.6% instead of 24.5%. The reduction in the operational bandwidth of the antenna can be attributed to the presence of small airgaps between the substrate layers and the spacer. Figure 3.65 shows the bandwidth reduction as a function of airgaps between the spacer and the antenna substrates for S_{11}. The larger the gap gets the lower the impedance bandwidth will be. From this we can also determine that there is an airgap of around 0.1 to 0.15 mm between layers. This can be corrected for either on the simulation level or by adding glue or a bonding layer between the substrates and the spacer. However, it is very important to simulate those bonding layers because they will affect the antenna S-parameters specially at mm-Wave frequencies. The presence of airgaps will also have a similar effect on S_{22} as shown in figure 3.66. in addition to bandwidth reduction a worsening in matching is also observed for S_{22}.

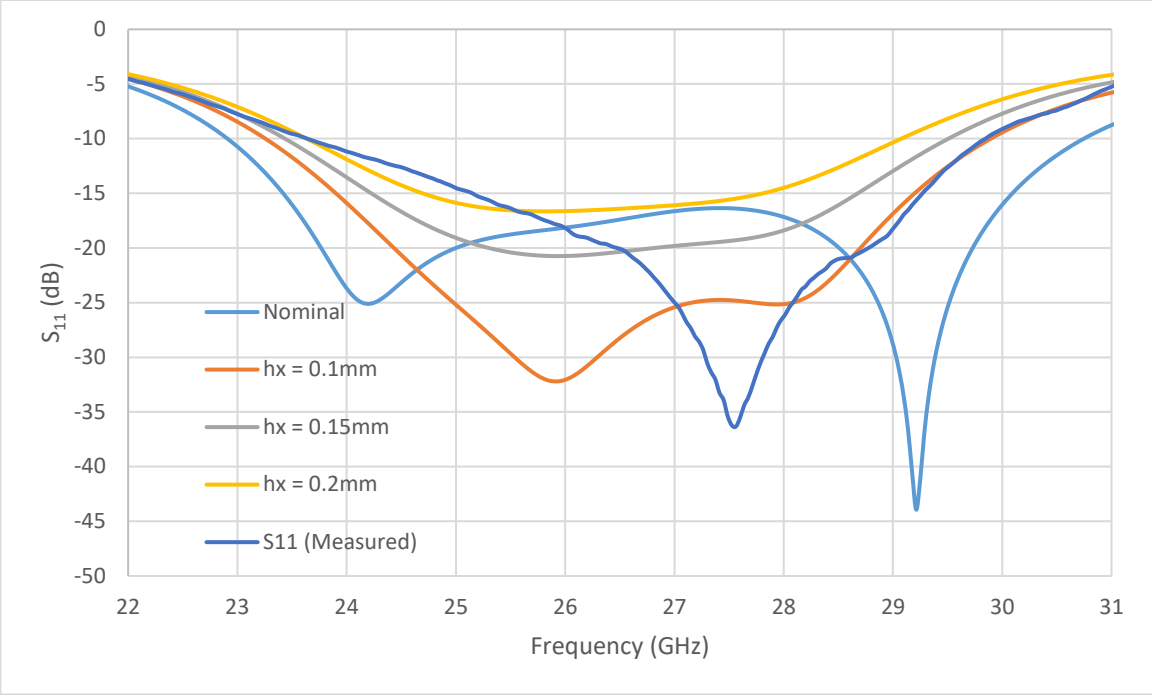

Figure 3.65: Effect of airgaps between the antenna substrates and the spacers on S_{11}

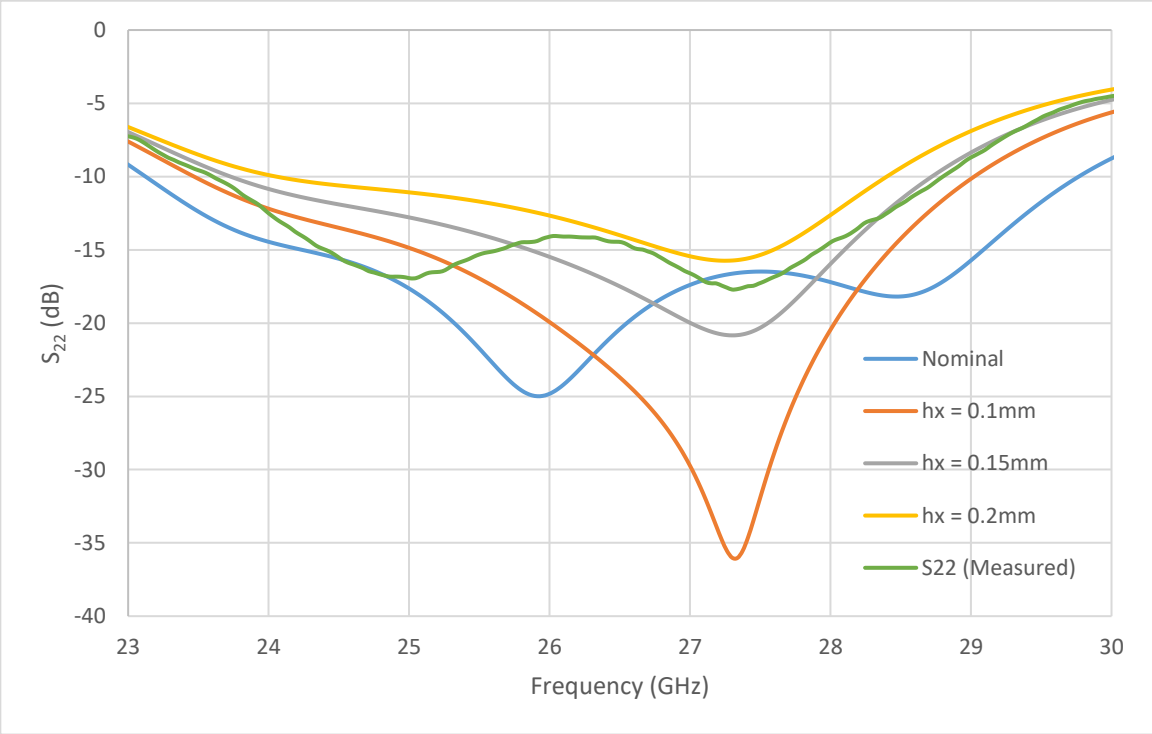

Figure 3.66: Effect of airgaps between the antenna substrates and the spacers on S_{22}

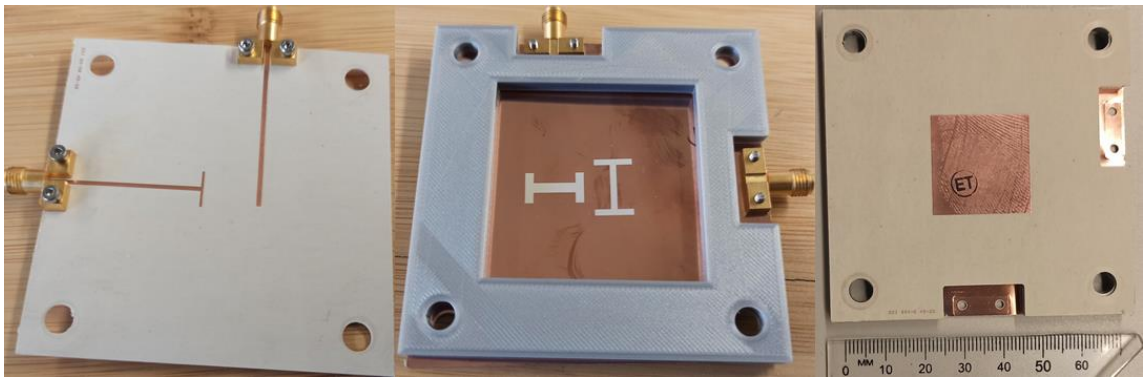

Figure 3.67: 4 GHz antenna with a 3D printed spacer

Another prototype like the one designed above is also manufactured around 4 GHz to cover one of the 5G NR (new radio) bands. Figure 3.67 shows the different layers of the designed antenna. Similar to the 28 GHz design here the antenna bandwidth is also reduced due to airgaps. The bandwidth of S_{11} drops from around 41% to 26% and S_{22} goes from 34.4% to 26%. Again, this can also be adjusted for either when simulating the antennas or by adding a thin layer of glue to hold everything together.

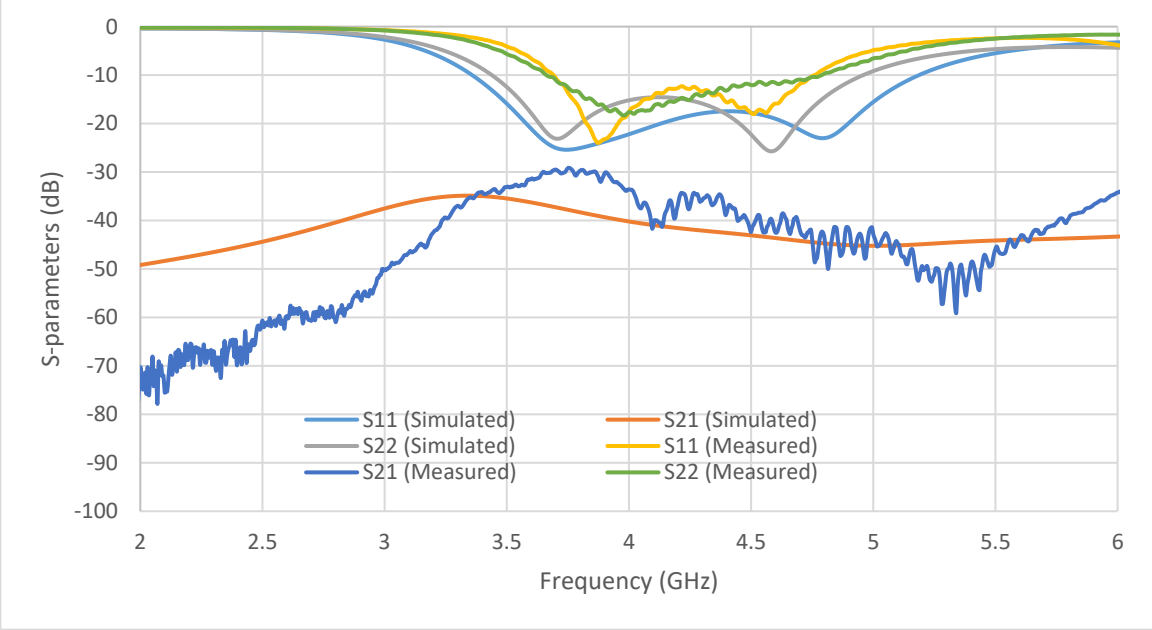

Figure 3.68: 4 GHz antenna with a 3D printed spacer measured and simulated results

3.5 Chapter Summary

To summarize, three types of stacked patch antennas with impedance bandwidth above 25% were proposed in this chapter. The effects of small airgaps and dimension variation from the manufacturing process and laminate properties and profiles could be more pronounced in comparison to similar designs at lower portions of the frequency spectrum. Therefore, a parametric study and sensitivity analysis were carried out for the most important parameters affecting the antenna performance. Techniques for port isolation enhancement were also examined, and a method capable of achieving better than 10 dB of isolation enhancement was proposed.

A dual linearly polarized slot coupled microstrip antenna such as the ones proposed in this chapter can be designed through the following design guidelines:

- To enhance the back-lobe radiation pattern, port coupling, and hence port isolation, an H shaped, or bowtie slot should be used.
- Ensuring that the feed lines are oriented orthogonally and increasing the offset between the slots as much as possible without degrading the level of coupling to the patch antenna, the best level of port isolation can be achieved.
- Tune the slot length to achieve the desired center frequency, and broader bandwidth can be achieved by increasing the slot length (resonant slot) at the expense of increased levels of back radiation or by adding multiple resonators.

All radiation patterns and gain plots presented in this chapter are for the case when port 1 is excited. Similar results are seen when the other port is excited, and therefore not shown here for the sake of brevity.

Table 3-2 shows the performance comparison of recently studied dual linearly polarized antenna designs in the literature at millimeter-wave frequencies. The three designs proposed in this work compare favorably in terms of bandwidth, profile, and port isolation. These new antenna element designs are promising candidates for 5G millimeter wave cellular applications. A higher percent impedance bandwidth and a lower profile is achieved in comparison to most designs proposed in the literature. Port isolation levels are also better than 40 dB over most of the band for all three designs proposed here, which are some of the highest levels of reported isolation at mm-Wave frequencies over such a broadband to the best of our knowledge.

Table 3-2 Performance comparison of millimeter-wave dual linearly polarized antennas

Reference	***Frequency (GHz)***	***Bandwidth (%)***	***Port Isolation (dB)***	***Antenna Profile***	***Number of PCB Layers for Feed Network***
[38]	60	15	≥ 37.2	0.066 λ_0	Single layer
[39]	60	17.6	≥ 26	0.226 λ_0	Multi-layer
[40]	24	18	≥ 35	0.153 λ_0	Multi-layer
[43]	29	22	≥ 20	0.285 λ_0	Single layer
[62]	33	42.4	NA	0.274 λ_0	Single layer
This work (Design I)	28	34.2	≥ 34	0.120 λ_0	Single layer
This work (Design II)	26.5	46.8	≥ 34	0.150 λ_0	Single layer
This work (Design III)	28	34.7	≥ 37	0.177 λ_0	Single layer

Chapter 4

Antenna Array Design and Results

With the growing demand for mobile services, mobile operators worldwide are turning to massive MIMO or mm-Waves to accommodate traffic. In the U.S., for example, more than 15% of adults use LTE all the time [65]. Mobile operators have started investing in mm-Wave bands such as the 28 and 39 GHz bands, mostly in the U.S., where large bandwidths are not available at sub 6 GHz to alleviate the traffic density problem. Moving to mm-Wave frequencies, however, comes with its challenges, such as power amplifier efficiencies and link budgets. For this reason, engineers have turned to the use of large antenna arrays of 64 to 256 elements to achieve antenna gains in the order of 25 to 30 dB. These types of dual linearly polarized arrays are capable of attaining the necessary linear EIRPs (Effective isotropically radiated power) in the range of 60 dBm[65]. In this chapter, a 4 and 16 element array are designed based on the patch and fractal antenna elements proposed in section 3.1. These antennas are a proof of concept for 5G antenna arrays operating in the mm-Wave frequency band from 24 to 30 GHz that can achieve a broadband gain of 12.5 and 18 dB, respectively. The antenna gain can be further increased to around 25 dB by using a 64-element array.

There are two types of antenna arrays, linear (one dimensional) or planar (two dimensional). Patch antennas are typically broadside radiators meaning that they have a maximum radiation pattern perpendicular to the surface of the antenna. Antenna array radiation patterns are a function of the single element radiation pattern and the array factor.

The array factor is calculated using the number elements, spacing, amplitude, and phase of element signals [66]. Larger element spacing and more antenna elements lead to a higher array directivity. In the interest of grating lobe suppression, though, it is best to space elements less than a half-wavelength apart. While keeping in mind that mutual coupling between closely spaced antennas can degrade its overall performance, there is a tradeoff to be made between the element spacing and the level of mutual coupling.

4.1 Feed Network Design

Different antenna array feeding techniques have been proposed by researchers over the years, such as series and corporate (parallel) feed networks [66]–[68]. These types of feed networks can also be used to scan the antenna beam in different directions. Corporate feed networks made up of 1: n dividers are typically utilized in patch antenna arrays. Progressive phase shifts or delay lines can be added between each element and the next to achieve the desired beam steering. Insertion losses of this type of feed can be high, especially in large antenna arrays at mm-Wave frequencies, which can degrade the antenna gain and reduce its efficiency.

Figure 4.1 shows the microstrip line corporate feed network designed to excite the antenna elements. For the 16-element array, four dividers are used to feed each column of 4 with a divider connecting them to the excitation point.

Figure 4.1: Corporate feed network

Bends in microstrip lines alter the input impedance of the divider. Therefore, mitering or chopping off a small section of the bend is necessary to compensate for the added capacitance from the 90-degree bend. Figure 4.2 below shows a mitered bend. The optimum miter dimensions can be calculated from the substrate height and microstrip line width using the equations proposed in [69], [70].

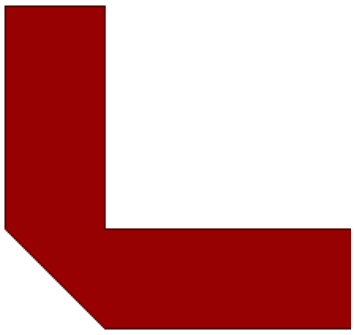

Figure 4.2: Mitered bend

At the T-junction of the divider, some of the power is reflected if the microstrip line widths are different. A V groove must be made at the junction of the two lines, as shown in figure 4.3, to compensate for this reflection.

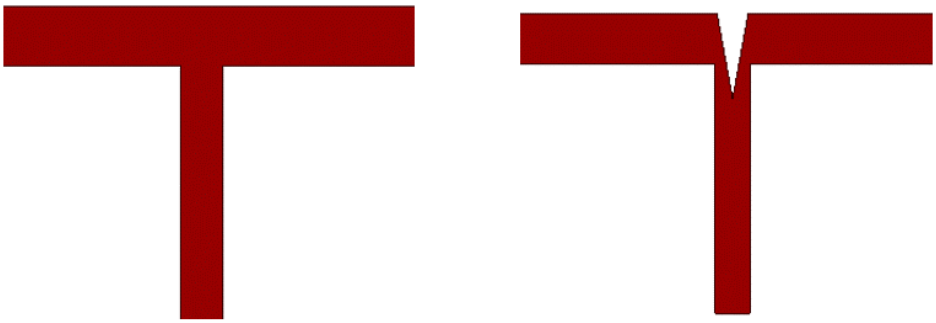

(a) (b)

Figure 4.3: T-junction (a) without and (b) with groove

Multi-section quarter-wave transformers are used here to improve the divider impedance matching over a wider bandwidth. Figure 4.4 shows the first 1:2 power divider. Two similar dividers can be added to make a complete corporate feed network.

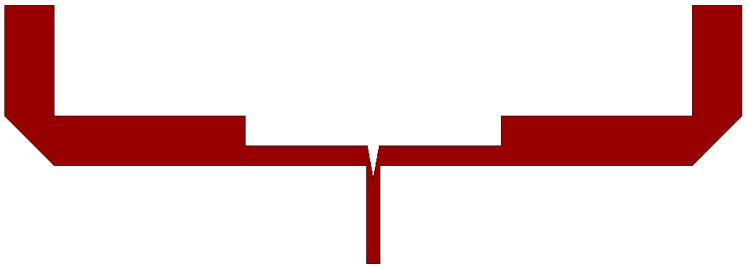

Figure 4.4: 3-dB power divider

4.2 4x1 Antenna Array

In this section, a linear 4 element antenna array operating in the frequency range from 24 to 30 GHz (VSWR ≥ 2) is designed. Figure 4.5 shows the exploded view of the antenna and the feed network. The goal here is to develop a linear array based on the single element proposed in section 3.1, with a better matching than 10 dB across the frequency band of interest.

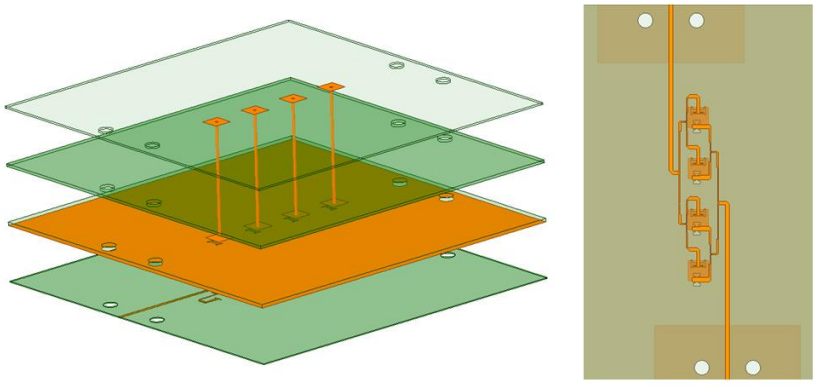

(a) (b)

Figure 4.5: 4x1 antenna array (a) stack-up (b) feed network

Figure 4.6 shows the S-parameter results of the optimized linear array, a 10 dB bandwidth above 21% is achieved in the frequency band from 24 to 30 GHz. The bandwidth of the proposed single element antenna is wider than the bandwidth of the array, which is limited by the bandwidth of the feed network.

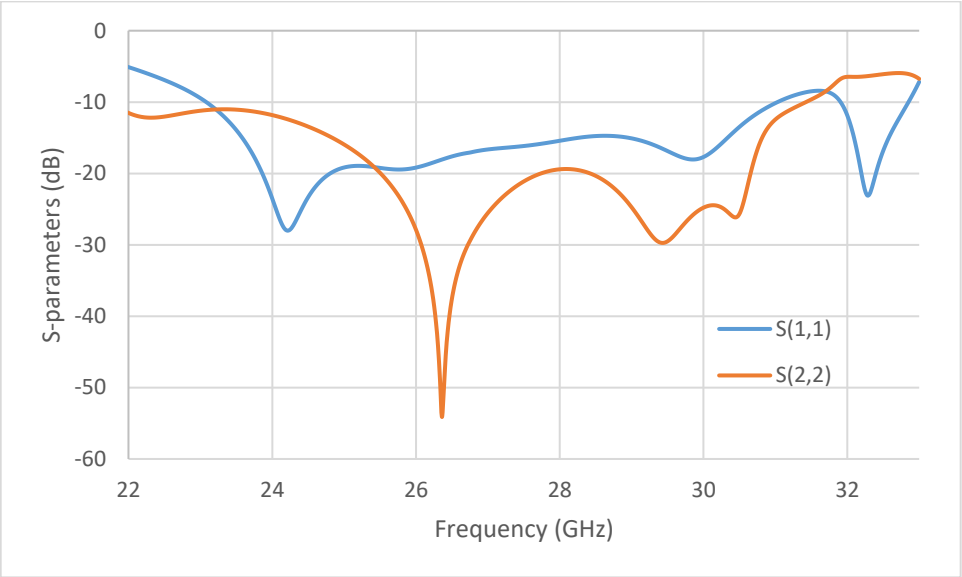

Figure 4.6: Optimized antenna S-parameters

The antenna array broadside gain is around 12.5 dB at 28 GHz. Figure 4.7 shows the E_Θ and E_Φ plots in the $\Phi = 0$ and $\Phi = 90$ planes, respectively, at 28 GHz. The cross-polarization levels for both $\Phi = 0$ and $\Phi = 90$ planes are 30 dB below the co-polar patterns at boresight.

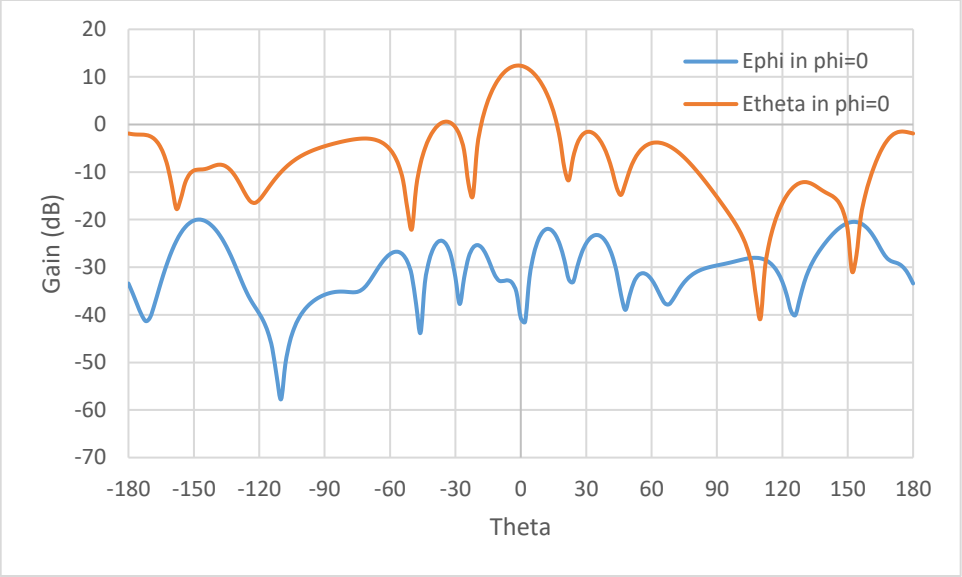

(a)

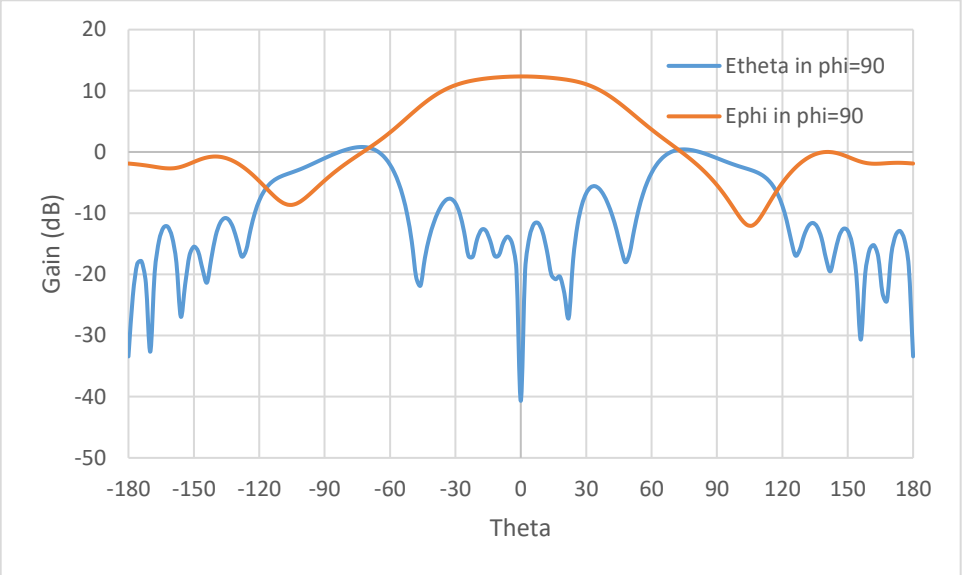

(b)

Figure 4.7: Gain patterns in (a) Φ = 0 and (b) Φ = 90 at 28 GHz

The array gain over frequency is stable from 24 to 30 GHz, as shown in figure 4.8. Gain values vary between 11 and 13 dB in the band of interest. The decrease in gain at the lower frequency edge can be attributed to the worsening of the impedance matching at those frequencies.

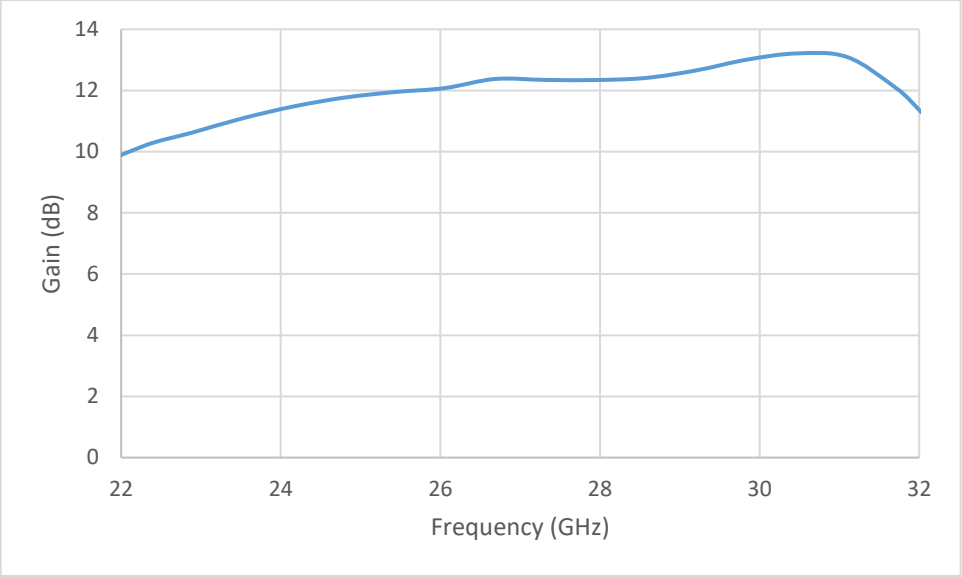

Figure 4.8: Gain as a function of frequency

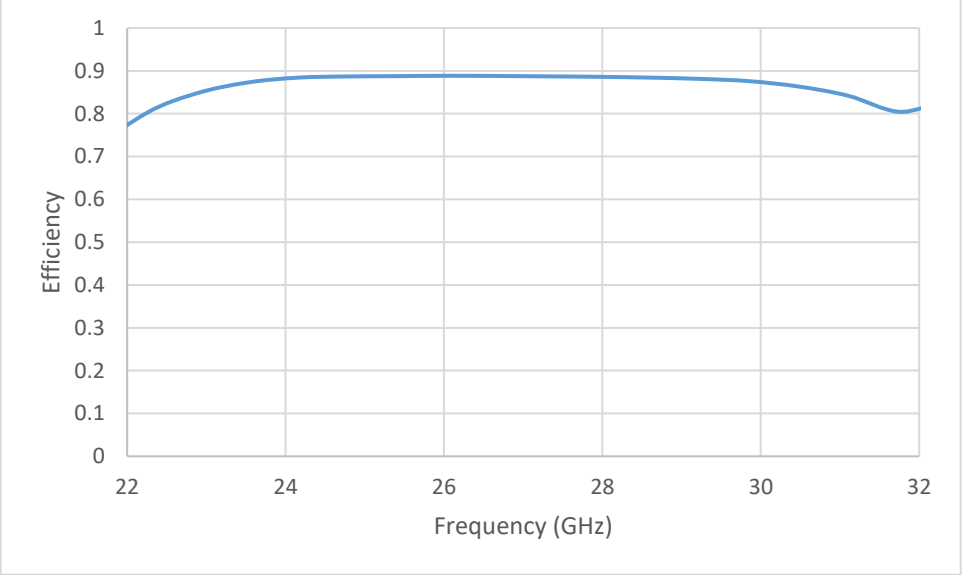

Figure 4.9: Antenna efficiency vs. frequency

Figure 4.9 shows the antenna efficiency of the array. As can be seen from the plot, the simulated antenna efficiency is better than 80% across the band of interest. The antenna front to back ratio is better than 15 dB across the band, and better than 20 dB from 24 to 30 GHz. Figure 4.10 shows the simulated antenna front to back ratio from 22 to 32 GHz.

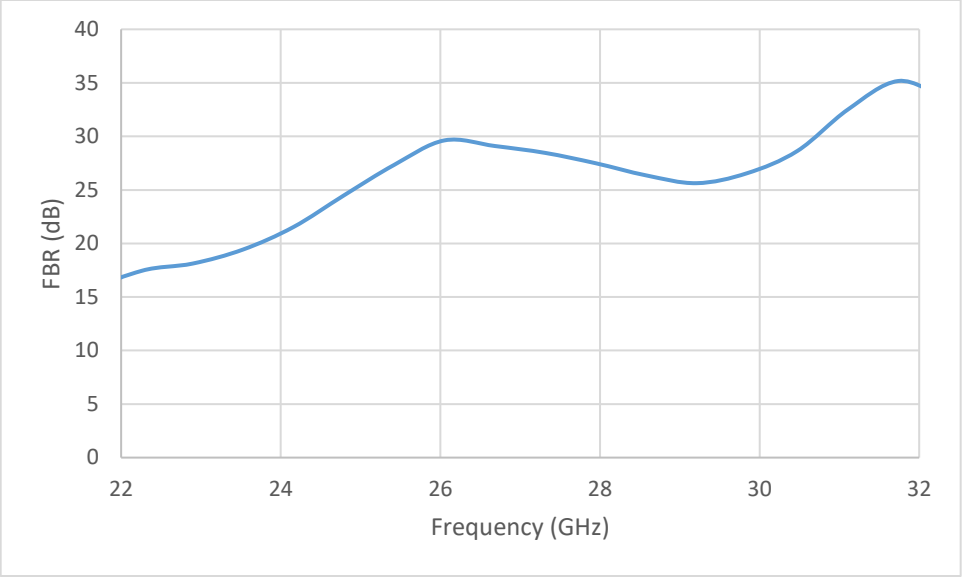

Figure 4.10: Antenna front to back ratio

4.3 4x4 Antenna Array

Two planar 16-element antenna arrays are designed and simulated in this section. The two antennas are based on the patch and fractal antenna elements proposed in section 3.1. Parameters to keep in mind when designing antenna arrays are the array directivity, sidelobe levels (SLL), element spacing (grating lobes), and mutual coupling. The antenna directivity or gain can be increased by increasing the element spacing or the number of elements in the array. Increasing the element spacing, however, causes the appearance of grating lobes, reducing the antenna broadside gain, and causing interference. Therefore, element spacing must always be kept around half a free space wavelength or less to avoid the generation of grating lobes. Mutual coupling between antenna elements is also a function of the element spacing, where closely spaced antennas have a worse degree of coupling. Sidelobe levels can be reduced either by increasing the number of elements in the array or the use of tapering (unequal excitations). More information on different tapering techniques and advantages can be found in [66]. All these parameters must be kept

in mind when designing an antenna array. The tradeoffs between them mostly depend on the application where the array is employed.

Figure 4.11 shows the planar array before the integration of the feed network. The antennas are surrounded by a set of metallic vias acting as a cavity. The center to center element spacing is 7mm, which is equivalent to 0.65 λ_0.

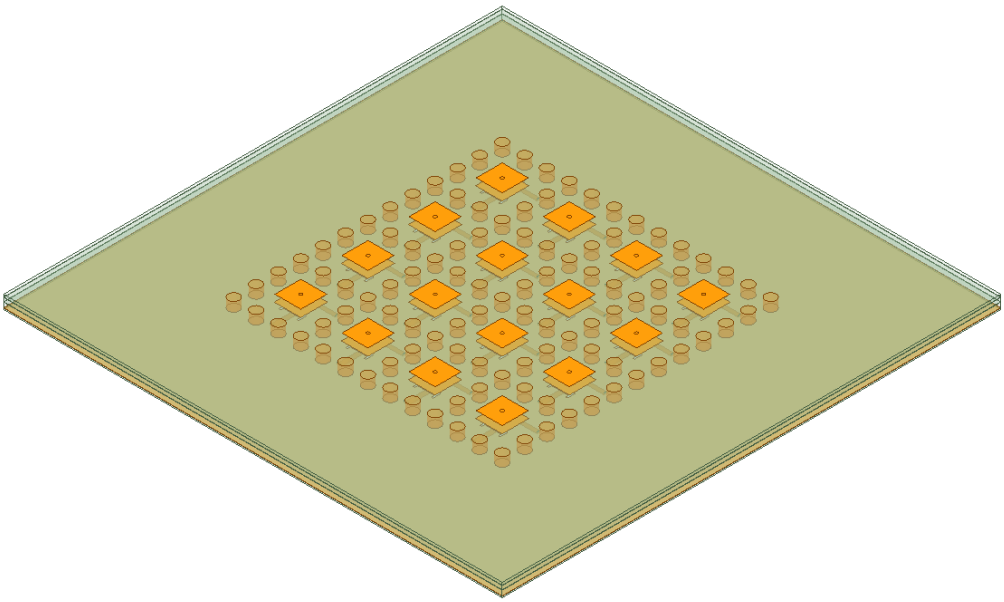

Figure 4.11: Antenna array without corporate feed network

Mutual coupling between the antenna elements is better than 17 dB across the band of interest, and sidelobe levels are better than 10 dB. Figure 4.12 shows the port S-parameters for all ports in the array. S-parameters for all ports are roughly the same, where the even ports are for one polarization, and the odd ports are for the other. Figure 4.13 shows the mutual coupling between some elements in the array; the coupling between all elements in the array is better than 17 dB.

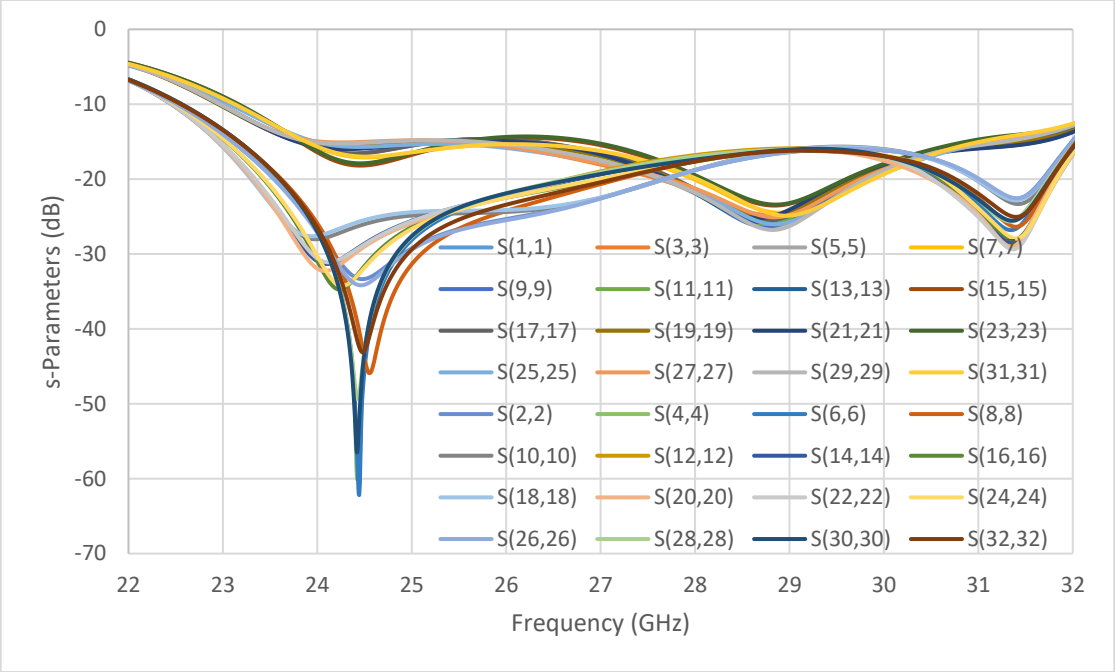

Figure 4.12: S-parameters for all ports

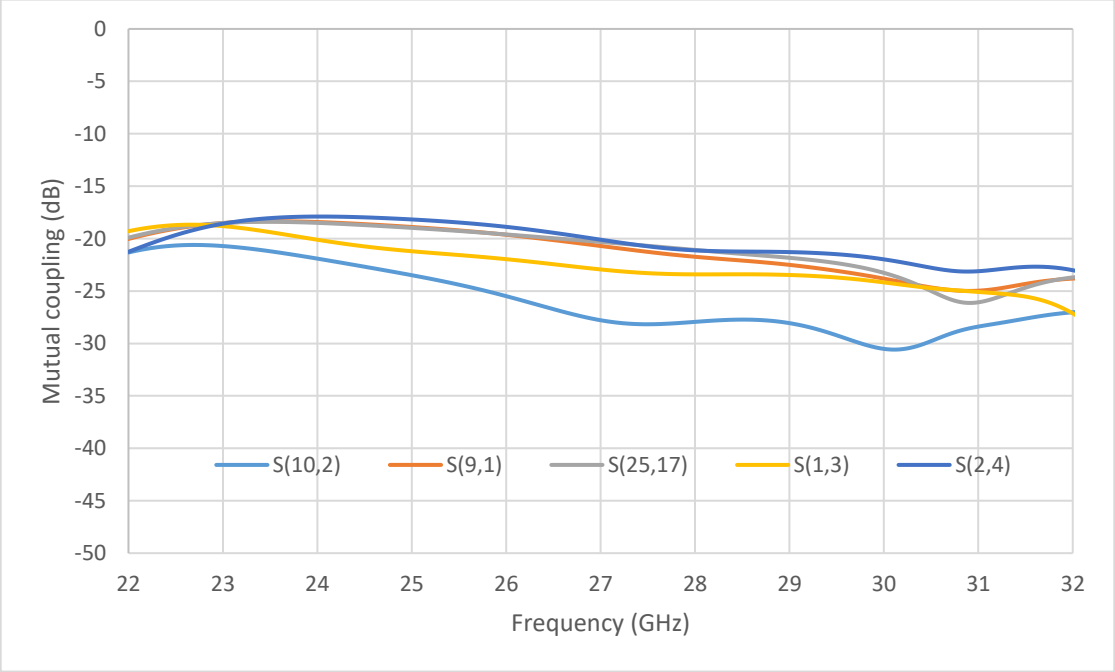

Figure 4.13: Mutual coupling between array elements

The array broadside gain is around 18 dB at 28 GHz. Figure 4.14 shows the E_Θ and E_Φ radiation patterns in the $\Phi = 0$ and $\Phi = 90$ planes respectively, at 28 GHz. The cross-

polarization levels are better than 20 dB in both the E and H planes. The array gain over frequency is stable and varies between 17.8 dB and 19 dB, as shown in figure 4.15.

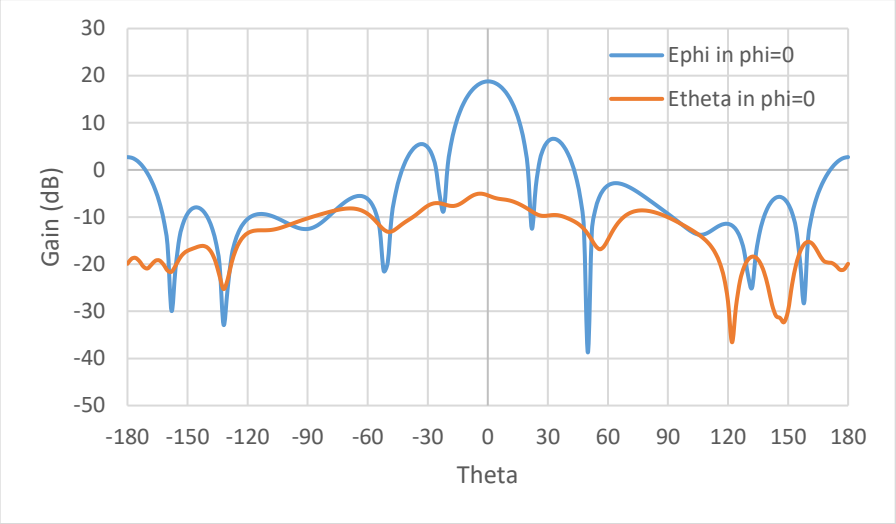

(a)

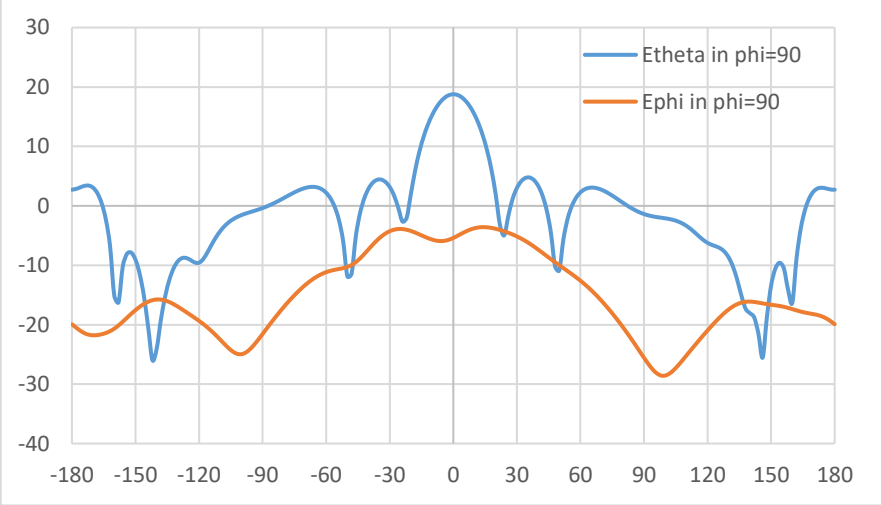

(b)

Figure 4.14: Gain patterns in (a) Φ = 0 and (b) Φ = 90 at 28 GHz

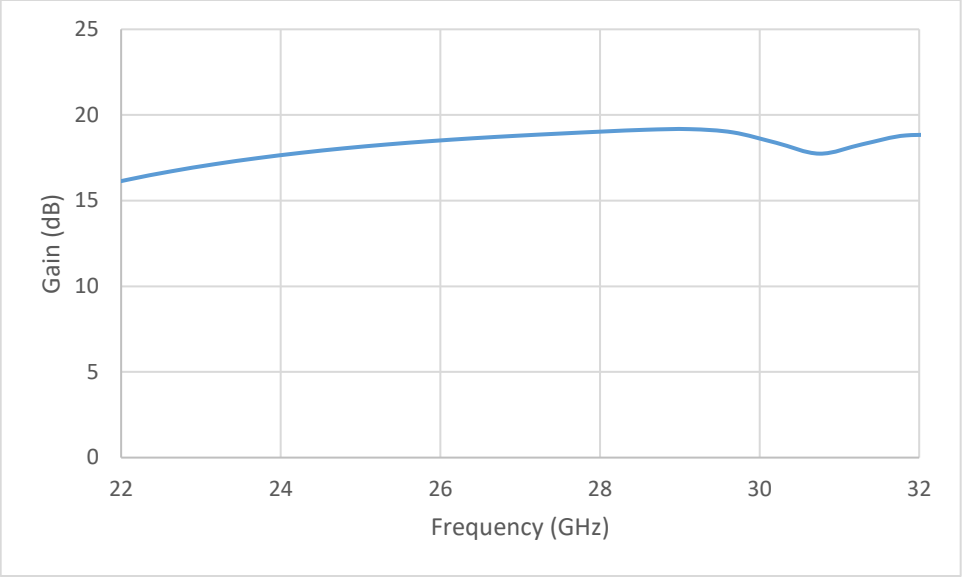

Figure 4.15: Antenna gain vs. frequency

Simulated antenna efficiency is shown in figure 4.16. The antenna efficiency is better than 90% across the band, like that of the single element antenna. The antenna front to back ratio is better than 10 dB, as shown in figure 4.17.

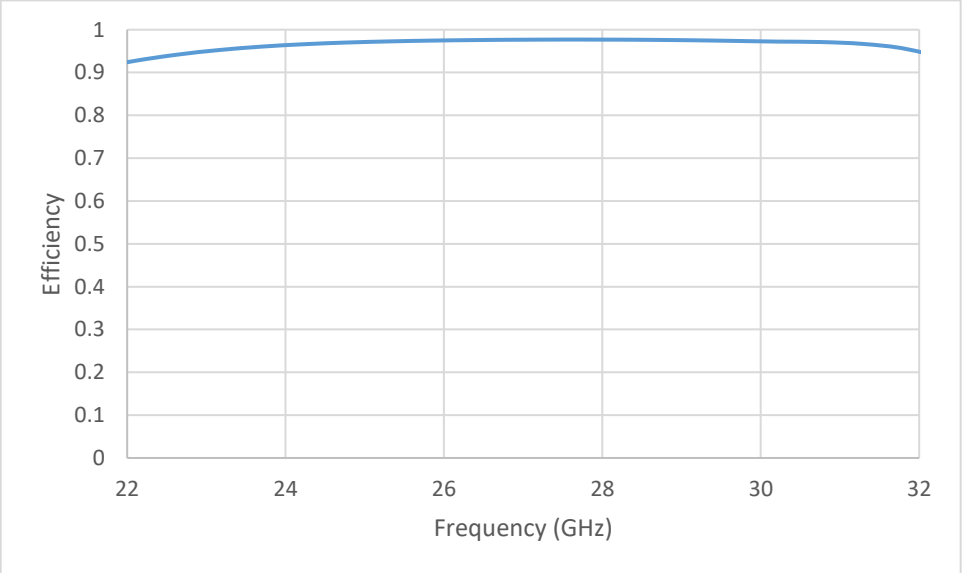

Figure 4.16: Simulated antenna efficiency

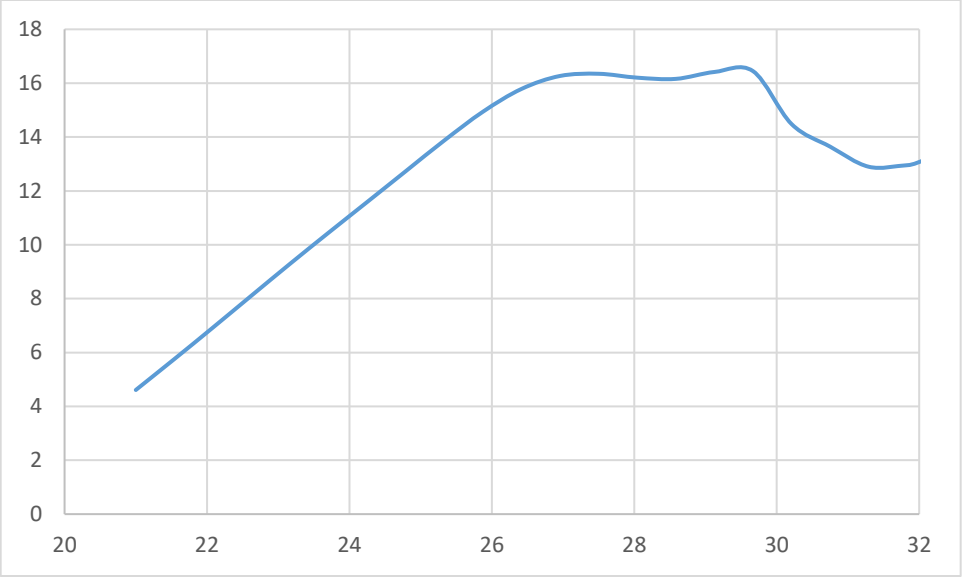

Figure 4.17: Antenna front to back ratio

Figure 4.18 shows the exploded view of the antenna and its corporate feed network on the right side of the figure. All layers are etched on a Rogers RT/Duroid 5880 laminates, like the stack-up of the single element antenna. The array performance requirements are a 10 dB impedance bandwidth of around 20% (24.25 – 29.5 GHz), sidelobe levels (SLL) of 10 dB or more below the main beam, and inter-element coupling that is better than 15 dB. Amplitude tapering can be employed to reduce the SLL further for other applications. Mutual coupling between array elements, on the other hand, can be improved by increasing the element spacing at the expense of a narrower scan range.

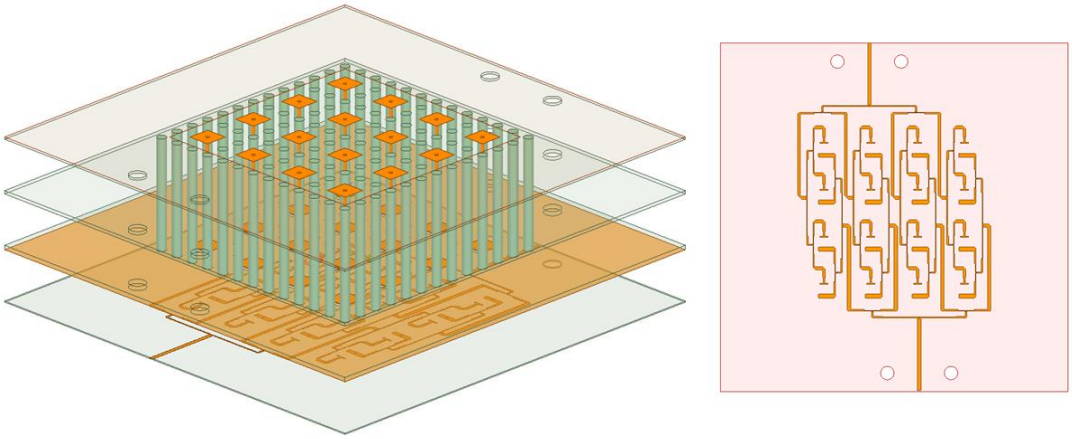

(a) (b)

Figure 4.18: 16-Element antenna array (a) exploded view (b) feed network

The antenna element and corporate feed network for this array were optimized separately and then integrated to reduce simulation times. Figure 4.19 shows the optimized S-parameters for the array. An impedance matching of 10 dB or better was achieved in the band of interest from 24.25 to 29.5 GHz. Therefore, covering both the 26 and 28 GHz millimeter wave bands proposed for the next generation of 5G by some countries.

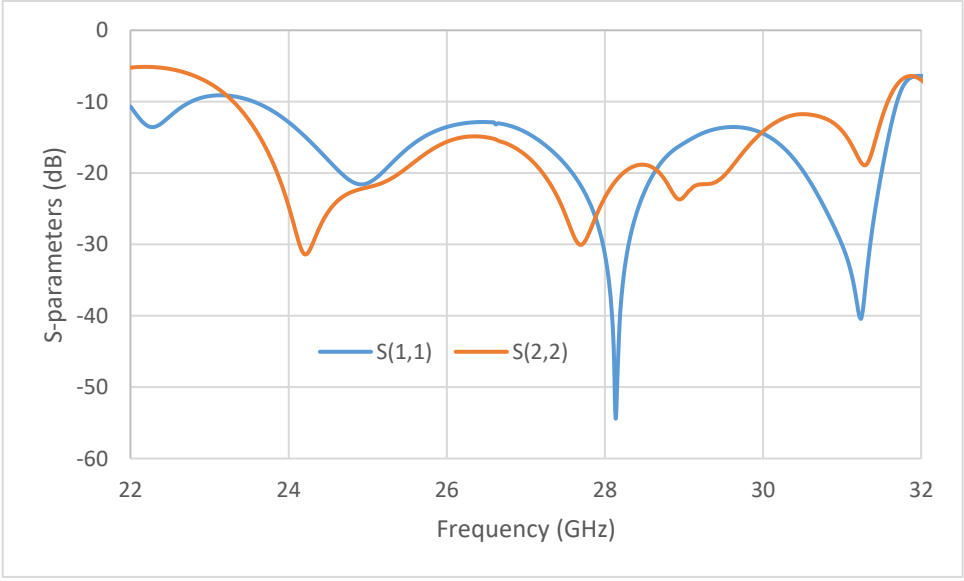

Figure 4.19: Optimized antenna S-parameters

The antenna array co-polar and cross-polar radiation patterns in the E and H planes at 28 GHz are shown in figure 4.20 (a) and (b), respectively. Cross-polarization levels are better than 20 dB in both planes.

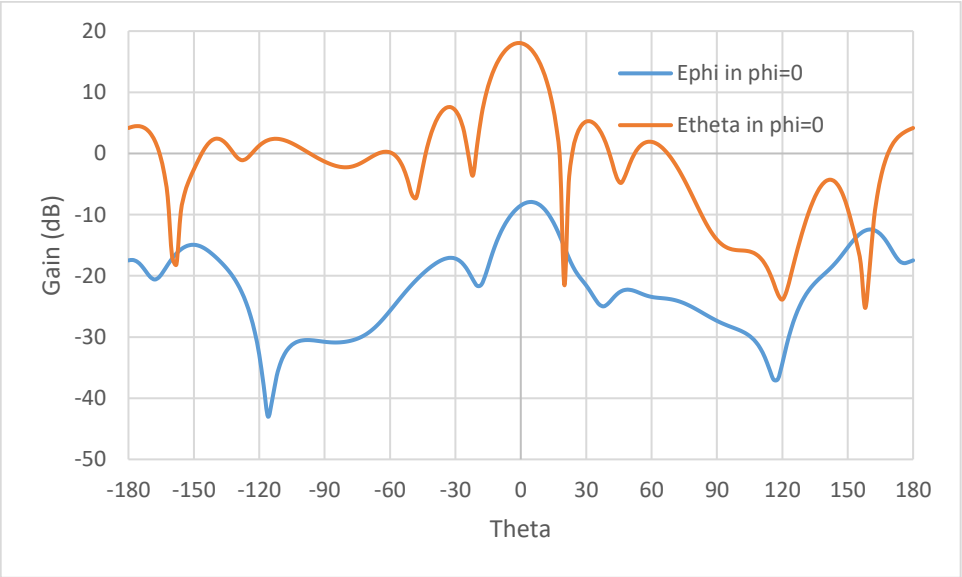

(a)

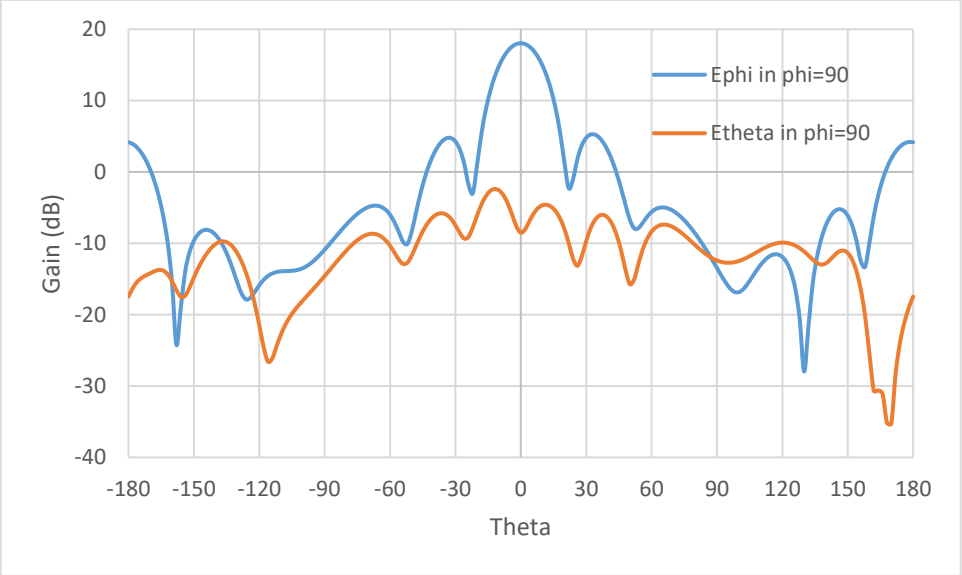

(b)

Figure 4.20: Gain patterns in (a) Φ = 0 and (b) Φ = 90 at 28 GHz

Figure 4.21 shows the array gain across the frequency band of interest. The gain is between 17 and 18.4 dB from 24 to 30 GHz. Simulated array efficiency is better than 85% from 24 to 30 GHz, as shown in figure 4.22.

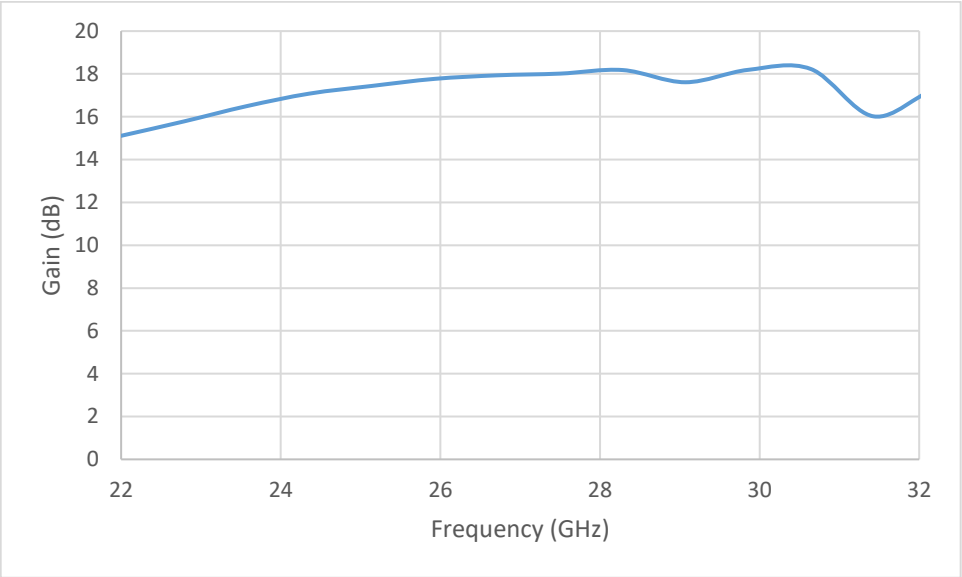

Figure 4.21: Array gain vs. frequency

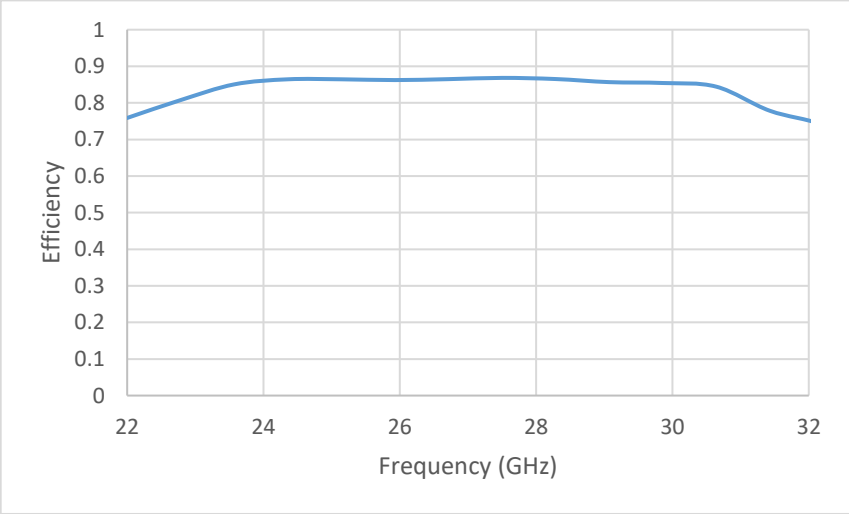

Figure 4.22: Simulated antenna array efficiency

The array front to back ratio is better than 12 dB from 24.25 to 29.5 GHz, as shown in figure 4.23. This value is slightly lower than the single element antenna, which has an FBR

of 15 dB across the band. This could be a result of differences in the slot lengths because the antenna had to be optimized again before corporate feed integration. The corporate feed network itself could also be decrease the FBR.

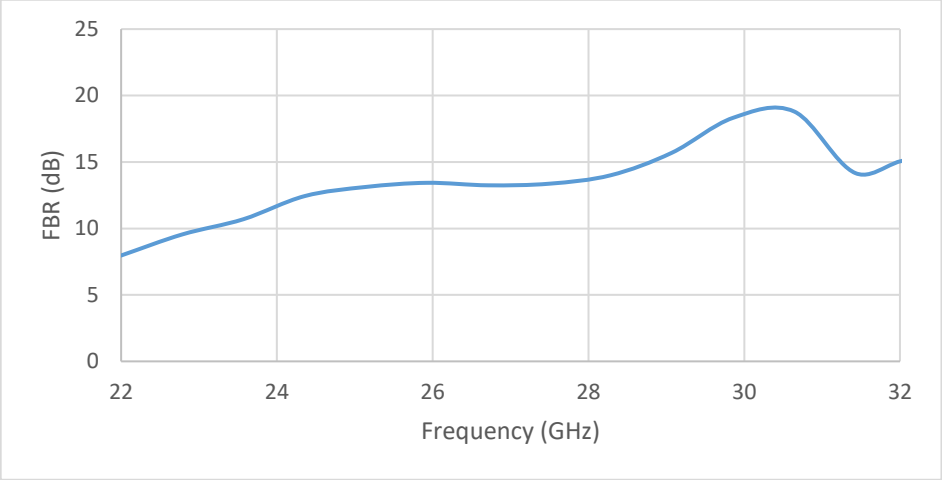

Figure 4.23: Antenna array front to back ratio

A 16-element fractal array based on the single element fractal proposed in section 3.1 is designed here. Figure 4.24 shows the optimized S-parameters for the array. The array is matched (return loss ≥ 10 dB) from 24.25 to 29.5 GHz, covering both the 26 and 28 GHz millimeter wave bands, which are two of the likely candidates for 5G.

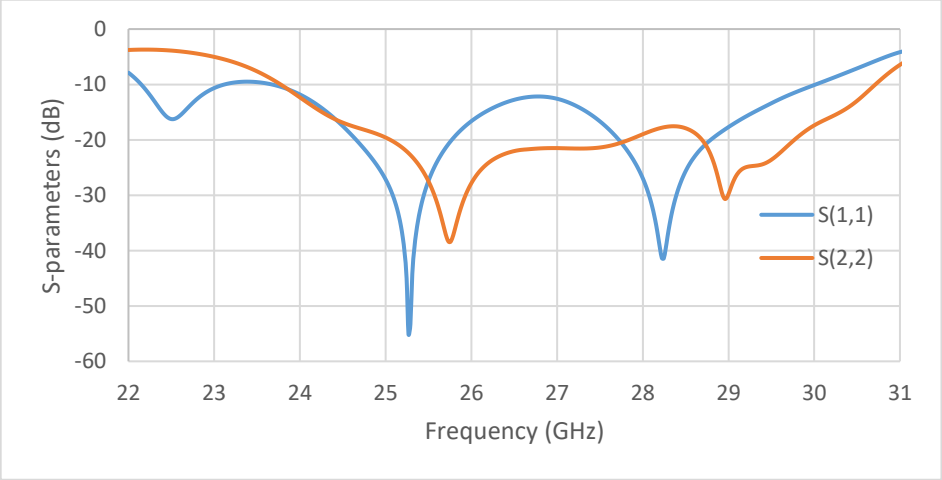

Figure 4.24: Optimized fractal antenna S-parameters

The antenna array broadside gain is around 18 dB at 28 GHz. Figure 4.25 (a) and (b) shows the E_Θ and E_Φ plots at 28 GHz in the $\Phi = 0$ and $\Phi = 90$ planes, respectively. The cross-polarization levels for both $\Phi = 0$ and $\Phi = 90$ planes are better than 20 dB.

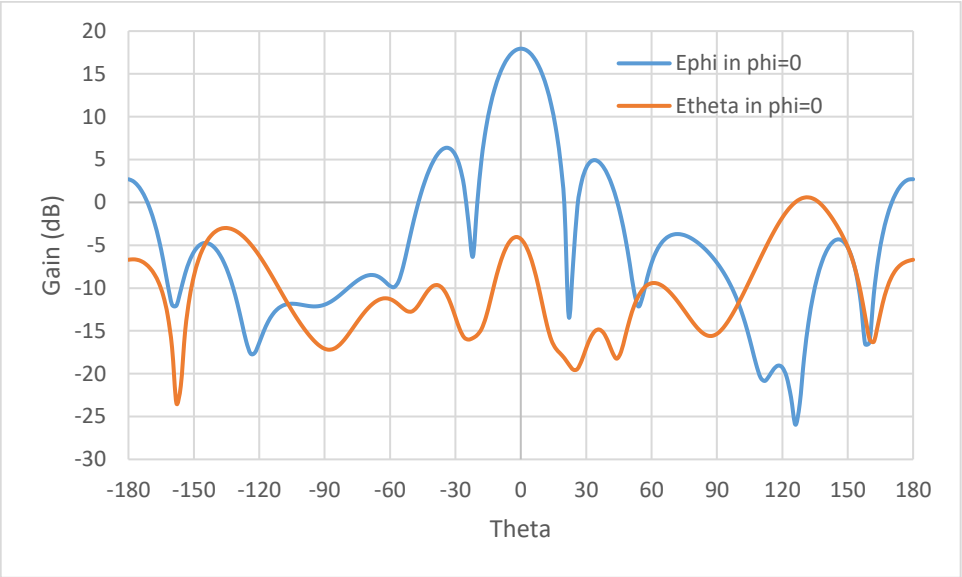

(a)

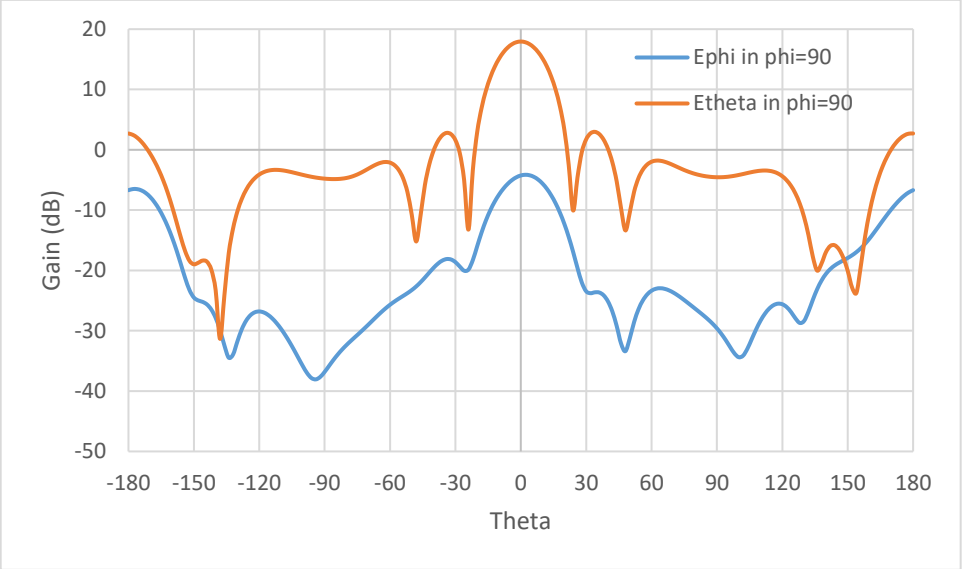

(b)

Figure 4.25: Fractal array gain patterns in (a) Φ = 0 and (b) Φ = 90 at 27 GHz

Figure 4.26 shows the fractal array gain vs. frequency. Where the array gain varies between 16 and 18 dB across the band of interest. The gain drop at the lower edge of the band around 24 GHz can be attributed to the rapid change in the antenna return loss. The array efficiency is slightly lower than that of the single element. However, a radiation efficiency above 82% is still maintained across the frequencies of interest, as seen in figure 4.27.

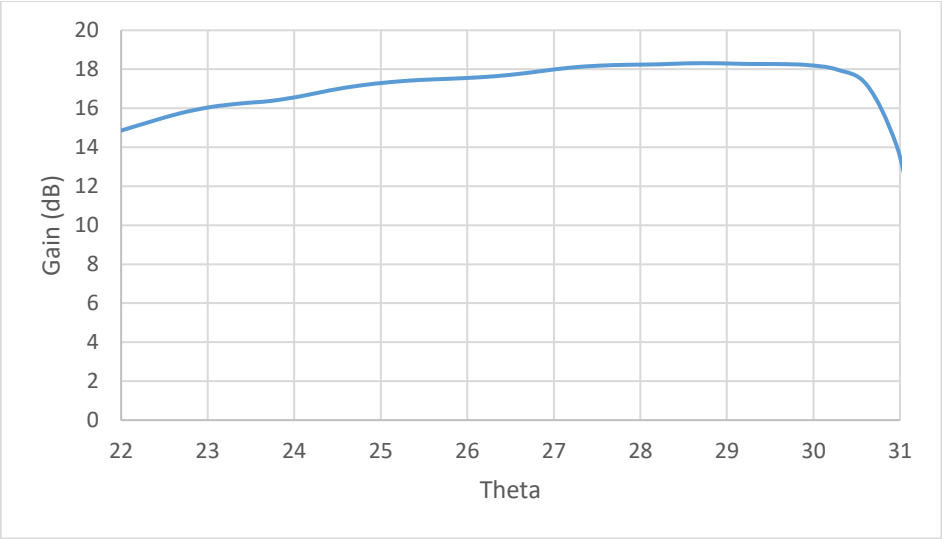

Figure 4.26: Fractal array gain vs. frequency

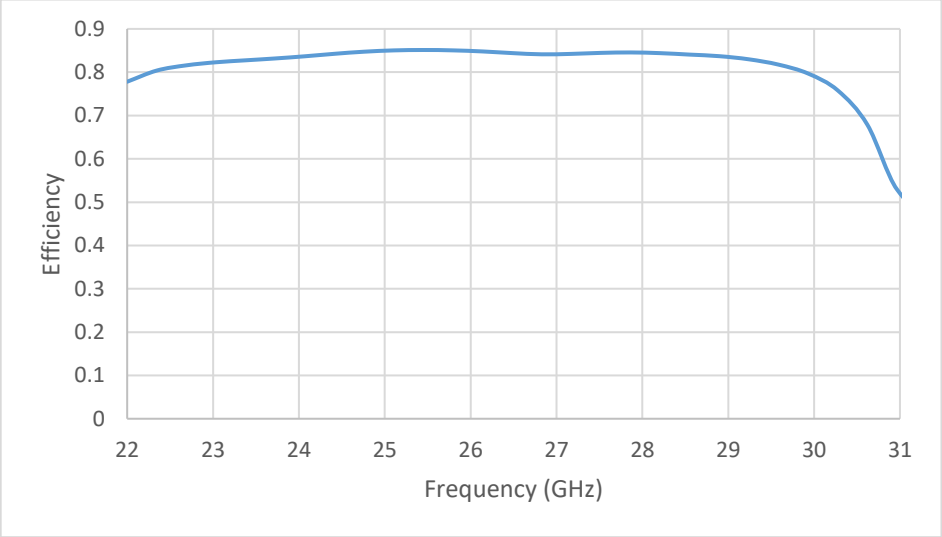

Figure 4.27: Fractal array simulated efficiency

Figure 24.8 shows the array front to back ratio from 22 to 31 GHz. This array has an FBR of 12 dB or more from 24.5 to 29.5. If a better FBR is required, a reflector can be used below the ground plane, or stripline feeding can be employed.

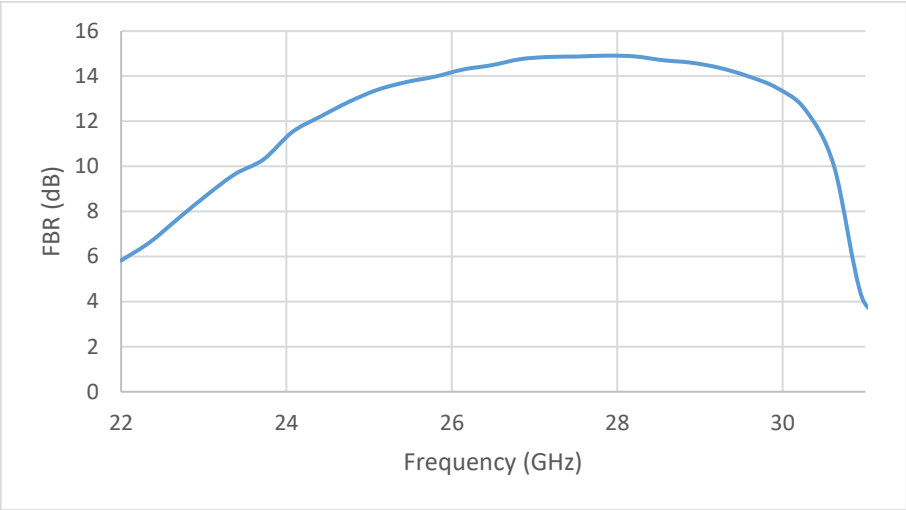

Figure 4.28: Fractal array front to back ratio

4.4 Chapter Summary

In this chapter, a four and sixteen element array operating from 24 to 30 GHz were designed to serve as a proof of concept for a mm-Wave 5G antenna array. These antennas have gains of 12.5 and 18 dB, respectively. Array types, array feeding techniques, and the concept of array factor were also briefly discussed. Next, important design parameters for a corporate feed network are covered, along with the four- and sixteen-way power divider designed to feed the arrays. Both antenna arrays designed in this chapter have an impedance bandwidth of 21%, covering the frequencies from 24 to 30 GHz, with a return loss better than 10 dB. The arrays also met the design goals they were designed for, with a gain of 12.5 dB for the linear array (4-element), and a gain of around 18 dB for the planar array (16-element). Sidelobe level in both designs were also lower than 10 dB. These designs are good candidates for 5G mmWave antenna arrays.

Chapter 5

Conclusions and Recommendations

5.1 Conclusions

The continuous growth in mobile communication technologies from the 1st generation to the currently under development 5th generation calls for the continuous development of new antenna systems. 5G will offer users a better experience through higher data rates and lower latency. The availability of larger millimeter wave bands worldwide will assist in rolling out these services. The benefits of designing advance antenna systems at the frequencies outweigh its challenges. Some of these benefits are increasing throughput and enhancing coverage in challenging propagation environments.

Microstrip antennas have many desirable characteristics but one of their main disadvantages are their narrow impedance bandwidth. Even though there is an abundance of publications showing techniques to increase the operation bandwidth of patch antennas below 6 GHz, there are not as many designs operating above 15 or 20 GHz. Hence the goal of this thesis was to design a broadband dual linearly polarized microstrip antenna with high port isolation to cover the 26 and 28 GHz bands (24.25 – 29.5 GHz) proposed for 5G. Three antenna designs with a similar stack-up were proposed offering an impedance bandwidth of more than 30% with port isolation levels that are better than 30 dB.

The first antenna design was built on a four-layer Rogers RT/Duroid 5880 substrate. Two capacitively coupled patch antenna fed through a slot in the ground plane was used to increase the antenna bandwidth. This antenna has an impedance bandwidth of 34.2% and

better than 34 dB port isolation across the band. A second design using a foam layer between the two antennas to increase its bandwidth was also proposed, achieving an impedance bandwidth of 46.8% and isolation above 34 dB. The antenna achieved a higher impedance bandwidth (around 5%) and its profile was also much lower (0.15 λ_0 in comparison to 0.27 λ_0) than similar designs. A shorting post extending from the ground plane to the radiating patch was used in both designs to increase the port isolation by more than 10 dB. A Sierpinski carpet fractal was also designed using a similar stack-up to both antenna designs I and II. Antenna design III replaced the foam layer in design II with a 3D printed spacer made of PLA. This design has port isolate better than 37 dB and 34.7% impedance bandwidth. Some of these results have been confirmed by measurements. However, obtaining satisfactory measurements are challenging as the effect of fabrication tolerances become more pronounced at these high frequencies.

Next two antenna arrays a four and a sixteen element were designed using the patch and fractal single elements from design I. The arrays had better than 10 dB return loss from 24 to 30 GHz, with sidelobe levels that are better than 9 dB. An SIW cavity was used between antenna elements to reduce the level coupling between arrays.

5.2 Future Directions

Future research possibilities include a second prototype of antenna design II can be manufactured and tested using a rigid foam such as LAST-A-FOAM RF-2200 that can withstand the heat and pressure applied during the manufacturing process. Antenna design I can also be fabricated again, but this time around a slightly thicker feed substrate, to reduce connector mismatches due to misalignment. Of course, one should keep in mind feedline radiation when this is being done, as thicker substrates will lead to thicker

microstrip line which in turn will lead higher levels of feedline radiation. A version with and without the SIW cavity can also be made to investigate if poor via metallization can be an issue in deteriorating the antenna performance.

Antenna design III can also be manufactured and tested by building the 3D printed spacer and manufacturing the rest of the layers on PCB. An initial prototype can be manufactured at a lower frequency to reduce the manufacturing cost, like what was shown in the measurements section.

For antenna arrays a different feeding technique should be investigated to reduce the losses from the microstrip feed network, an SIW corporate feed network is a good example, since it can reduce the level of back radiation from the feed network itself, something along the lines of what is proposed in [71], [72] is a good place to start. The integration of active elements (switches and phase shifters) for beam steering should also be investigated. Larger arrays for a 5G base station array can also be manufactured, integrated with other transmitter/receiver building blocks, and tested.

Appendix A. Slot Coupled Microstrip Antenna Design Equations and Guidelines

Figure A-5.1 shows the exploded view of slot coupled microstrip antenna. The antenna is made up of two substrate layers, a low permittivity substrate for the patch, and a second substrate for the feed network. This allows us to choose a high permittivity substrate for the integration of MMIC's if needed [67].

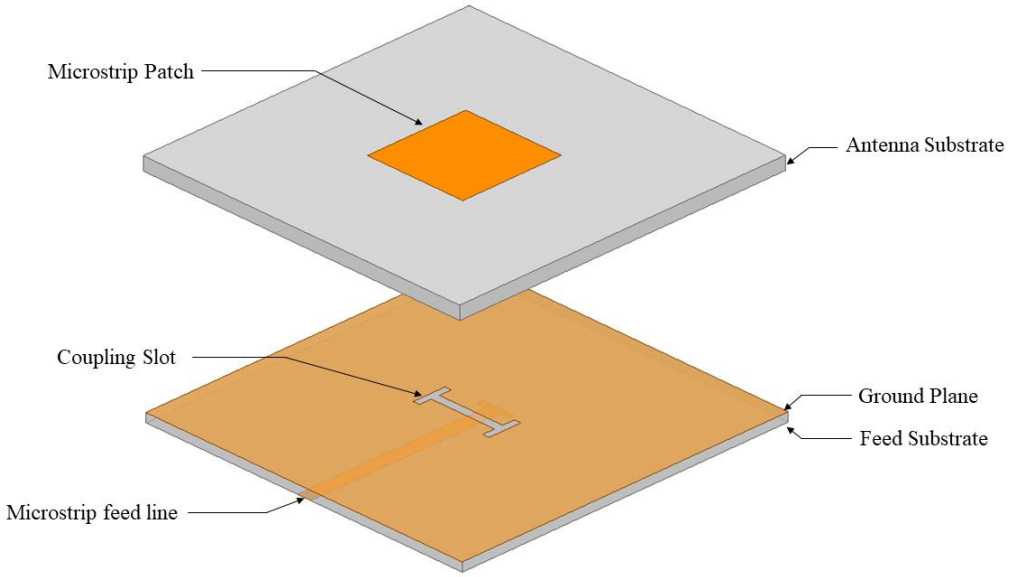

Figure A-1: Slot coupled microstrip antenna geometry

The most important material and dimensional properties are summarized below:

Antenna substrate parameters:

The antenna substrate thickness and dielectric constant effect both the antenna impedance bandwidth and radiation efficiency. Where antennas etched on thin low permittivity materials have a better radiation efficiency. As the substrate thickness is increased, the impedance bandwidth gets wider, its efficiency drops, however. Antennas mounted on thicker substrates will also have a lower level of coupling, therefore requiring a larger slot and resulting in a higher level of back radiation. Figure A-5.2 shows the achievable antenna bandwidth and efficiency as a function of dielectric constant and antenna profile. From this we can conclude that the antenna dielectric properties and substrate thickness are typically determined based on the desired impedance bandwidth and antenna efficiency. Using thicker substrates will lead to a larger impedance bandwidth at the expense of radiation efficiency and worse scan angles due to the excitation of surface waves.

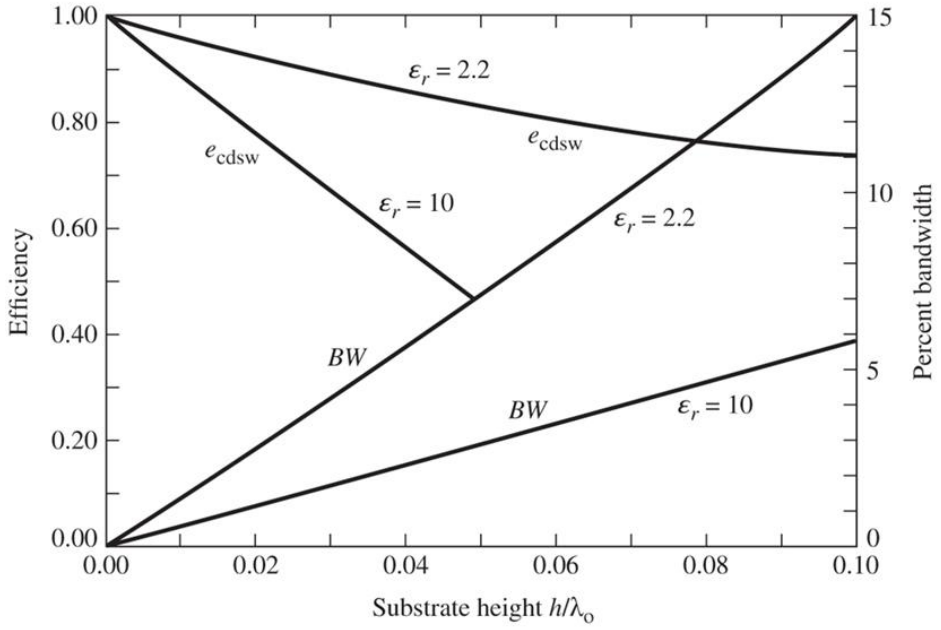

Figure A-2: Efficiency and impedance bandwidth versus substrate thickness for a rectangular microstrip antenna © IEEE 1992 [Reprinted with permission from John Wiley & Sons]

Patch antenna Dimensions:

The required patch dimensions to excite the dominant mode of a microstrip patch antenna is approximately half a wavelength. Where antennas are typically designed to have a length slightly less than half a wavelength to account for the fringing fields. A good estimate to start with is:

$$L = \frac{\lambda_e}{2}$$

Where λ_e is the effective wavelength,

$$\lambda_e = \frac{\lambda_0}{\varepsilon_e}$$

Where ε_e is the effective dielectric constant of the substrate, and can be approximated as follows,

$$\varepsilon_e = \frac{\varepsilon_r + 1}{2}$$

Once the antenna is simulated the patch length can be adjusted to achieve the exact center frequency. That is why a simple approximation is used here to estimate the effective dielectric constant. Unless the antenna is to be used for dual or circular polarization, square patches should not be used because of their high cross polarization generation.

Antenna feed parameters:

A thinner feed substrate with a relative permittivity from 2 to 10, and a profile of 0.01λ to 0.02λ (profiles in this range result in a good compromise between higher loss and spurious feed radiation) should be chosen to reduce spurious feed radiation [73]. Centering the slot below the patch antenna typically results in the best level of coupling to the antenna. Similarly, the feedline must also be positioned at a right angle to the slot center for optimal coupling levels. The tuning stub length is typically around $\lambda_g/4$ long and can be used to optimize the reactance of the slot. Increasing the stub length moves the impedance locus in the smith chart to the inductive side and vise versa. A smith chart plot of the impedance locus versus frequency is shown in figure A-5.3. The impedance locus diameter is controlled primarily by the slot length, where a longer slot leads to a larger diameter of the circular portion of the locus [73].

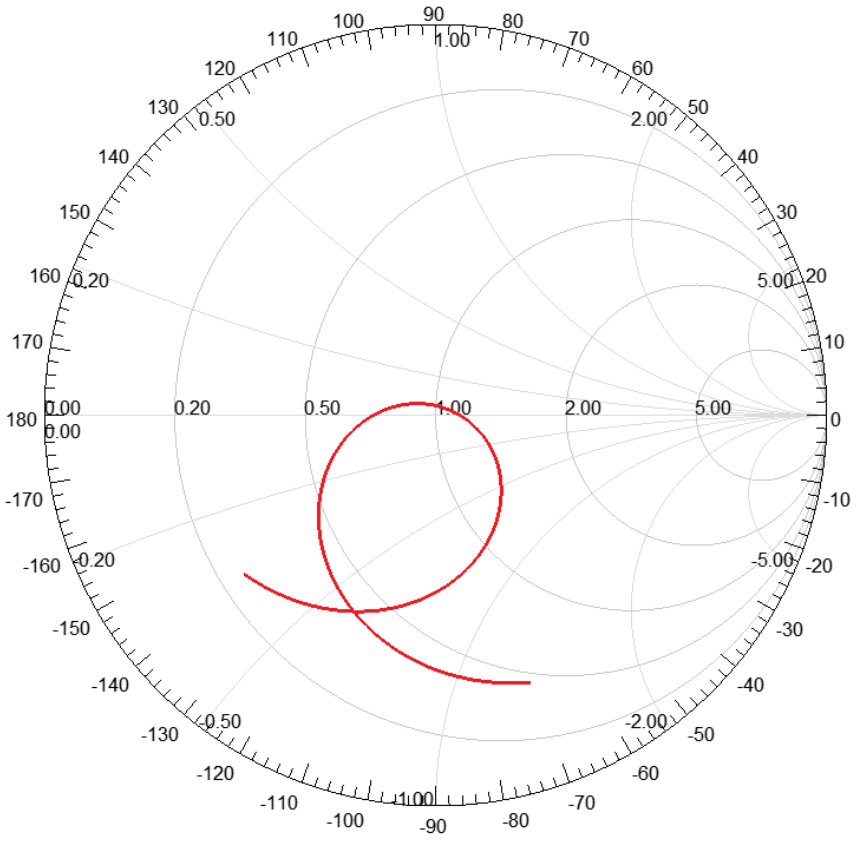

Figure A-3: Slot coupled microstrip antenna impedance locus versus frequency

Coupling Slot:

A key parameter to an aperture coupled design is to get a starting impedance response that is not confined to the edge of the smith chart. Typically, a good starting point is a slot length of about half that of the patch length. This however will depend on the thickness of the material being used. H or bow-tie slot shapes were demonstrated to result in a better level of coupling in comparison to rectangular or round slots.

Slot coupled microstrip antennas will result in a larger percent impedance bandwidth in comparison to antennas fed using other excitation techniques. Bandwidths of up to 50% or more have been demonstrated by using stacked patches and resonant slots [73].

Appendix B. Figure Reprint Permissions

Thesis / Dissertation Reuse

The IEEE does not require individuals working on a thesis to obtain a formal reuse license, however, you may print out this statement to be used as a permission grant:

Requirements to be followed when using any portion (e.g., figure, graph, table, or textual material) of an IEEE copyrighted paper in a thesis:

1) In the case of textual material (e.g., using short quotes or referring to the work within these papers) users must give full credit to the original source (author, paper, publication) followed by the IEEE copyright line © 2011 IEEE.
2) In the case of illustrations or tabular material, we require that the copyright line © [Year of original publication] IEEE appear prominently with each reprinted figure and/or table.
3) If a substantial portion of the original paper is to be used, and if you are not the senior author, also obtain the senior author's approval.

Requirements to be followed when using an entire IEEE copyrighted paper in a thesis:

1) The following IEEE copyright/ credit notice should be placed prominently in the references: © [year of original publication] IEEE. Reprinted, with permission, from [author names, paper title, IEEE publication title, and month/year of publication]
2) Only the accepted version of an IEEE copyrighted paper can be used when posting the paper or your thesis on-line.
3) In placing the thesis on the author's university website, please display the following message in a prominent place on the website: In reference to IEEE copyrighted material which is used with permission in this thesis, the IEEE does not endorse any of [university/educational entity's name goes here]'s products or services. Internal or personal use of this material is permitted. If interested in reprinting/republishing IEEE copyrighted material for advertising or promotional purposes or for creating new collective works for resale or redistribution, please go to http://www.ieee.org/publications_standards/publications/rights/rights_link.html to learn how to obtain a License from RightsLink.

If applicable, University Microfilms and/or ProQuest Library, or the Archives of Canada may supply single copies of the dissertation.

Permission to reprint figure A-5.2 from John Wiley & Sons.

JOHN WILEY AND SONS LICENSE TERMS AND CONDITIONS

Nov 02, 2020

This Agreement between Mr. Mohamed Nasser ("You") and John Wiley and Sons ("John Wiley and Sons") consists of your license details and the terms and conditions provided by John Wiley and Sons and Copyright Clearance Center.

License Number	4940890559880
License date	Nov 02, 2020
Licensed Content Publisher	John Wiley and Sons
Licensed Content Publication	Wiley Books
Licensed Content Title	Antenna Theory: Analysis and Design, 4th Edition
Licensed Content Author	Constantine A. Balanis
Licensed Content Date	Feb 1, 2016
Licensed Content Pages	1
Type of Use	Dissertation/Thesis
Requestor type	University/Academic
Format	Print and electronic
Portion	Figure/table
Number of figures/tables	29
Will you be translating?	No
Title	Design of Broad-band Dual-polarized Microstrip Patch Antennas
Institution name	Ontario Tech University
Expected presentation date	Nov 2020
Portions	figure 14.29
Attachment	image.png
Requestor Location	Mr. Mohamed Nasser 2000 Simcoe Street North Oshawa, ON L1H7K4 Canada Attn: Ontario Tech University
Publisher Tax ID	EU826007151
Billing Type	Invoice
Billing Address	Ontario Tech University 2000 Simcoe Street North Oshawa, ON L1H7K4 Canada Attn: Ontario Tech University
Total	0.00 CAD
Terms and Conditions	

TERMS AND CONDITIONS

This copyrighted material is owned by or exclusively licensed to John Wiley & Sons, Inc. or one of its group companies (each a"Wiley Company") or handled on behalf of a society with which a Wiley Company has exclusive publishing rights in relation to a particular work (collectively "WILEY"). By clicking "accept" in connection with completing this licensing transaction, you agree that the following terms and conditions apply to this transaction (along with the billing and payment terms and conditions established by the Copyright

Permission to reprint figure 1.2 from 3GPP.

Mohamed Nasser
Ontario Tech University
2000 Simcoe Street North, Oshawa, Ontario,
Canada, L1H 7K4

5 November 2020

Our ref: L2020-002-025

Subject: COPYRIGHT LICENCE from 3GPP to reproduce 3GPP material

Dear Mohamed Nasser,

In response to your copyright request, and on behalf of the Third Generation Partnership Project (3GPP™), ETSI is pleased to hereby grant you the non-exclusive right to reproduce, free of charge, the copyrighted material provided in the Annex, to be used as described in your request, provided that you insert the paragraph provided in the Annex, as due acknowledgement of the source, wherever appropriate.

Please note that:

- The Third Generation Partnership Project (3GPP™) is not a legal entity;
- 3GPP Technical Specifications (TSs) and Technical Reports (TRs) are not stable by nature and therefore may be subject to modifications;
- 3GPP TSs and most TRs are, by nature, intended to be transposed into Deliverables of the regional recognised standards developing organisations.

As a result, the present authorisation can only be granted for the 3GPP TRs and TSs "as is".

This copyright licence allows for reproduction only, on a world-wide basis and for an unlimited period of time. Please note that the herewith granted licence does not encompass the right of modification (including but not limited to slight adaptations) and the right of translation into other languages.

Should the above information fall under patent protection, the present copyright licence is not to be construed as an authorisation to use and/or implement patent information without fulfilling any attached obligations.

Yours sincerely,

Christian Loyau
Legal and Governance Affairs Director

www.etsi.org

ETSI | 650 Route des Lucioles | 06921 Sophia Antipolis CEDEX | France | +33 (0)4 92 94 42 00 | info@etsi.org

Institut Européen des Normes de Télécommunication | SIRET N° 348 623 562 00017 – APE 7112B Association à but non lucratif enregistrée à la Sous-Préfecture de Grasse (06) N° W061004871 | N° TVA : FR 14 348 623 562

ANNEX

3GPP TR 38.815	V15.0.0 (2018)	Figure 4.1-1: NR spectrum plans in the range between 24.25-29.5 GHz

Paragraph to be inserted wherever appropriate:

www.etsi.org

ETSI | 650 Route des Lucioles | 06921 Sophia Antipolis CEDEX | France | +33 (0)4 92 94 42 00 | info@etsi.org

Institut Européen des Normes de Télécommunication | SIRET N° 348 623 562 00017 – APE 7112B Association à but non lucratif enregistrée à la Sous-Préfecture de Grasse (06) N° W061004871 | N° TVA : FR 14 348 623 562

References

[1] C. Mercer, “What is 5G? Everything you need to know about 5G,” *Techworld*, pp. 1–15, 2017.

[2] A. Bahai, B. Haroun, and N. Klemmer, “Analog advancements make waves in 5G wireless communications,” *Texas Instruments Inc.*, 2016.

[3] Ericcson, “Ericsson Mobility Report June 2020,” *Ericsson*, no. June, p. 36, 2020.

[4] 5G Americas, “Advanced Antenna Systems for 5G,” *5G Am.*, 2019.

[5] R. B. Waterhouse, *Microstrip Patch Antennas: A Designer’s Guide*. 2003.

[6] D. M. Pozar, “Microstrip Antenna Aperture-Coupled To A Microstripline,” *Electron. Lett.*, vol. 21, no. 2, pp. 49–50, 1985.

[7] D. M. Pozar and B. Kaufman, “Increasing the bandwidth of a microstrip antenna by proximity coupling,” *Electron. Lett.*, vol. 23, no. 8, pp. 368–369, 1987.

[8] S. D. Targonski, R. B. Waterhouse, and D. M. Pozar, “Design of wide-band aperture-stacked patch microstrip antennas,” *IEEE Trans. Antennas Propag.*, vol. 46, no. 9, pp. 1245–1251, 1998.

[9] R. F. Jimenez Broas, D. F. Sievenpiper, and E. Yablonovitch, “A high-impedance ground plane applied to a cellphone handset geometry,” *IEEE Trans. Microw. Theory Tech.*, vol. 49, no. 7, pp. 1262–1265, 2001.

[10] J. J. Schuss *et al.*, “The iridium main mission antenna concept,” *IEEE Trans. Antennas Propag.*, vol. 47, no. 3, pp. 416–424, 1999.

[11] C. R. Rowell and R. D. Murch, “A capacitively loaded PIFA for compact mobile telephone handsets,” *IEEE Trans. Antennas Propag.*, vol. 45, no. 5, pp. 837–842, 1997.

[12] 3GPP, “3rd generation partnership project; Technical Specification Group Radio Access Network;Radio resource management strategies,” 2007.

[13] M. Mirmozafari, G. Zhang, C. Fulton, and R. J. Doviak, “Dual-Polarization Antennas with High Isolation and Polarization Purity: A Review and Comparison of Cross-Coupling Mechanisms,” *IEEE Antennas Propag. Mag.*, vol. 61, no. 1, pp. 50–63, 2019.

[14] P. K. Mishra, D. R. Jahagirdar, and G. Kumar, “A review of broadband dual linearly polarized microstrip antenna designs with high isolation [education column],” *IEEE Antennas Propag. Mag.*, vol. 56, no. 6, pp. 238–251, 2014.

[15] L. Lewin, “Spurious Radiation From Microstrip.,” *Proc. Inst. Electr. Eng.*, vol. 125, no. 7, pp. 633–642, 1978.

[16] M. J. Cryan and P. S. Hall, “Integrated active antenna with simultaneous transmit-receive operation,” *Electron. Lett.*, vol. 32, no. 4, pp. 286–287, 1996.

[17] S. S. Zhong, X. X. Yang, S. C. Gao, and J. H. Cui, “Corner-fed microstrip antenna element and arrays for dual-polarization operation,” *IEEE Trans. Antennas Propag.*, vol. 50, no. 10, pp. 1473–1480, 2002.

[18] S. C. Gao, L. W. Li, T. S. Yeo, and M. S. Leong, “Low cost, dual linearly polarised microstrip patch array,” *IEE Proc. Microwaves, Antennas Propag.*, vol. 148, no. 1, pp. 21–24, 2001.

[19] E. Chang, S. A. Long, and W. F. Richards, “An Experimental Investigation of Electrically Thick Rectangular Microstrip Antennas,” *IEEE Trans. Antennas Propag.*, vol. 34, no. 6, pp. 767–772, 1986.

[20] A. Petosa, A. Ittipiboon, and N. Gagnon, “Suppression of unwanted probe radiation in wideband probe-fed microstrip patches,” *Electron. Lett.*, vol. 35, no. 5, pp. 355–357, 1999.

[21] A. A. Kishk and L. Shafai, “The Effect of Various Parameters of Circular Microstrip Antennas on Their Radiation Efficiency and the Mode Excitation,” *IEEE Trans. Antennas Propag.*, vol. 34, no. 8, pp. 969–976, 1986.

[22] A. Adrian and D. H. Schaubert, “Dual Aperture-Coupled Microstrip Antenna for Dual or Circular Polarisation,” *Electron. Lett.*, vol. 23, no. 23, pp. 1226–1228, 1987.

[23] Y. Murakami, W. Chujo, and M. Fujise, “Mutual coupling between two ports of dual slot-coupled circular patch antennas,” in *AP-S International Symposium (Digest) (IEEE Antennas and Propagation Society)*, 1993, vol. 3, pp. 1469–1472.

[24] D. M. Pozar and S. D. Targonski, “Improved coupling for aperture coupled microstrip antennas,” *Electron. Lett.*, vol. 27, no. 13, pp. 1129–1131, 1991.

[25] V. Rathi, G. Kumar, and K. P. Ray, “Improved coupling for aperture coupled microstrip antennas,” *IEEE Trans. Antennas Propag.*, vol. 44, no. 8, pp. 1196–1198, 1996.

[26] P. Brachat and J. M. Baracco, “Dual-Polarization Slot-Coupled Printed Antennas Fed by Stripline,” *IEEE Trans. Antennas Propag.*, vol. 43, no. 7, pp. 738–742, 1995.

[27] K. M. Luk, C. L. Mak, Y. L. Chow, and K. F. Lee, “Broadband microstrip patch antenna,” *Electron. Lett.*, vol. 34, no. 15, pp. 1442–1443, 1998.

[28] K. S. Ryu and A. A. Kishk, “Wideband dual-polarized microstrip patch excited by hook shaped probes,” *IEEE Trans. Antennas Propag.*, vol. 56, no. 12, pp. 3645–3649, 2008.

[29] H. Wong, K. L. Lau, and K. M. Luk, “Design of dual-polarized L-probe patch antenna arrays with high isolation,” *IEEE Trans. Antennas Propag.*, vol. 52, no. 1, pp. 45–52, 2004.

[30] S. C. Gao, L. W. Li, M. S. Leong, and T. S. Yeo, “Dual-polarized slot-coupled planar antenna with wide bandwidth,” *IEEE Trans. Antennas Propag.*, vol. 51, no. 3, pp. 441–448, 2003.

[31] S. Hienonen, A. Lehto, and A. V. Räisänen, “Simple broadband dual-polarized aperture-coupled microstrip antenna,” in *IEEE Antennas and Propagation Society International Symposium: Wireless Technologies and Information Networks, APS 1999 - Held in conjunction with USNC/URSI National Radio Science Meeting*, 1999, vol. 2, pp. 1228–1231.

[32] S. J. Li, J. Gao, X. Cao, Z. Zhang, and D. Zhang, “Broadband and high-isolation dual-polarized microstrip antenna with low radar cross section,” *IEEE Antennas Wirel. Propag. Lett.*, vol. 13, pp. 1413–1416, 2014.

[33] K. Ghorbani and R. B. Waterhouse, “Dual polarized wide-band aperture stacked patch antennas,” *IEEE Trans. Antennas Propag.*, vol. 52, no. 8, pp. 2171–2174, 2004.

[34] S. D. Targonski and D. M. Pozar, “Design of Wideband Circularly Polarized Aperture-Coupled Microstrip Antennas,” *IEEE Trans. Antennas Propag.*, vol. 41, no. 2, pp. 214–220, 1993.

[35] B. G. Porter, “Dual-polarized slot-coupled patch antennas on duroid with teflon lenses for 76.5-GHz automotive radar systems,” *IEEE Trans. Antennas Propag.*, vol. 47, no. 12, pp. 1836–1842, 1999.

[36] J. K. Du *et al.*, “Dual-polarized patch array antenna package for 5G communication systems,” in *2017 11th European Conference on Antennas and Propagation, EUCAP 2017*, 2017, pp. 3493–3496.

[37] D. Liu, X. Gu, C. W. Baks, and A. Valdes-Garcia, “Antenna-in-Package Design Considerations for Ka-Band 5G Communication Applications,” *IEEE Trans. Antennas Propag.*, vol. 65, no. 12, pp. 6372–6379, 2017.

[38] T. H. Jang, H. Y. Kim, D. M. Kang, S. H. Kim, and C. S. Park, “60 GHz Low-Profile, Wideband Dual-Polarized U-Slot Coupled Patch Antenna with High Isolation,” *IEEE Trans. Antennas Propag.*, vol. 67, no. 7, pp. 4453–4462, 2019.

[39] S. Liao and Q. Xue, “Dual polarized planar aperture antenna on LTCC for 60-GHz antenna-in-package applications,” *IEEE Trans. Antennas Propag.*, vol. 65, no. 1, pp. 63–70, 2017.

[40] M. A. Islam and N. C. Karmakar, “A 4 × 4 dual polarized mm-wave ACMPA array for a universal mm-wave chipless RFID tag reader,” *IEEE Trans. Antennas Propag.*, vol. 63, no. 4, pp. 1633–1640, 2015.

[41] M. Yamazaki, E. T. Rahardjo, and M. Haneishi, “Construction of a slot-coupled planar antenna for dual polarisation,” *Electron. Lett.*, vol. 30, no. 22, pp. 1814–1815, 1994.

[42] W. Wang, J. Wang, A. Liu, and Y. Tian, “A Novel Broadband and High-Isolation Dual-Polarized Microstrip Antenna Array Based on Quasi-Substrate Integrated

Waveguide Technology," *IEEE Trans. Antennas Propag.*, vol. 66, no. 2, pp. 951–956, 2018.

[43] T. Chaloun, V. Ziegler, and W. Menzel, "Design of a Dual-Polarized Stacked Patch Antenna for Wide-Angle Scanning Reflectarrays," *IEEE Trans. Antennas Propag.*, vol. 64, no. 8, pp. 3380–3390, 2016.

[44] J. L. Vazquez-Roy, V. Krozer, and J. Dall, "Wideband dual-polarization microstrip patch antenna array for airborne ice sounder," *IEEE Antennas Propag. Mag.*, vol. 54, no. 4, pp. 98–107, 2012.

[45] R. J. Mailloux, "On the Use of Metallized Cavities in Printed Slot Arrays with Dielectric Substrates," *IEEE Trans. Antennas Propag.*, vol. 35, no. 5, pp. 477–487, 1987.

[46] F. Zavosh and J. T. Aberle, "Infinite Phased Arrays of Cavity-Backed Patches," *IEEE Trans. Antennas Propag.*, vol. 42, no. 3, pp. 390–398, 1994.

[47] M. A. González de Aza, J. Zapata, and J. A. Encinar, "Broad-band cavity-backed and capacitively probe-fed micro strip patch arrays," *IEEE Trans. Antennas Propag.*, vol. 48, no. 5, pp. 784–789, 2000.

[48] M. H. Awida, A. H. Kamel, and A. E. Fathy, "Analysis and design of wide-scan angle wide-band phased arrays of substrate-integrated cavity-backed patches," *IEEE Trans. Antennas Propag.*, vol. 61, no. 6, pp. 3034–3041, 2013.

[49] J. Wang, W. Wang, A. Liu, M. Guo, and Z. Wei, "Cross-Polarization Suppression of a Dual-Polarized Microstrip Antenna Using Enclosed Substrate-Integrated Cavities," *IEEE Antennas Wirel. Propag. Lett.*, vol. 19, no. 1, pp. 64–68, 2020.

[50] M. H. Awida and A. E. Fathy, "Design guidelines of substrate-integrated cavity-backed patch antennas," *IET Microwaves, Antennas Propag.*, vol. 6, no. 2, pp. 151–157, 2012.

[51] M. H. Awida, S. H. Suleiman, and A. E. Fathy, "Substrate-integrated cavity-backed patch arrays: A low-cost approach for bandwidth enhancement," *IEEE Trans. Antennas Propag.*, vol. 59, no. 4, pp. 1155–1163, 2011.

[52] J. R. Bray and L. Roy, "Resonant frequencies of post-wall waveguide cavities," in *IEE Proceedings: Microwaves, Antennas and Propagation*, 2003, vol. 150, no. 5, pp. 365–368.

[53] D. Deslandes and K. Wu, "Accurate Modeling, Wave Mechanisms, and Design Considerations of a Substrate Integrated Waveguide," *IEEE Trans. Microw. Theory Tech.*, vol. 54, no. 6, pp. 2516–2526, 2006.

[54] P. Applications, "Last-a-foam ® rf-2200 dielectric foam series," 2015.

[55] D. H. Schaubert, F. G. Farrar, A. Sindoris, and S. T. Hayes, "Microstrip Antennas with Frequency Agility and Polarization Diversity," *IEEE Trans. Antennas Propag.*, vol. 29, no. 1, pp. 118–123, 1981.

[56] P. L. Sullivan and D. H. Schaubert, “Analysis of an Aperture Coupled Microstrip Antenna,” *IEEE Trans. Antennas Propag.*, vol. 34, no. 8, pp. 977–984, 1986.

[57] F. Croq and D. M. Pozar, “Millimeter-Wave Design of Wide-Band Aperture-Coupled Stacked Microstrip Antennas,” *IEEE Trans. Antennas Propag.*, vol. 39, no. 12, pp. 1770–1776, 1991.

[58] P. R. Haddad and D. M. Pozar, “Analysis of two aperture-coupled cavity-backed antennas,” *IEEE Trans. Antennas Propag.*, vol. 45, no. 12, pp. 1717–1726, 1997.

[59] F. A. Ghaffar and A. Shamim, “Design of silicon-based fractal antennas,” *Microw. Opt. Technol. Lett.*, vol. 55, no. 1, pp. 180–186, 2013.

[60] F. A. Ghaffar, M. U. Khalid, K. N. Salama, and A. Shamim, “24-GHz LTCC fractal antenna array SoP with integrated Fresnel lens,” *IEEE Antennas Wirel. Propag. Lett.*, vol. 10, pp. 705–708, 2011.

[61] D. M. Pozar, “Considerations for Millimeter Wave Printed Antennas,” *IEEE Trans. Antennas Propag.*, vol. 31, no. 5, pp. 740–747, 1983.

[62] R. B. Waterhouse, D. Novak, A. Nirmalathas, and C. Lim, “Broadband Printed Millimeter-Wave Antennas,” *IEEE Trans. Antennas Propag.*, vol. 51, no. 9, pp. 2492–2495, 2003.

[63] J. S. Dahele, S. H. Tung, and K. F. Lee, “Normal and Inverted Configurations of the Broadband Electromagnetic-Coupled Microstrip Antenna.,” in *IEEE Antennas and Propagation Society, AP-S International Symposium (Digest)*, 1986, pp. 841–844.

[64] G. Boussatour, P. Y. Cresson, B. Genestie, N. Joly, and T. Lasri, “Dielectric Characterization of Polylactic Acid Substrate in the Frequency Band 0.5-67 GHz,” *IEEE Microw. Wirel. Components Lett.*, vol. 28, no. 5, pp. 374–376, 2018.

[65] S. Ima *et al.*, “5G Phased Array Technologies,” no. September, 2019.

[66] J. W. Wevers, “Chapter 14,” in *Notes on the Greek Text of Genesis*, 2019, pp. 185–201.

[67] D. M. Pozar and D. H. Schaubert, *Microstrip Antennas: The Analysis and Design of Microstrip Antennas and Arrays Electrical engineering, antennas and propagation*. 1995.

[68] R. E. Munson, “Conformal Microstrip Atennas and Microstrip Phased Arrays,” *IEEE Trans. Antennas Propag.*, vol. AP-22, no. 1, pp. 74–78, 1974.

[69] R. J. P. Douville and D. S. James, “Experimental Study of Symmetric Microstrip Bends and Their Compensation,” *IEEE Trans. Microw. Theory Tech.*, vol. 26, no. 3, pp. 175–182, 1978.

[70] H. J. Visser, “Equivalent length design equations for right-angled microstrip bends,” in *IET Seminar Digest*, 2007, vol. 2007, no. 11961.

[71] J. Xu, W. Hong, Z. H. Jiang, and H. Zhang, “Wideband, low-profile patch array

antenna with corporate stacked microstrip and substrate integrated waveguide feeding structure," *IEEE Trans. Antennas Propag.*, vol. 67, no. 2, pp. 1368–1373, 2019.

[72] Y. Li and K. M. Luk, "60-GHz Dual-Polarized Two-Dimensional Switch-Beam Wideband Antenna Array of Aperture-Coupled Magneto-Electric Dipoles," *IEEE Trans. Antennas Propag.*, vol. 64, no. 2, pp. 554–563, 2016.

[73] D. M. Pozar, "A review of aperture coupled microstrip antennas: History, operation, development, and applications," *Univ. Massachusetts Amherst*, no. May, pp. 1–9, 1996.